A MURINE MODEL OF THE ACUTE RESPONSE OF BONE TO A MARROW ABLATING DOSE OF IONIZING RADIATION IN PEDIATRIC ACUTE LYMPHOBLASTIC LEUKEMIA TREATMENT

Angelica B. de Rosa

A thesis submitted to the faculty at the University of North Carolina at Chapel Hill
in partial fulfillment of the requirements for the degree of Master of Science
in the Joint Department of Biomedical Engineering in the School of Medicine.

Chapel Hill
2014

Approved by:

Ted A. Bateman

Jacqueline Cole

Jeffrey S. Willey

ABSTRACT

Angelica B. de Rosa: A Murine Model of the Acute Response of Bone to a Marrow Ablating Dose of Ionizing Radiation in Pediatric Acute Lymphoblastic Leukemia Treatment
(Under the direction of Ted A. Bateman)

Acute lymphoblastic leukemia (ALL) survivors experience chronic health conditions from treatment, including osteoporosis. ALL radiation therapy is known to induce bone resorption, but animal models for this loss do not exist.

Five-week-old C57Bl/6 mice were either irradiated with 8 Gy X rays or kept as non-irradiated controls. Bones were collected at 2, 4, and 6 days post-irradiation. MicroCT and finite element analysis assessed microarchitectural and structural parameters. Serum osteocalcin and TRAP-5b levels were quantified.

At 2 days post-irradiation, osteocalcin and trabecular bone volume fraction (BV/TV) were elevated in irradiated mice compared to controls. By 6 days, BV/TV, connectivity density, and trabecular stiffness declined, while TRAP-5b levels and cortical volume and stiffness increased.

In conclusion, radiation exposure in young mice causes an acute increase in bone mass followed by rapid loss. This suggests less than a one-week window after irradiation to prevent or mitigate bone loss due to radiation therapy.

To my parents.

ACKNOWLEDGEMENTS

Thank you to the Bateman Lab for all your help and support, especially Dr. Anthony G. Lau for your extensive help with finite element modeling of bone and mentorship through graduate school, Dr. Sheila Rao-Dayton for your expertise with ELISAs, Eric W. Livingston for your patience and help with all things lab-related and μCT, and Dr. Ted A. Bateman for giving me a chance at a graduate education and believing that good engineers can also learn biology. Thank you also to my family and the future Dr. Christopher J. Payne for your unending love and support. This research was funded by the Initiative for Maximizing Student Diversity, the North Carolina Space Grant, and the National Institutes of Health.

TABLE OF CONTENTS

LIST OF TABLES

LIST OF FIGURES

LIST OF ABBREVIATIONS

6-MP	mercaptopurine
ALL	acute lymphoblastic leukemia
BALP, BSAP	bone specific alkaline phosphatase
BMD	bone mineral density
BMI	body mass index
BMT	bone marrow transplantation
BMU	bone multicellular unit
BRC	bone remodeling compartment
BV/TV	trabecular bone volume fraction
CLP	common lymphoid progenitor cell
CMP	common myeloid progenitor cell
CNS	central nervous system
ConnD	connectivity density
CtBV	cortical bone volume
CtPo	cortical porosity
CtTh	cortical thickness
CTX	C-terminal crosslinking telopeptide of type I collagen
CY	cyclophosphamide
DXA	dual x-ray absorptiometry
ELISA	enzyme-linked immunosorbent assay
FEA	finite element analysis

FGF	fibroblast growth factor
FRAX	Fracture Risk Assessment Tool
G-CSF	granulocyte colony stimulating factor
GMP	granulocyte macrophage progenitor cell
GVHD	graft-versus-host-disease
GVL	graft-versus-leukemia
GVT	graft-versus-tumor
Gy	Gray
HRCT	high resolution computed tomography
HSC	hematopoietic stem cell
HSCT	hematopoietic stem cell transplant
IGF	insulin-like growth factor
IL	interleukin
IRR	irradiated
M-CSF	macrophage colony stimulating factor
MDCT	multi-detector computed tomography
MEP	megakaryocyte/erythroid progenitor cell
microCT, μCT	microcomputed tomography
MRI	magnetic resonance imaging
MSC	mesenchymal stem cell
MTX	methotrexate
NK	natural killer cell
NR	non-irradiated

NTX	N-terminal crosslinking telopeptide of type I collagen
OC	osteocalcin
OPG	osteoprotegerin
P1CP	procollagen I carboxyl terminal propeptide
P1NP	procollagen type 1 N-terminal propeptide
pMOI	polar moment of inertia
pQCT	peripheral quantitative computed tomography
PTH	parathyroid hormone
QCT	quantitative computed tomography
QUS	quantitative ultrasound
RANK	receptor activator of nuclear factor (NF)-kappa-B
RANKL	receptor activator of nuclear factor (NF)-kappa-B ligand
RUNX	Runt-related transcription factor
Sv	Sieverts
SZ	sealing zone
TBI	total body irradiation
TbN	trabecular number
TbSp	trabecular separation
TbTh	trabecular thickness
TGF	transforming growth factor
TNF	tumor necrosis factor
TRAP-5b	tartrate-resistant alkaline phosphatase
UNC	University of North Carolina at Chapel Hill

vBMD	volumetric bone mineral density
VCR	vincristine
WHO	World Health Organization

CHAPTER 1: INTRODUCTION

Bone is a dynamic substance that is constantly adapting to its environment. Bone will strategically increase or decrease in mass and microarchitecture to accommodate growth, external loading, or chronic conditions. This is possible through the work of osteoblasts, which build bone and are more active during growth and development, and osteoclasts, which resorb bone and are more active when bone loss occurs. Osteoblast and osteoclast activity can be detected through several biomarkers, including osteocalcin (OC), procollagen type I N-terminal propeptide (P1NP), and bone specific alkaline phosphatase (BSAP) for osteoblasts, and tartrate-resistant acid phosphatase (TRAP-5b), N-terminal cross-linking telopeptides of type I collagen (NTX), and deoxypyridinoline for osteoclasts. Their cell numbers and surface area can also be visualized and quantified using histology, and their effects can be measured through microcomputed tomography (μCT) as microarchitectural parameters and finite element analysis (FEA) as structural parameters.

The response of bone is often complex and not well understood in cases with multiple sources of influence on overall bone health. Such is the case in treating children with acute lymphoblastic leukemia (ALL), in which bone can be subjected to radiation therapy, chemotherapy, and bone marrow transplantation at the same time to achieve remission, in addition to the disease and disuse from bed rest. Although ALL is the most common form of childhood cancer, treated patients enjoy an over 80% long-term remission rate (Pui et al., 2008). However, treatment therapies also have significant long-term effects on the body,

including reduced bone mineral density (BMD) and increased fracture rate in bone (McClune et al., 2011).

Reduced BMD and osteoporosis are common side effects of radiation exposure (Oeffinger et al., 2006). Osteoporosis occurs when bone resorption exceeds formation, and is characterized by reduced bone strength, mass, and density. Patients typically undergo dual-energy x-ray absorptiometry (DXA) or quantitative computed tomography (QCT) scans periodically to assess BMD, microarchitecture, and overall bone health. This information helps clinicians craft patient-specific recovery regimens, which may include calcium and vitamin D supplements, pharmacological intervention, exercise regimens, and lifestyle changes with the goal of increasing BMD and reducing fracture risk.

Although BMD is commonly measured alone, it is not an all-inclusive determinant of fracture risk. Microarchitectural parameters such as trabecular number and connectivity density are also important to maintain the mechanical contribution of the cancellous region. These parameters can be combined with computer modeling to assess fracture risk more accurately.

The response of bone to radiation is established in scientific literature (Green & Rubin, 2014; Willey et al., 2011), but few reports of the effects of a myeloablating dose of radiation on bone in young subjects exist. With a high cure rate for ALL, improving quality of life and preventing fracture risk are increasing concerns. The study presented in this work aims to characterize the response of bone to a marrow-ablating dose of radiation in young subjects to model treatment for ALL. The results can be correlated with actual bone loss observed in children, and the model can be expanded to include the effects of bone marrow transplantation and chemotherapy as well. Overall, this work contributes information needed

to make informed decisions to provide the best care possible for ALL treatment patients and survivors.

Significance

There are several motivations to focus on ALL patients, radiation therapy, and bone as the context for this study. Many cancer patients receive radiation therapy, making a cancer model an appropriate choice to study the biological effects of radiation. Most patients diagnosed with ALL are cured and experience chronic conditions related to cancer therapy, with osteoporosis and increased fracture risk contributing to reduced quality of life (Rueegg et al., 2013).

Significance of the Effects of Total Body Irradiation

Radiation therapy is needed during treatment for an estimated 50-60% of all cancer cases (Beyzadeoglu et al., 2010; Zeman et al., 2014). Clinical radiation therapy is known to damage bone and increase fracture risk, although the increase in risk associated with standard fractionation is not well characterized (Baxter et al., 2005). Interacting factors, such as immunosuppressants, physical inactivity, and nutritional deficiencies are acknowledged in addition to radiation as the main causes of bone loss associated with ALL treatment (Mussa et al., 2010) and make it difficult to establish a scientific basis for total body irradiation (TBI) (Barrett, 1999). Our goal is to characterize one of these main causes of treatment-related bone loss, irradiation, and its effects on bone in a mouse model.

In ALL patients, the most prominent bone loss occurs during therapy (Mussa et al., 2010), with radiation and chemotherapy largely contributing to bone marrow suppression and bone loss (Green et al., 2012). Increased bone fragility in patients treated for ALL may be due to a combination of leukemic cell expansion into the bone marrow, inactivity, renal

electrolyte wasting, nutritional deficiencies, steroid and chemotherapeutic drug use, radiotherapy, and treatment-induced endocrine dysfunctions (Mussa et al., 2010). Radiation compromises bone marrow and depletes stem cell populations, increasing the risk of fracture (Green et al., 2012). For example, the risk of pelvic fracture is known to increase after pelvic exposure to irradiation, and is associated with up to a 20% higher mortality rate than in people who did not receive this type of clinical irradiation (Baxter et al., 2005). Therefore, prevention of damage during radiation therapy will improve bone injury recovery later on (Cao et al., 2011).

Application to Acute Lymphoblastic Leukemia

In the United States, about 13 new cases of leukemia are diagnosed each year for every 100,000 people, and over 1.1 million people live with or are in remission from leukemia, lymphoma, and myeloma, all of which use radiation therapy (Green & Rubin, 2014). For children, about 45 new cases of leukemia per million people per year (Imbach, 2011b), ALL appearing most frequently (Pui et al., 2008). Survival rates for ALL are estimated between 80-90% (Pui et al., 2008) and improving, allowing clinical focus to shift to reducing severe acute and late effects of treatment (Pui & Evans, 2006). Thus, the number of investigators for long-term effects of leukemia and its treatment is growing and becoming part of clinical trial development, with the goal of optimizing therapy intensity, efficacy, and short- and long-term health effects (O'Brien & Lacayo, 2008). One of the most prominent effects to be mitigated is treatment-related bone loss, which results in an almost doubled fracture rate for ALL survivors (Mussa et al., 2010).

Radiation therapy is used to treat cancer, making a cancer model an appropriate choice to study the effects of radiation. Curative radiotherapy is used to cure cancers such as

Hodgkin's lymphoma and nasopharyngeal cancers, and prophylactic radiotherapy is used to prevent metastases or recurrences in leukemias and small cell lung cancer (Beyzadeoglu et al., 2010). Total body irradiation is used especially in leukemia to eradicate leukemic cells, suppress the immune system, and clear space for bone marrow transplantation (Beyzadeoglu et al., 2010). Scientifically, the effects of clinical radiation are not easy to establish because other factors, such as graft-versus-host disease (GVHD) and bone marrow transplantation (BMT), affect treatment outcome, and patient treatment is the top priority (Barrett, 1999). For example, over 50,000 people worldwide can undergo BMT in a year, primarily due to leukemia (Green & Rubin, 2014).

Analysis of Bone

Osteoporosis is the most common bone disease, and its prevalence and associated fractures are expected to increase due to aging populations (Damilakis et al., 2010; Shuler et al., 2012). In the U.S., about 1.5 million osteoporotic fractures occur each year (Shuler et al., 2012). Over 970,000 hip fractures are expected in the European Union alone (Damilakis et al., 2010) and 6.26 million hip fractures are expected worldwide by 2050, compared to 1.66 million worldwide in 1950 (Shuler et al., 2012). The financial burden of osteoporotic fractures is also expected to increase, with direct care costs related to osteoporotic fractures estimated up to 18 billion dollars per year in 2002, and expected to double or triple by 2040 (Shuler et al., 2012).

Bone fractures are life threatening for individuals with osteoporosis, and over 70 million people worldwide are at risk of developing osteoporotic fractures (Boyle et al., 2003). Hip fractures alone result in over 300,000 hospitalizations per year in the U.S., have a 24% mortality for senior citizens within one year, and are associated with a 250% increased risk of

fracture at another location (Shuler et al., 2012). Patients who do not achieve an optimal peak BMD are more likely to suffer from osteoporotic fractures later in life (McClune et al., 2011). Therefore, addressing bone health early in life can help optimize BMD and thus reduce fracture risk (McClune et al., 2011).

Osteoporosis and increased fracture risk are acknowledged as results of radiation exposure and stem cell transplantation related to cancer treatment. Long-term survivors of hematopoietic stem cell transplantation are at risk for reduced bone mineral density, osteoporosis, and fracture (McClune et al., 2011) that contributes to morbidity and mortality (Schimmer et al., 2000). Osteoporosis and osteopenia are pathological long-term complications of radiation treatment (Green & Rubin, 2014; Willey et al., 2008). Bone loss causes reduced bone strength and increased fracture risk (Green & Rubin, 2014; Willey et al., 2011), and associated fractures are difficult to treat (Green & Rubin, 2014). X-ray based imaging techniques are also being used more frequently due to low doses of radiation absorbed, with DXA use growing to over 2 million scans in the U.S. alone by 2002 (Damilakis et al., 2010). With an increasing number of bone scans performed, optimization and justification of radiation exposure becomes necessary to ensure radiation doses are kept as low as reasonably achievable (Damilakis et al., 2010).

Improving Quality of Life

Health-related quality of life is becoming increasingly important for childhood cancer survivors, who experience a lower quality of life compared to their unafflicted siblings and often report musculoskeletal problems (Rueegg et al., 2013). In fact, chronic health conditions affect almost 75% of childhood cancer survivors within 30 years of diagnosis (Oeffinger et al., 2006). A growing number of patients cured from BMT and TBI (Sanders,

1990) and a high cure rate for leukemia already exist; therefore quality of life of those who are cured can and must be addressed (Tucci & Aricò, 2008). Complex treatments, large expenses, and toxic side effects can all be mitigated (Pui et al., 2008), and preventative measures, risk-targeted follow-up, and interventions may also help improve the quality of life for childhood cancer survivors (Rueegg et al., 2013).

More cancer patients are undergoing radiation therapy, so maintaining bone architecture to prevent long-term risk of fracture from treatment is of increasing importance (Green & Rubin, 2014). Findings about the inflammatory response may be applicable to other conditions in bone, whether inflicted by radiation, chemotherapy, or other perturbations. Identification of when osteoblasts and osteoclasts are active in children and their mode of action has potential to mitigate long-term skeletal effects of medical procedures affecting bone by providing appropriate targets for preventative and treatment therapies.

A Comprehensive Report

This manuscript is written with the intention of continued work in the refinement of a murine model for human radiation treatment. Inasmuch as it is undesirable and inhumane to withhold additional treatments from persons who receive radiation therapy, it is important to be aware of and understand confounding factors that occur necessarily in the clinical setting. Therefore, although the model aims to represent the effects of radiation on bone most accurately, it is in the best interests of investigators, clinicians, and patients that the results of these studies and their clinical corollaries are understood in light of the additional factors presented (and perhaps some not yet known).

CHAPTER 2: GENERAL BONE BIOLOGY AND PHYSIOLOGY

Introduction

Bone has three main functions: structural support of the body, mineral storage to maintain blood pH values, and blood and immune cell formation. We will discuss mainly load-bearing bones such as long bones in the leg (femur and tibia) and the vertebrae in the spine. Due to their load-bearing function, fracture risk is greatest in these bones, especially with aging or radiation treatment. BMD and bone mineral content, measures of bone mass or the amount of bone present, serve as partial indications of bone strength (Burr & Akkus, 2014). However, microarchitecture must be considered as well. Bone marrow is also the site of blood cell formation, or hematopoiesis, including immune cells. Here we will discuss bone anatomy and the juvenile skeleton; the three bone cells osteoblasts, osteoclasts, and osteocytes; normal bone remodeling, and hematopoiesis.

Bone Anatomy

Long bones consist of cortical and trabecular sections and a bone marrow cavity (Figure 1). The diaphysis is the shaft of the long bone that is made of thick cortical bone and contains yellow marrow in adults. The metaphysis is found at each end of the diaphysis and contains trabecular bone and red marrow and is surrounded by a thin cortical shell. The epiphysis serves as the end of the bone and is made of trabecular bone also incased by a thin cortical shell. Between the epiphysis and metaphysis is the growth plate, which is active during bone formation and growth until it solidifies. Long bones grow outward from the growth plates, lengthening the bone (Humphries, 2011). The periosteum is the membrane

covering the outer surface of bone that aids in formation and nutrition. The endosteum is the membrane that covers the inner surface of the bone. Each section serves its own function critical to structural support and cell generation.

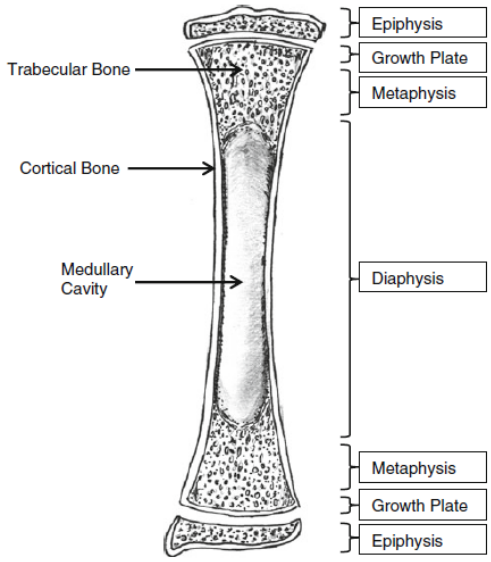

Figure 1: Standard anatomy of a long bone. (Drawing by Humphries, 2011)

Cortical and Trabecular Bone

The two main types of bone organization on the macro-scale are cortical and trabecular bone (Figure 2). Cortical bone, also called compact bone, is dense and forms the outer shell of bones, especially the skull, shafts of long bones, and vertebrae (Burr & Akkus, 2014; Hadjidakis & Androulakis, 2006). It composes 80% of the adult skeleton by weight and has a porosity of 5-10%, which together provides compressive strength and resistance to torsion and bending (Buck & Dumanian, 2012; Christenson, 1997; Hadjidakis & Androulakis, 2006). Cortical bone has an overall remodeling rate of 2-5% per year in normal, healthy individuals (Hadjidakis & Androulakis, 2006).

Trabecular bone, also called cancellous or spongy bone, is made up of thin interconnected struts that direct load forces to the stronger outer cortical bone. It composes 20% of the adult skeleton but has between 50-90% porosity (Buck & Dumanian, 2012; Christenson, 1997; Hadjidakis & Androulakis, 2006) and provides mechanical support by allowing deformations and absorption of loads (Buck & Dumanian, 2012) without significantly increasing the weight of the bone. The thickness and number of trabeculae will optimize according to the location and direction of loading, and loss of connectivity or trabecular number reduces bone stiffness and strength up to three times more than reducing trabecular thickness (Burr & Akkus, 2014). Due to its greater surface area compared to cortical bone, trabecular bone has higher rates of bone turnover for structural remodeling and maintaining metabolic equilibriums (Christenson, 1997; Hadjidakis & Androulakis, 2006).

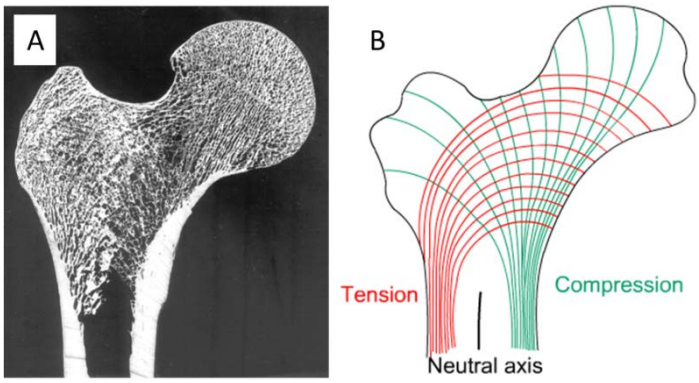

Figure 2: Cross section depicting the cortical shell in the proximal femur and supporting trabecular network. Note the visible trabecular tension and compression lines. A) Actual cross-section of a proximal femur (from GeoScienceWorld). B) Illustration of compression and tension lines visible in an actual cross-section of a proximal femur (University of Cambridge).

Although the macrostructure of bone can be described as cortical or cancellous, the microscopic structure of both cortical and trabecular structures is similar (Burr & Akkus,

2014). Microscopically, bone is organized into osteons that are composed of concentric lamellae organized around Haversian canals, the channels through which nerves and blood vessels run (Figure 3). In bone cross sections, the Haversian canals typically appear as dark, circular holes. The lamellae around the Haversian canals can sometimes be visualized by the deposition line, but canaliculi, the smaller dots circling the Haversian canal that contain osteocytes, are more visible signs of lamellar boundaries (Burr & Akkus, 2014). The outermost boundary of a lamella where bone resorption stopped is known as a cement line. Cement lines act as natural barriers to microcrack propagation, maintaining structural integrity of the osteon on the microscale (Burr & Akkus, 2014).

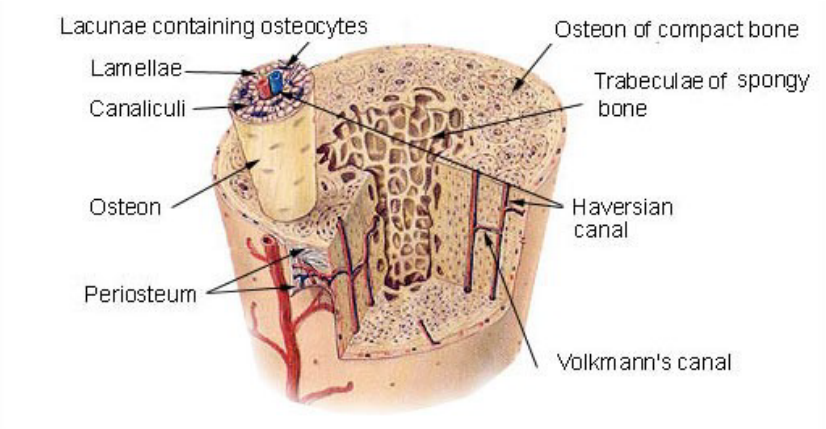

Figure 3: Microscopic structure of bone. Note the concentric lamellae, canaliculi, and Haversian canals. (From http://s1.hubimg.com/u/7534464_f520.jpg)

In cortical bone, osteons will grow large and are oriented offset from the long axis of the bone (Burr & Akkus, 2014). In cancellous bone, osteons are typically half-osteons, or hemiosteons, due to the small diameter of trabeculae, and blood supply can be accessed from the surrounding marrow rather than a Haversian canal (Burr & Akkus, 2014). Hemiosteons are oriented along the long axis of the trabeculae (Burr & Akkus, 2014).

Composite Material

Bone is composed of approximately 65% mineral or inorganic matrix by weight, 25% organic material, and 10% water (Burr & Akkus, 2014). Structurally on the nano-scale, it is a mineralized cross-linked collagen matrix (Burr & Akkus, 2014).

The organic phase of bone is secreted by osteoblasts and provides ductility and resilience (Burr & Akkus, 2014). It is composed primarily (90%) (Christenson, 1997; Hadjidakis & Androulakis, 2006; Teitelbaum, 2000) of type I collagen organized into fibers (Burr & Akkus, 2014) but also contains glycoproteins, proteoglycans, and growth factors (Buck & Dumanian, 2012), including bone morphogenetic proteins. The mineral phase of bone is dispersed throughout the collagen fibers, and the crystals are oriented in the same direction (Hadjidakis & Androulakis, 2006).

Mineral composes 50-70% of the bone matrix (Bellido et al., 2014). It acts as storage for the body's supply of calcium, phosphorus, magnesium, and sodium (Buck & Dumanian, 2012). The mineral phase of bone provides strength, stiffness, and compressive resistance to the material (Buck & Dumanian, 2012; Burr & Akkus, 2014) and is composed primarily of carbonated apatite (hydroxyapatite) organized into plate-like structures (Burr & Akkus, 2014; Teitelbaum, 2000). Calcium is a major component of bone and provides strength and stiffness. Calcium ions are also used in blood clotting, muscle contraction, and enzyme reactions (Burr & Akkus, 2014).

Bone Marrow

Bone marrow exists inside bones among the trabecular network, encased by the cortical shell. It contains capillaries and cells, including stem cells, stromal cells, macrophages, osteoblasts and osteoclasts, and megakaryocytic, erythroid, lymphocytic, and

myeloid cells (Paessler & Bourne, 2011). Stromal cells, which include fibroblasts and adipose cells, secrete proteins, adhesion molecules, and regulatory products required for hematopoiesis, stem cell survival, and osteogenesis (Paessler & Bourne, 2011).

During growth and development, the bone marrow cavities of the long bones contain mostly red marrow (Burr & Akkus, 2014; Guillerman, 2013). Red marrow is indicative of hematopoiesis, while yellow marrow is indicative of fat. By adulthood, much of the bone marrow cavity is filled with yellow fat (Burr & Akkus, 2014; Guillerman, 2013). Red marrow is highly vascularized and active in hematopoiesis, with the number of hematopoietic cells reducing with age (Guillerman, 2013). Yellow marrow is composed mostly of adipocytes and has little to no vasculature or hematopoietic activity (Guillerman, 2013). Conversion from red marrow to yellow marrow begins around the time of ossification of the epiphyses and occurs distal to proximal, diaphyseal to metaphyseal, and central to peripheral (Guillerman, 2013). Figure 4 below illustrates the conversion of red marrow to yellow marrow through adolescence using MRI images.

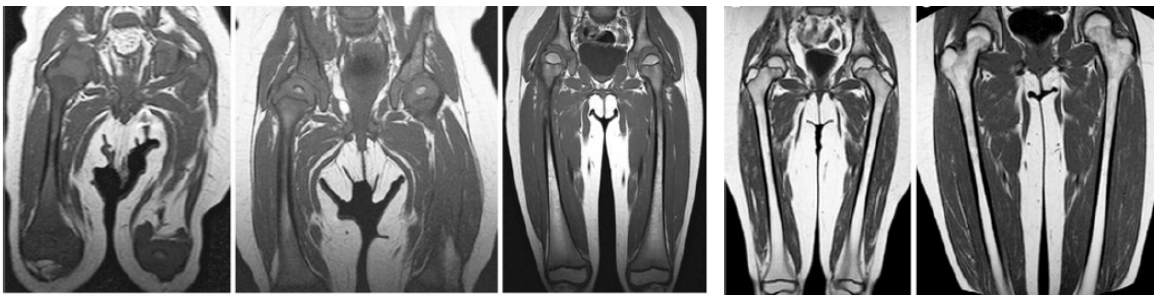

Figure 4: Normal conversion of red bone marrow to yellow bone marrow through childhood and adolescence. Shown from left to right are MRI images of the femur taken at 3 months, 10 months, 4 years, 8 years, and 16 years of age. (Adapted from Guillerman, 2013)

Juvenile Skeleton

The juvenile skeleton differs from the adult skeleton in 3 main ways: 1) it is not fully fused, 2) it has a thick periosteum, and 3) it is porous and flexible (Humphries, 2011). At birth about 460 centers of ossification exist that eventually fuse to form the 206 bones in the adult skeleton, and bones that are not completely done forming are present between birth and adulthood (Humphries, 2011). The embryonic skeleton is composed of woven bone, a flexible but weak matrix of disorganized collagen fibrils and mineralization, which is replaced with organized lamellar bone before adulthood (Buck & Dumanian, 2012). The periosteum is thicker in young bones because it is involved in growth and repair (Humphries, 2011) and contains osteoprogenitor cells before skeletal maturity (Buck & Dumanian, 2012). Young bone is more porous because it contains more Haversian canals and collagen than adult bones, resulting in greater flexibility, elasticity, and strength (Humphries, 2011).

Long bones form from a cartilage template in a process called endochondral ossification (Figure 5) (Buck & Dumanian, 2012; Humphries, 2011) . They mineralize from the center of the diaphysis toward the ends, forming a hollow bone marrow cavity and eventually lengthening from the epiphyseal growth plate (Humphries, 2011). Porosity may be observable before the completion of mineralization. Bone cells are responsible for modeling bone first in the juvenile skeleton, and remodeling throughout life.

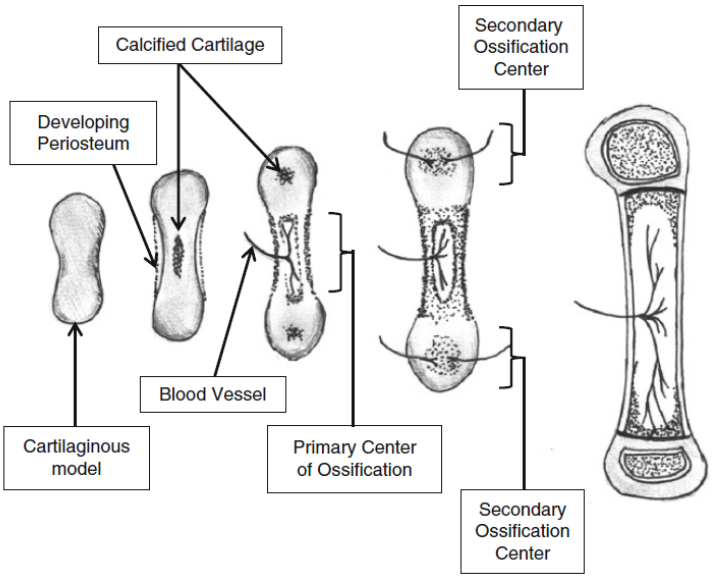

Figure 5: Endochondral ossification. Long bones are formed from a cartilage template that mineralizes and lengthens from the center of the diaphysis toward the epiphysis. (Drawing by Humphries, 2011)

Bone Cells

Bone is made up of three main types of cells. Osteocytes reside within the bone structure itself and monitor internal health. Osteoblasts are bone forming cells, and osteoclasts resorb bone. Osteoblasts and osteoclasts are key components in bone remodeling.

Osteoblasts

Osteoblasts form bone by secreting bone matrix protein and mineralizing bone (Bellido et al., 2014; Hadjidakis & Androulakis, 2006). They are cuboidal cells with large nuclei, enlarged Golgi apparatus, many mitochondria and free ribosomes, and extensive granular endoplasmic reticulum (Aarden et al., 1994; Bellido et al., 2014; Triffitt & Oreffo, 1998) (Figure 6). Osteoblasts secrete high levels of protein including osteocalcin and alkaline phosphatase (ALP), whose blood concentrations reflect the rate of bone formation (Bellido et al., 2014; Buck & Dumanian, 2012). They rapidly produce type I collagen and other matrix

proteins to form osteoid during bone formation (Bellido et al., 2014; Hadjidakis & Androulakis, 2006).

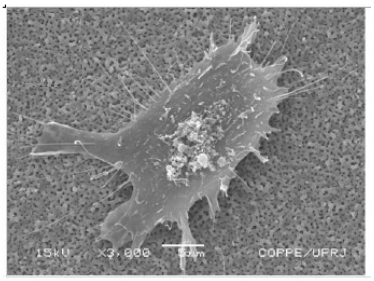

Figure 6: Scanning electron micrograph of an osteoblast cultured on a titanium film. (From http://www.scielo.br/img/revistas/rmat/v12n1/a18fig03.jpg)

Osteoblasts are derived from mesenchymal progenitor cells (Bellido et al., 2014; Buck & Dumanian, 2012; Marie, 1998), proliferate into preosteoblasts, and differentiate into osteoblasts (Figure 7). Preosteoblastic cells adhere to the bone matrix through focal adhesion points (Marie, 1998). At the early stage of osteoblast differentiation, alkaline phosphatase is expressed (Marie, 1998; Triffitt & Oreffo, 1998). Type I collagen is expressed before the extracellular matrix is secreted (Marie, 1998). At the late stage of osteoblast differentiation and the onset of calcification, osteocalcin, osteonectin, osteopontin, bone sialoprotein and other products are expressed (Marie, 1998; Triffitt & Oreffo, 1998). After matrix synthesis is complete, osteoblasts may flatten and cover the inactive bone surface to become lining cells, become embedded in the bone matrix to become osteocytes, or undergo apoptosis (Bellido et al., 2014; Triffitt & Oreffo, 1998).

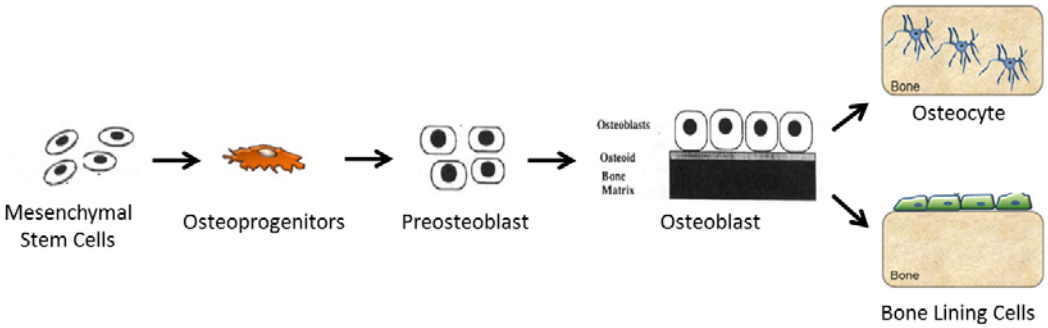

Figure 7: Stages of the osteoblast lifecycle. Osteoblasts are formed from osteoprogenitor cells that derive from mesenchymal stem cells. Once the osteoid has been laid, osteoblasts either become lining cells, osteocytes, or undergo apoptosis. (Figure adapted from Marie, 1998; Triffitt & Oreffo, 1998, and bioscience.org)

Osteoblast proliferation, differentiation, and activities are regulated by a number of pathways and proteins. Wnt signaling pathways influence mesenchymal stem cells to follow osteoblastic pathways, stimulate differentiation of preosteoblasts, and inhibit osteoblastic apoptosis (Bellido et al., 2014). The helix-loop-helix family of transcription factors proliferate osteoblast progenitors (Bellido et al., 2014) and may increase osteoblast differentiation (Marie, 1998), and AP-1 family of transcription factors are expressed during proliferation (Bellido et al., 2014). Bone morphogenetic protein (BMP) signaling pathways control osteoblast differentiation (BMP-2, -3, and -7), promote bone matrix protein synthesis, and induce apoptosis at the end of the lifecycle (Bellido et al., 2014; Marie, 1998). Osteoblasts can stimulate bone matrix protein synthesis and the proliferation of osteoblast precursor cells by producing fibroblast growth factor (FGF), insulin-like growth factor (IGF), and transforming growth factor beta (TGF-β) (Marie, 1998). TGF-β also inhibits bone formation by inhibiting genes that express type I collagen, osteopontin, osteocalcin, and alkaline phosphatase (Triffitt & Oreffo, 1998). Prostaglandins stimulate bone formation by promoting cell proliferation and collagen and non-collagen protein synthesis (Triffitt & Oreffo, 1998). IGF-1 stimulates osteoblast proliferation and bone collagen synthesis (Triffitt

& Oreffo, 1998). Runt-related transcription factor 2 (RUNX2) and osterix promote mineralization. Osteoblasts can also produce receptor activator of nuclear factor kappa-B ligand (RANKL), interleukin 1 (IL-1), tumor necrosis factor alpha (TNF-α), IL-6, and macrophage colony stimulating factor (M-CSF), which may increase osteoclastogenesis and bone resorption (Bellido et al., 2014; Despars & St-Pierre, 2011; Marie, 1998). RANKL expression is upregulated by IL-1, IL-6, parathyroid hormone (PTH), and vitamin D (Bellido et al., 2014). IL-1 is a major stimulator of bone resorption (Triffitt & Oreffo, 1998). Osteoblasts are also influenced by Wnt pathways to secrete osteoprotegerin (OPG), a protein in the TNF receptor family that inhibits osteoclastogenesis by binding to RANKL (Bellido et al., 2014).

Osteocytes

Up to 20% of osteoblasts are embedded in bone, flatten, and develop dendrites to become osteocytes (Aarden et al., 1994; Bellido et al., 2014; Bonewald, 2011; Hadjidakis & Androulakis, 2006). Osteocytes signal osteoblasts and osteoclasts to remodel the matrix in response to mechanical and hormonal influences such as microcracks and mechanical loading (Aarden et al., 1994; Bellido et al., 2014). The cell bodies reside in lacunae and monitor bone through their dendrites, which lie in canaliculi (Aarden et al., 1994; Bellido et al., 2014) (Figure 8). Dendrites of neighboring osteocytes are in contact with each other, and this network allows signaling communication and protein exchange throughout the network (Bellido et al., 2014). Compared to osteoblasts, osteocytes have up to 70% less volume and a greatly reduced number of organelles (Aarden et al., 1994). Osteocytes also express more proteins related to mineralization and phosphate metabolism than osteoblasts (Bellido et al., 2014) such as osteocalcin, but less alkaline phosphatase (Aarden et al., 1994).

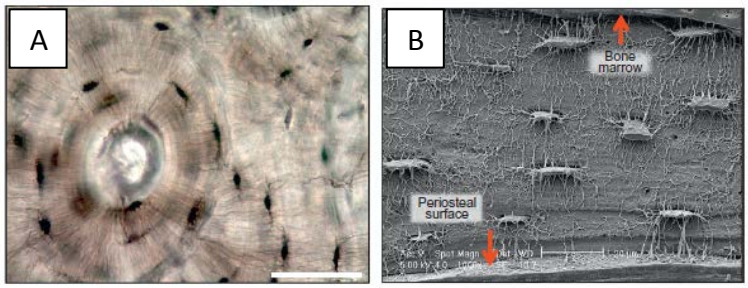

Figure 8: Osteocyte morphology. A) Depiction of osteocytes in an osteon, lacunae and fine canaliculi organized perpendicular to a Haversian canal. B) Osteocytes form a network among each other, bone marrow, and other bone surfaces through connecting dendrites. (Adapted from Bellido et al., 2014)

The osteocyte lifecycle has four stages: formative, steady-state, resorptive, and degenerative (Aarden et al., 1994) (Figure 9). Osteocytes are derived from osteoblasts, and in the formative phase the osteoblast commits to the osteocyte lineage and becomes embedded in the secreted osteoblastic matrix (Aarden et al., 1994). Next comes the steady-state phase devoid of most metabolic activity (Aarden et al., 1994), followed by maturation and the resorptive phase in which the osteocyte may be capable of bone resorption (Aarden et al., 1994; Bonewald, 2011). Indeed, osteocytes are capable of remodeling their perilacunar matrix (Bonewald, 2011). The degenerative phase in which the osteocyte deteriorates precedes cell death (Aarden et al., 1994).

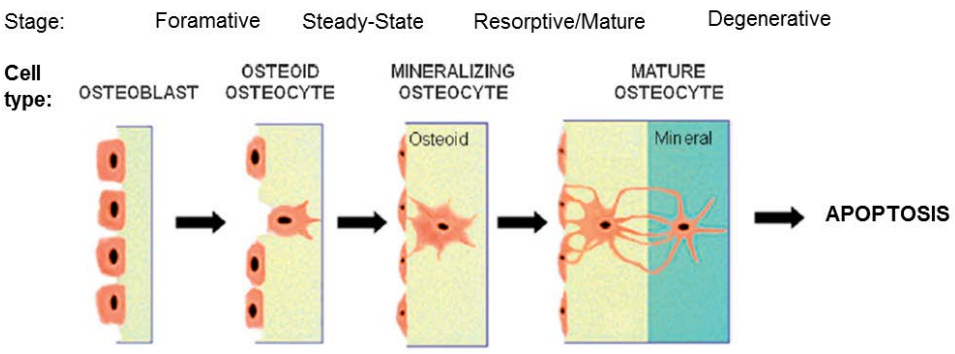

Figure 9: Osteocyte stages and life cycle. Osteocytes are derived from osteoblasts that have been embedded in the forming bone matrix. They monitor the bone matrix and signal remodeling in response to mechanical and hormonal stimuli. (Figure adapted from Bonewald, 2011)

Osteocytes secrete M-CSF and RANKL, which are proteins that promote osteoclastogenesis and osteoclast survival (Bellido et al., 2014). M-CSF causes osteoclast differentiation by binding to its receptor on osteoclast precursor cells (Bellido et al., 2014). RANKL binds directly to its receptor on osteoclasts to stimulate activity (Bellido et al., 2014). It promotes precursor fusion, attachment to bone surfaces, and stimulation of resorption (Bellido et al., 2014). Osteocytes also secrete OPG, a protein in the TNF receptor family that inhibits osteoclastogenesis (Bellido et al., 2014). OPG binds to RANKL, inhibiting RANKL from binding to and activating osteoclasts. These together help to regulate the remodeling cycle to resorb and build bone as needed. RANKL and OPG are mainly produced by osteocytes (Plotkin & Bivi, 2014), making osteocytes the main regulators of bone remodeling activity. Osteocytes also produce sclerostin, which stimulates bone loss by antagonizing BMP signaling pathways and preventing Wnt signaling, which promote and regulate osteoblast activity (Bellido et al., 2014).

Osteoclasts

Osteoclasts are multinucleated cells that resorb bone (Figure 10), although they can only resorb mineralized bone (Buck & Dumanian, 2012). They have several Golgi complexes, transport vesicles, and mitochondria and lysosomal enzymes for resorbing and processing bone (Hadjidakis & Androulakis, 2006). The sealing zone (SZ) is the circumferential region of bone-cell interface composed of podosomes, which are filamentous actin structures of F-actin, alpha-actin, vinculin and talin proteins (Teitelbaum, 2000) that allow osteoclasts to adhere to bone (Bellido et al., 2014; Boyle et al., 2003; Teitelbaum, 2000). Once attached, the cell polarizes and creates a ruffled border (RB) (Hadjidakis & Androulakis, 2006; Teitelbaum, 2000), which resorbs bone through the use of an H^+-adenosine triphosphate (H^+-ATPase) mediator and a process similar to exocytosis (Teitelbaum, 2000). The RB secretes hydrolytic enzymes (Bellido et al., 2014) such as hydrogen ions, TRAP, and pro-cathepsin K (pro-CATK) (Boyle et al., 2003; Hadjidakis & Androulakis, 2006) to acidify and dissolve bone (Bellido et al., 2014; Hadjidakis & Androulakis, 2006). Degraded products include collagen fragments, calcium, and phosphate, which are processed by the osteoclast and discharged into circulation (Boyle et al., 2003). This resorption of bone results in the creation of a resorptive pit called Howship's lacunae (Bellido et al., 2014).

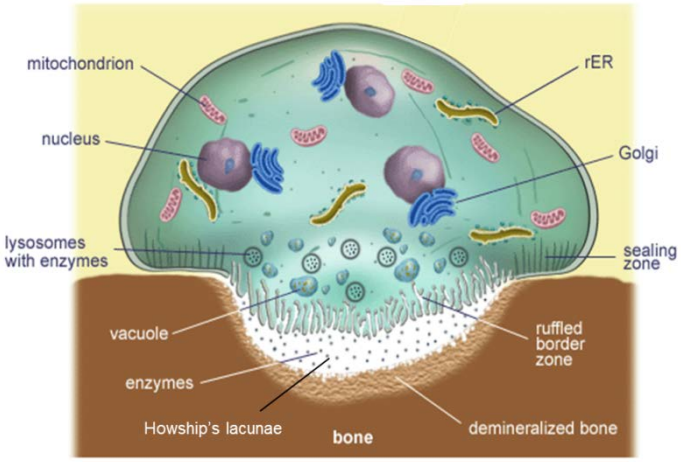

Figure 10: Osteoclast morphology. Note especially the multiple nuclei, sealing zone, ruffled boarder, and Howship's lacuna. (Adapted from oerafrica.org)

Osteoclasts are derived from the hematopoietic monocyte/macrophage line (Bellido et al., 2014; Boyle et al., 2003; Buck & Dumanian, 2012; Teitelbaum, 2000) (Figure 11). M-CSF causes monocytes to develop into preosteoclasts (Teitelbaum, 2000). These preosteoclasts cluster and fuse together under the influence of M-CSF and RANKL, which are secreted by osteoblasts and osteocytes (Bellido et al., 2014; Boyle et al., 2003). The protein beta-catenin is also known to directly control osteoclastogenesis and bone resorption (Bellido et al., 2014). Osteoclasts then resorb bone and may detach and move to a new site of bone degradation (Teitelbaum, 2000), or undergo apoptosis (Bellido et al., 2014).

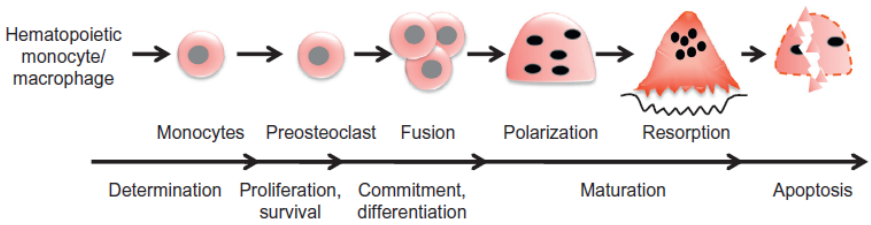

Figure 11: Osteoclast lifecycle and derivation. Osteoclasts are derived from hematopoietic stem cells that commit to the osteoclastic lineage. They fuse to form multinucleated osteoclasts that resorb bone. (From Bellido et al., 2014)

OPG, receptor activator of nuclear factor kappa-B (RANK), RANKL together are known to regulate osteoclast function (Boyle et al., 2003). RANK is a member of the TNF receptor superfamily (Teitelbaum, 2000) and is required for osteoclast differentiation, activation, and bone resorption (Boyle et al., 2003). RANKL is a polypeptide member of the TNF superfamily that binds to and activates RANK on osteoclasts (Boyle et al., 2003; Teitelbaum, 2000), and can prolong survival of mature osteoclasts (Boyle et al., 2003). RANKL is also expressed by T-lymphocytes (Teitelbaum, 2000). OPG is produced by osteoblasts and binds to RANKL to inhibit osteoclastogenesis (Bellido et al., 2014; Boyle et al., 2003; Teitelbaum, 2000). Calcitonin is also known to be active in osteoclast regulation (Buck & Dumanian, 2012), and IL-6, IL-1β, and TNF-α are known pro-resorption cytokines (Despars & St-Pierre, 2011).

Together, osteoblasts, osteoclasts, and osteocytes are responsible for one remodeling.

Bone Remodeling

Bone remodeling is a term defined by Harold Frost in 1990 (Frost, 1990) to identify the process by which bone is restored or renewed in response to loading, microdamage, cell death, or blood mineral homeostasis (Allen & Burr, 2014; Hadjidakis & Androulakis, 2006). It is characterized by a coupled response of bone resorption and bone formation on an existing bone surface mediated by cell signaling within the bone multicellular unit (BMU) of osteoblasts, osteoclasts, and associated blood vessels (Allen & Burr, 2014).

Bone Remodeling Process

The remodeling cycle consists of five stages: activation, resorption, reversal, formation, and quiescence (Allen & Burr, 2014; Hadjidakis & Androulakis, 2006) (Figure 12).

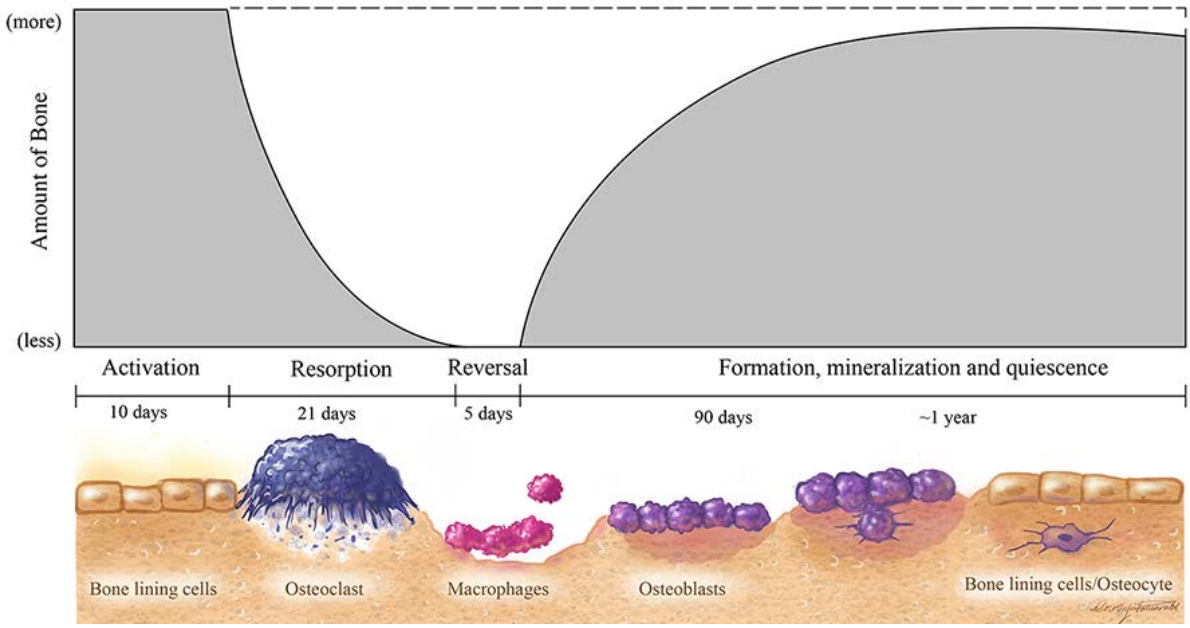

Figure 12: Bone remodeling process. Mechanical or molecular stimuli initiate the activation phase, which results in the resorption of bone by osteoclasts. After resorption, the reverse occurs and osteoblasts lay down new osteoid that will later mineralize to become bone. When mineralization is complete, bone lining cells monitor the remodeled resting bone. (Adapted from Allen & Burr, 2014. Image by Dorothy Fatumnbi)

The bone remodeling process begins with activation. In most cases, bone remodeling is triggered by osteocyte signaling prior to apoptosis (Allen & Burr, 2014). When an osteocyte is cut off from the network due to microdamage, or the osteocyte network is otherwise disrupted, the affected cells undergo apoptosis (Allen & Burr, 2014). Prior to death, they produce RANKL and other factors that signal osteoclast development (Allen & Burr, 2014). Preosteoclasts migrate to the remodeling cite (Hadjidakis & Androulakis, 2006).

Unaffected osteocytes produce antiapoptotic signals, such as OPG, to prevent their resorption and constrain remodeling to affected regions (Allen & Burr, 2014).

Bone resorption begins after activation. Mature osteoclasts form and signal bone lining cells to retract from the surface, forming a bone remodeling compartment (BRC) within which bone remodeling takes place (Figure 13) (Allen & Burr, 2014). Podosomes in the SZ allow osteoclasts to adhere to the exposed surface of bone. Osteoclasts then acidify the enveloped region by producing protons from carbonic anhydrase and secreting them through the RB, and internalize the degraded bone. This results in a resorption lacuna (Figure 10) (Bellido et al., 2014).

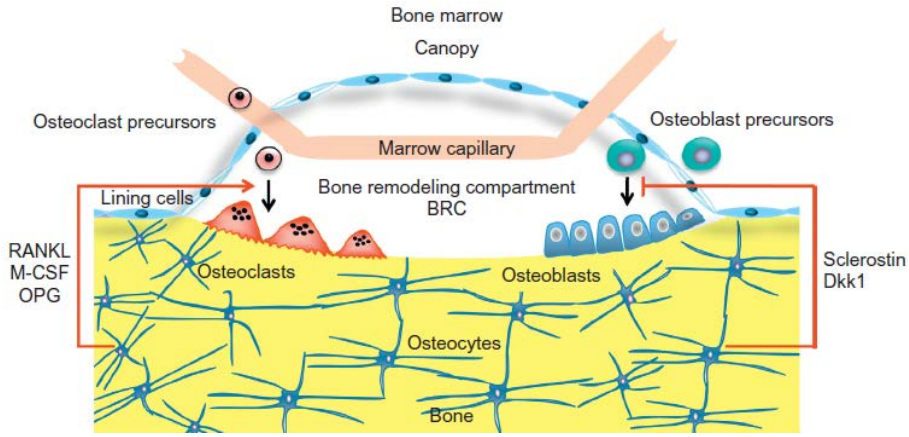

Figure 13: Bone remodeling compartment. Lining cells retract at the onset of the bone remodeling process to create an enclosed space in which bone remodeling takes place. Note osteoblasts and osteoclasts, and their precursor cells, at work in the BRC. (From Bellido et al., 2014)

During the reversal phase, osteoclast activity ends and bone formation begins (Allen & Burr, 2014). Macrophages prepare the bone surface for bone formation and signal osteoblast differentiation and migration to the remodeling site (Hadjidakis & Androulakis,

2006). Any remaining collagen fragments are removed, and the cement line matrix is laid down (Allen & Burr, 2014).

When reversal is complete, bone formation may be triggered by osteoblastic chemoattractants or growth factors, such as TGF-β, which is released during bone resorption and stimulates bone formation (Marie, 1998). Osteoblasts then secrete the organic phase of bone, namely type 1 collagen and other matrix proteins, to form osteoid and serve as a template for mineral hydroxyapatite deposition (Allen & Burr, 2014; Bellido et al., 2014; Hadjidakis & Androulakis, 2006). Mineralization occurs, and soluble calcium and phosphate in the organic matrix become solid calcium phosphate crystals (Buck & Dumanian, 2012). Osteoblasts then either die by apoptosis or become osteocytes or lining cells (Allen & Burr, 2014).

Mineral deposition occurs in two phases (Figure 14). During the initial phase, primary mineralization causes a rapid increase in the number of calcium and phosphate ions in the collagen framework and reaches up to 70% of the maximum limit within about three-weeks. The secondary phase then begins at a much slower rate to accumulate the remaining 30% mineral saturation limit over the next months or years (Allen & Burr, 2014; Burr & Akkus, 2014).

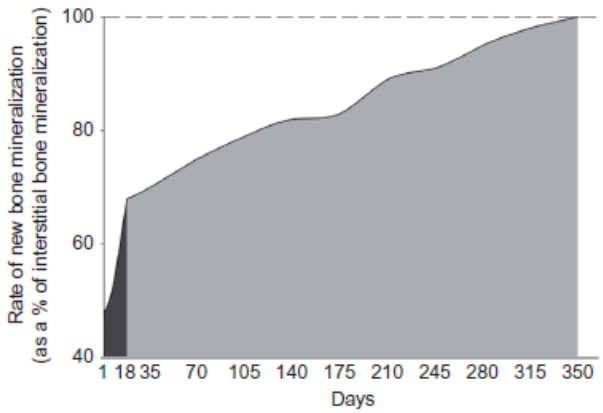

Figure 14: Mineral deposition during bone remodeling. Primary mineralization saturates bone up to 70% of its limit within 3 weeks. Secondary mineralization accumulates the remaining 30% over the next months or years (Burr & Akkus, 2014).

At the end of the remodeling cycle is the quiescence phase in which bone rests as it accumulates mineral (Allen & Burr, 2014).

Molecular Markers

The following table summarizes molecular markers of bone formation and resorption that can be detected in blood serum or urine (Allen & Burr, 2014). Key molecules are highlighted in more detail following the table.

Table 1: Bone formation and resorption markers that can be detected in urine or blood serum. *Osteocalcin is produced primarily by osteoblasts but also by osteoclasts to a much lesser extent. (Adapted from Allen & Burr, 2014 and Christenson, 1997)

Molecule	Abbreviation	Matrix	Source
Formation			
Osteocalcin*	OC	Serum	Allen 2014, Christenson, 1997
Bone-specific alkaline phosphatase	BSAP, BALP	Serum	Allen 2014, Christenson 1997
Procollagen type I N propeptide	PINP	Serum	Allen 2014, Christenson 1997
Procollagen type I C propeptide	PICP	Serum	Christenson 1997
Resorption			
Tartrate-resistant acid phosphatase	TRAP	Serum	Allen 2014, Christenson 1997
Pyrindoline	PYD	Urine	Allen 2014
Deoxypyrindoline	DPD	Urine and serum	Allen 2014, Christenson 1997
Osteoprotegerin	OPG		Plotkin 2014
N-terminal cross-linking telopeptide of type I collagen	NTX-I	Urine and serum	Allen 2014, Christenson 1997
C-terminal cross-linking telopeptide of type I collagen	CTX-I	Urine and serum	Allen 2014, Christenson 1997
Urinary calcium		Urine	Christenson 1997

Bone Formation

Biomarkers of bone formation indicate organic matrix formation in bone and osteoblast activity (Christenson, 1997).

Osteocalcin (OC, or the Gla protein) is the most abundant noncollagenous protein in the bone matrix (Christenson, 1997). It enhances calcium binding and controls mineral deposition and is overexpressed in cancer and some autoimmune diseases (Burr & Akkus, 2014). It is produced by osteoblasts during active matrix secretion, and a small amount is normally released into the circulation (Christenson, 1997). Along with ALP, OC reflects the rate of bone formation (Allen & Burr, 2014; Bellido et al., 2014) when formation and resorption are coupled (Christenson, 1997). However, OC is also released during osteoclastic degradation and indicates turnover when formation and resorption are uncoupled

(Christenson, 1997). Osteocalcin is specifically expressed by osteoblasts late in the differentiation pathway in the presence of mineralized bone matrix (Triffitt & Oreffo, 1998).

Alkaline phosphatase (ALP) is a glycoprotein and potential Ca^{2+} (calcium ion) carrier (Burr & Akkus, 2014). It hydrolyzes pyrophosphate, an inhibitor of calcium phosphate and mineral deposition (Burr & Akkus, 2014; Christenson, 1997). It is produced by osteoblasts during active matrix secretion and may be clipped off the osteoblastic membrane (Christenson, 1997). ALP, along with osteocalcin, also reflects the rate of bone formation (Allen & Burr, 2014; Bellido et al., 2014; Christenson, 1997).

Procollagen I extension peptides are produced by osteoblasts from collagen fragments that are cleaved during collagen synthesis (Allen & Burr, 2014; Christenson, 1997), yielding procollagen I amino terminal propeptide (PINP) and procollagen I carboxyl terminal propeptide (PICP) (Christenson, 1997).

Bone Resorption

Biomarkers of bone resorption indicate a degradation of type I collagen and osteoclast activity (Christenson, 1997).

TRAP is a lysosomal enzyme expressed and secreted by osteoclasts between the sealing zone and bone matrix during bone remodeling (Bellido et al., 2014; Christenson, 1997). It may be involved in dephosphorylizing bone sialoprotein and osteopontin, which are used in generating reactive oxygen species used in matrix degradation (Bellido et al., 2014). Bone acid phosphatase can be inhibited by L (+) tartrate, so most analyzed specimens are treated with (+) tartrate to make them tartrate resistant (hence, TRAP) (Christenson, 1997).

OPG is a receptor protein secreted by stromal cells, osteoblasts, and osteocytes (Plotkin & Bivi, 2014). It has an N-terminal similar to RANK, allowing it to act as a decoy

for RANKL, which decreases osteoclastogenesis (Plotkin & Bivi, 2014). OPG can be used to gauge bone resorption (Plotkin & Bivi, 2014).

Collagen fragments, including N-terminal and C-terminal crosslinking telopeptides of type I collagen (NTX-I and CTX-I, respectively), are released from the bone matrix during resorption and can be detected in urine and serum (Allen & Burr, 2014; Christenson, 1997). The formation of these fragments is specific to bone due to osteoclastic metabolization of type I collagen in bone that does not occur in other tissues (Christenson, 1997). Crosslinks such as pyridinoline and deoxypridinoline are also released from the matrix during resorption (Allen & Burr, 2014; Christenson, 1997).

Hematopoiesis

Hematopoiesis is the process by which blood cells are formed, and it occurs throughout life. After birth, blood cells are made in the red marrow where pluripotent hematopoietic stem cells (HSCs) produce all types of blood cells from common myeloid progenitor cells (CMPs) and common lymphoid progenitor cells (CLPs) (Jagannathan-Bogdan & Zon, 2013; Murre, 2009; Orkin & Zon, 2008) (Figure 15) to osteoclasts (Despars & St-Pierre, 2011). HSCs are pluripotent but also have the ability to self-renew if they do not differentiate (Murre, 2009). CMPs give rise to granulocyte/macrophage progenitor cells (GMPs) and megakaryocyte/erythroid progenitor cells (MEPs) (Murre, 2009; Orkin & Zon, 2008). GMPs produce mast cells, eosinophils, neutrophils, and macrophages (Orkin & Zon, 2008). CLPs differentiate into T-cells, B-cells, or natural killer (NK) cells (Murre, 2009). B-lymphocytes, which produce antibodies, and T-lymphocytes, which either stimulate the immune system or destroy cells, compose the adaptive immune system (Staal et al., 2011). NK cells inject toxic proteins into pathogens to destroy them (Staal et al., 2011).

Granulocytes and macrophages are part of the innate immune system and engulf and digest pathogens (Staal et al., 2011).

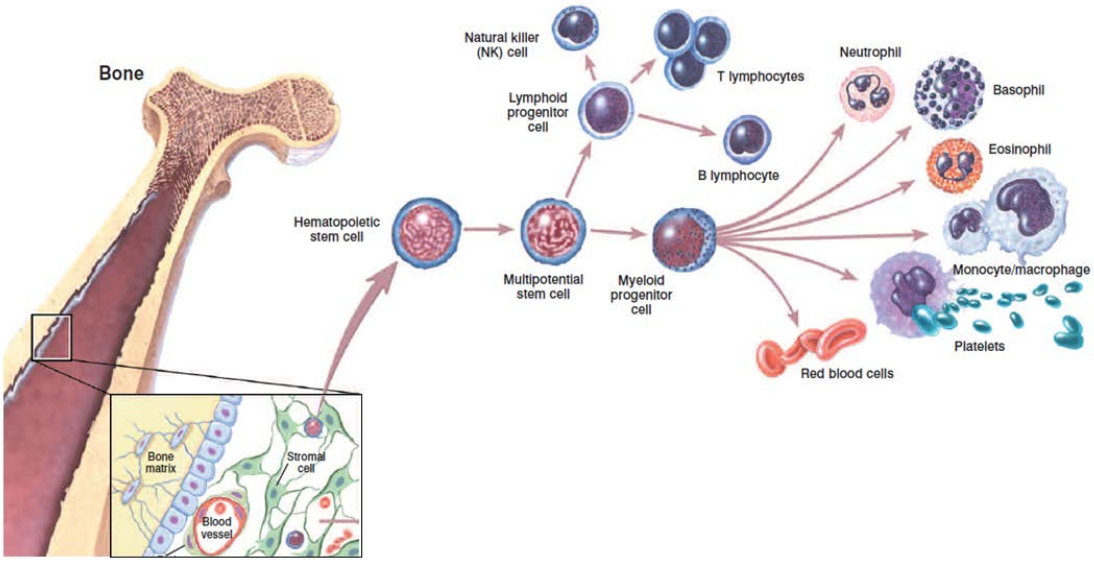

Figure 15: Blood cell generation. All blood cells derive from hematopoietic stem cells, which can differentiate into lymphoid cells (natural killer cells, B-cells, T-cells) or myeloid cells (macrophages, basophils, eosinophils, neutrophils, platelets, and red blood cells). (Adapted from Domen et al., 2011, image by Terese Winslow 2001)

HSCs are located in the bone marrow cavity, with hematopoietic reconstitutive HSCs near the endosteum and long-term reconstitutive HSCs in hypoxic marrow regions (Despars & St-Pierre, 2011). Mesenchymal stem cells (MSCs) that produce osteoblasts, chondrocytes, and other skeletal cells are located in oxygen-rich areas of the bone marrow (Despars & St-Pierre, 2011).

Many proteins affect hematopoiesis and influence terminal differentiation. RUNX1 is important for the definitive production of erythroid, myeloid, and lymphoid cells (Jagannathan-Bogdan & Zon, 2013; Murre, 2009). The Notch signaling pathway promotes HSC expansion and self-renewal upon activation (Jagannathan-Bogdan & Zon, 2013). Myeloid cell lines are promoted by high levels of transcription factor PU.1 and

CCAAT/enhancer binding protein alpha (C/EBPα), while lymphoid cell lines are promoted by the combination of PU.1, Ikaros, and transcription factor E2A (Murre, 2009). B-cells are promoted by early B-cell factor (EBF) and paired box protein Pax5, which suppress the T-cell lineage, and E2A (Murre, 2009). T-cells are promoted and matured by E2A and Notch signaling proteins, as well as the transcription factor GATA-3, zinc finger protein Gfi-1, DNA-binding transcription factor TCF1, and Ikaros (Murre, 2009). Kit ligand from stromal cells is also required for stem cell homeostasis (Jagannathan-Bogdan & Zon, 2013).

Cell signaling from osteoblasts and osteoclasts may also influence hematopoiesis. Wnt signaling and BMPs may be important in hematopoiesis, and osteoblasts may interact with HSCs in the bone marrow (Jagannathan-Bogdan & Zon, 2013). Increased osteoblast activity increases the HSC population in the bone marrow, while decreased osteoblast numbers and bone loss cause HSCs to relocate outside of the bone marrow (Despars & St-Pierre, 2011). Adhesion molecules and matrix protein secretion by osteoblasts can regulate HSC function through cell-to-cell interactions (Despars & St-Pierre, 2011). Osteoclast precursors and mature osteoclasts contribute to the retention of HSCs in the marrow (Despars & St-Pierre, 2011). RANKL activates osteoclasts and results in hematopoietic progenitor cell migration to the blood, while calcitonin inhibits osteoclast function and reverses this mobilization (Despars & St-Pierre, 2011).

Summary

Bone provides structural support for the body and adapts to external conditions to provide adequate strength for daily tasks. The cortical shell and inner network of trabeculae provide resistance to bending and add strength with minimal weight respectively, while the mineral composition of both components provides stiffness and organic collagen provides

ductility. Bone modeling occurs in the immature skeleton, and remodeling occurs throughout life as a result of bone cell activity and interactions, and bone cell activity can be observed through urinary or blood serum biomarkers produced by osteoblasts and osteoclasts. Bone is also the site of hematopoiesis, and is thus the location of stem cell differentiation into immune cells and osteoclasts. Skeletal growth and remodeling in young subjects as well as bone cell activities and hematopoietic responsibilities are important factors to keep in mind when analyzing the response of bone to radiation therapy for ALL, as they characterize the condition studied in this work.

CHAPTER 3: OSTEOPOROSIS

Introduction

Osteoporosis is a condition of low bone density and microarchitectural deficits that greatly increases fracture risk (Damilakis et al., 2010; Sebestyen et al., 2012; Shuler et al., 2012; Weilbaecher, 2000). It can be caused by hormonal imbalances, diseases, treatments, lifestyle choices, or a combination of them (Green & Rubin, 2014). No cure currently exists, making prevention the best treatment option. In ALL patients, premature osteoporosis and low bone density are largely a result of disease treatment, particularly radiation, chemotherapy, and disuse from bed rest (Green & Rubin, 2014; Schimmer et al., 2000; Weilbaecher, 2000). Radiation is believed to be the main source of acute bone loss (Weilbaecher, 2000). In this section we will explore the normal pathology of osteoporosis and focus on radiation-specific mechanisms. We will also present standard treatments and treatment regimens accepted for pediatrics.

Defining Osteoporosis

The World Health Organization (WHO) defines osteoporosis as a disease in which decreased bone mass and microarchitectural deterioration of bone tissue leads to increased bone fragility and fracture risk (Damilakis et al., 2010; Sebestyen et al., 2012; Shuler et al., 2012; Weilbaecher, 2000). Osteoporosis is the most common bone disease, and is detectable, preventable, and treatable (Shuler et al., 2012). Fracture is the largest threat to patients, with about 1.5 million osteoporosis-related fractures occurring each year in the United States

alone (Shuler et al., 2012) and over 70 million people worldwide at risk (Boyle et al., 2003). Osteoporosis is considered a silent disease because it is often detected only after a low-energy fracture (Shuler et al., 2012), and patients are susceptible to spontaneous bone fractures (Teitelbaum, 2000).

Osteoporosis and osteopenia, a pre-osteoporotic condition, result from an uncoupling of bone formation and resorption, with the resorption rate greater than formation (Shuler et al., 2012; Weilbaecher, 2000), and can result from reduced bone formation or accelerated bone resorption (von Scheven, 2007). Trabecular plates of bone are lost with increased bone resorption, resulting in reduced bone strength, mass, and density (Shuler et al., 2012). Trabecular thinning occurs over time until the struts become so thin that the remodeling unit causes a disconnection (Allen & Burr, 2014). Trabecular struts cannot be reconnected once disconnected, as this would require de novo formation to create woven bone bridges (Allen & Burr, 2014). Therefore, high rates of bone remodeling are a greater risk factor for fracture than low rates of bone remodeling (Allen & Burr, 2014), and osteoporotic bones are more fragile than non-osteoporotic bones (Shuler et al., 2012). Fractures occur most commonly in patients with osteopenia (Shuler et al., 2012) and areas rich in trabecular bone, such as the vertebrae, wrist, and hip (Damilakis et al., 2010) (Figure 16).

Figure 16: Normal and osteoporotic vertebrae. Osteoporotic bone has a thinner cortical shell and thinner or fewer trabeculae than healthy bone. (Image from http://www.ottawaosteopath.com/images/stories/osteoporosis_ottawa.jpg)

Maximizing peak bone mass is critical to minimizing fracture risk later in life, and low childhood growth rate (height and weight) can be a significant predictor of hip fracture later in life (Khosla, 2013). Peak bone density is reached around 20-25 years of age, and the overall outcome of osteoporosis depends on this peak bone mass and the rate of bone loss (Haddy et al., 2001; Khosla, 2013; Mandel et al., 2004; Putman & Gordon, 2014). During puberty, total bone strength increases linearly, and 25-50% of peak adult bone mass can be achieved (Khosla, 2013). Bone formation-inhibiting sclerostin decreases at the onset of puberty, and cortical thickness increases at the end of puberty (Khosla, 2013).

Osteoporosis is now defined and detected using T-scores and the WHO Fracture Risk Assessment Tool (FRAX) (Shuler et al., 2012). The FRAX is a tool that identifies patients at the greatest absolute fracture risk for the next decade based on country, BMD, age, gender, body mass index (BMI), previous personal and family fracture history, smoking status, glucocorticoid use, alcohol consumption, and presence of rheumatoid arthritis in addition to T-score (Shuler et al., 2012). T-scores are generated based on the standard deviation of a patient's bone mineral density from a young reference population near peak bone mass, and relative fracture risk doubles for every standard deviation below peak bone mass (Haddy et al., 2001; Schimmer et al., 2000). According to the WHO, a patient has osteoporosis if his or her bone mineral density is 2.5 standard deviations or greater below the mean of a young reference population (Damilakis et al., 2010; Haddy et al., 2001; Schimmer et al., 2000; Shuler et al., 2012) and osteopenia between 1 and 2.5 standard deviations below the young adult mean (Haddy et al., 2001; Schimmer et al., 2000; Shuler et al., 2012). The overriding advantage of the FRAX is that it can predict fracture risk and identify patients in need of treatment before fracture without BMD testing (Shuler et al., 2012). Limitations are that it is

only valid between the ages of 40 and 90, not applicable to pharmacologically managed patients, does not account for fracture-related risk factors such as falls and biochemical markers, and does not account for dose response effects (Shuler et al., 2012).

Detecting Bone Loss

Bone density and other parameters can be assessed through several X-ray and non-X-ray imaging and bone turnover detection techniques. The most commonly used technique DXA, which produces T-scores used to determine osteoporotic status (Shuler et al., 2012). A low energy x- ay scans the site of interest, usually the proximal femur or lumbar spine, and calculates bone density based on the amount of X-ray transmission through the tissue (Schimmer et al., 2000). Areal bone mineral density can be obtained in a short time while maintaining image quality using fan-beam DXA (Damilakis et al., 2010), but it cannot separately analyze trabecular and cortical bone (Khosla, 2013). DXA has an effective dose of less than 0.01 mSv for a peripheral scan, 0.0052 mSv for a 5-year-old child whole body scan, and 0.0042 mSv for an adult whole body scan (Damilakis et al., 2010).

Other X-ray methods for skeletal quantitative assessment include quantitative computed tomography (QCT), multi-detector CT (MDCT), peripheral QCT (pQCT), high resolution CT (HRCT), radiographs, and single energy absorptiometry (Damilakis et al., 2010; Shuler et al., 2012). QCT has high spatial resolution, can detect structural abnormalities, and can characterize bone density but uses larger amounts of radiation than DXA (Khosla, 2013; Shuler et al., 2012). It can be performed in 2D or 3D at central or peripheral sites and gives an effective dose of up to 0.3 mSv (Damilakis et al., 2010). MDCT cannot depict individual trabeculae and so is not used for vertebral fracture detection but can accurately assess microarchitectural patterns (Damilakis et al., 2010). pQCT is associated

with a low radiation dose (less than 0.01 mSv) and can assess bone morphology *in vivo* and obtain trabecular number, thickness and separation, and cortical porosity and thickness (Damilakis et al., 2010). HRCT can image the texture of trabecular bone but provides a much higher dose of radiation than a typical X ray at about 3 mSv (Damilakis et al., 2010). Spinal radiographs are commonly used for vertebral fracture identification due to lower radiation doses than CT scans, good tissue contrast, and ability to characterize bone density but cannot assess 3D architecture and can have a false negative rate of up to 45% (Damilakis et al., 2010; Shuler et al., 2012).

Non X-ray imaging techniques include ultrasound and magnetic resonance imaging (MRI). Ultrasound can characterize bone density but does not produce a T-score value (Shuler et al., 2012). Quantitative ultrasound is smaller, cheaper, and more mobile than DXA while maintaining similar fracture risk assessment abilities but is difficult to maintain calibration and quality control (Shuler et al., 2012). MRI can be used to characterize bone density and analyze 3D trabecular structures without the radiation exposure of QCT and may be developed to wider use in the future (Shuler et al., 2012). DXA, QCT, pQCT, and ultrasound can be used to measure bone density in pediatric patients, although clinically, DXA is used the most (Sebestyen et al., 2012; von Scheven, 2007).

Bone turnover can be assessed using histomorphometry and immunoassays in adults (Christenson, 1997). Decreases in bone mass are associated with increases in biochemical markers of bone resorption (Khosla, 2013). Assays to monitor NTX, CTX, pyridinoline and deoxypyridinoline, and urinary calcium concentrations can be used to monitor bone resorption and loss (Christenson, 1997). Serum levels of bone specific alkaline phosphatase, which is produced by osteoblasts, are used clinically as an indication of bone metabolism

(Christenson, 1997). Serum and urinary biomarkers can also be used to measure bone turnover, including hydroxyproline, osteocalcin, calcium, alkaline phosphatase, and thyroid-stimulating hormone (Christenson, 1997; Schimmer et al., 2000).

Age Related Bone Loss

Bone mass is stabilized by fairly equal amounts of formation and resorption until age 35-40 (Mandel et al., 2004). After about age 40, bone resorption exceeds formation, and bone mass begins to decline (Mandel et al., 2004). About 40% of lifetime expected trabecular bone loss occurs by age 50 (Khosla, 2013). Decreases in trabecular bone and volumetric bone mineral density (vBMD) can occur as early as the 20s, with increased rate of loss during menopause for women (Khosla, 2013). Cortical vBMD is stable until it begins decreasing in mid-life for women and in the early 70s for men (Khosla, 2013). Women experience bone loss through decreases in trabecular number and increases in trabecular separation (Khosla, 2013). Men experience bone loss largely through a reduction in trabecular thickness (Khosla, 2013).

Fracture risk associated with BMD varies with age (Shuler et al., 2012). Older individuals have more apoptotic cells, shorter telomere lengths, increases in oxidative stress, and greater inflammatory microenvironments compared to younger subjects (Khosla, 2013). Human mesenchymal stem cells, which differentiate into osteoblasts, take 1.7 times longer to double in older subjects than young subjects (Khosla, 2013). Sclerostin levels are also known to increase with age (Khosla, 2013).

A rapid phase of estrogen-dependent bone loss occurs in women at menopause and lasts 5-10 years (Haddy et al., 2001). BMD decreases by about 5% within the first 2 years of menopause (Schimmer et al., 2000). This can be prevented by hormone replacement therapy

within the first 3 years of the onset of menopause, although it may increase the risk of breast cancer (Schimmer et al., 2000). In men, both estrogen and testosterone maintain bone formation, but estrogen protects against bone resorption much more than testosterone (Khosla, 2013). Total testosterone and estrogen levels decline with aging due to increased hormone binding globulin levels (Khosla, 2013).

Osteoporosis in women is related to estrogen deficiency (Khosla, 2013). Bone resorption increases and bone formation markers decrease significantly with acute estrogen deprivation (Khosla, 2013). Estrogen and androgens inhibit apoptosis in osteocytes and osteoblasts (Bellido et al., 2014) and suppress osteoclast formation and activity, increase transcription of IGF-1 and TGF-beta which stimulate osteoblast replication and bone matrix synthesis, and repress osteoblast transcription of RANKL, IL-6 and M-CSF which activate osteoclasts (Khosla, 2013; Weilbaecher, 2000). Postmenopausal women have more than 3 times the percentage of bone marrow cells expressing RANKL than premenopausal women (Khosla, 2013). Therefore, after menopause, women have a period of rapid bone loss due to estrogen decreases and increased bone remodeling (Allen & Burr, 2014).

Radiation-Induced Osteoporosis

Ionizing radiation can eject electrons from atoms, breaking molecular bonds and damaging surrounding material or tissue (Willey et al., 2011). Body tissues absorb radiation, and while the dose can be substantial, radiation only impacts bone in the radiation field (Willey et al., 2011). Absorbed dose is measured in gray (Gy), or energy per unit mass (Damilakis et al., 2010; Willey et al., 2011). The effective dose is measured in Sieverts (Sv), and is the absorbed dose multiplied by a weighting factor or relative radiation risk (Damilakis et al., 2010; Willey et al., 2011). The average person receives 2.4 mSv/year from background

radiation (Damilakis et al., 2010), but cancer patients can receive up to 2Gy doses of radiation delivered over several minutes for several days in a row (Willey et al., 2011). Hematopoietic stem cell transplantation (HSCT) patients, who often receive preparative radiation therapy, experience the most bone loss within 6 months of irradiation (Green et al., 2012).

Radiation exposure is followed by an acute increase in bone resorption and subsequent reduced bone formation (Willey et al., 2011). Bone loss occurs in fewer than 10 days following radiation exposure (Green & Rubin, 2014) and can be observed within one week (Willey et al., 2011). TBI decreases growth hormone secretion, which may lead to hypogonadism and increased bone loss from reduced sex hormone production (Weilbaecher, 2000). Radiation also depletes bone marrow, allowing adipocytes to fill in rather than hematopoietic repopulation (Green & Rubin, 2014). Vasculature within bone can be damaged, including the marrow cavity and Haversian systems (Willey et al., 2011). The amount of bone loss sustained depends on the absorbed dose, energy of radiation beam, fraction size, and age and developmental stage of the patient (Willey et al., 2011), but cumulative low doses (fractionation) may prevent bone architecture devastation while still maintaining efficacy for therapeutic applications (Green et al., 2012).

Radiation can induce bone changes in the epiphyseal and metaphyseal regions (Miyazaki et al., 2009; Weilbaecher, 2000), including sclerosis, thinning of bones, loss of trabecular connections, and thickening of trabeculae (Willey et al., 2011). In children, metaphyseal sclerosis and fraying, longitudinal metaphyseal striations, abnormal epiphyseal ossification, and immature primary spongiosa have been observed after TBI, along with bone pain and short stature (Miyazaki et al., 2009). Ionizing radiation exposure can cause a

dramatic 20-40% reduction in trabecular bone and a minor reduction of cortical bone (Green & Rubin, 2014), and functional bone loss can be observed as early as 3 days post-irradiation (Kondo et al., 2009). Bone volume fraction (BV/TV) and trabecular number were found to be greatly reduced by 10-days post-irradiation, and trabecular separation increased (Green et al., 2012). Volumetric bone mineral density and mineral apposition rate have been observed to increase within a week of radiation exposure (Willey et al., 2010). Finite element analysis revealed an increase in compressive strength at 2 weeks post-irradiation, followed by a long term loss of strength (Wernle et al., 2010). Microarchitectural quality was still damaged at 8-weeks post-irradiation (Green et al., 2012).

Radiation can directly damage bone cells, enlarge resorption lacunae, and increase osteoclast number and activity without an increase in bone formation (Weilbaecher, 2000). It also promotes cell cycle arrest and apoptosis, inhibits osteoblast proliferation, and reduces collagen production (Willey et al., 2008). Bone marrow cell populations are greatly reduced 2 days post-irradiation, with recovery by 8-weeks (Green et al., 2012). Mesenchymal stem cell populations are reduced following irradiation (Willey et al., 2011), but hematopoietic stem cells are relatively radiation resistant (Green et al., 2012). Radiation can upregulate specific hematopoietic lineages, and its effects are dependent on the phenotypic cell population (Green et al., 2012). Younger mice have been found to repopulate marrow cell populations faster than older animals, as the number of cells in the bone marrow is reduced by over 60% by 2 days post-irradiation, with no recovery at 10-days but recovery in young mice by 8-weeks (Green et al., 2012).

Radiation damages osteoblast precursors (Willey et al., 2011) and directly inhibits osteoblast formation and growth hormone and IGF-1 production, reducing bone formation

long-term (McClune et al., 2011), but osteoblast numbers and bone formation are unchanged when acute bone loss occurs after radiation exposure (Willey et al., 2011). Irradiation reduces the number of osteoblasts, reduces osteoblast proliferation and differentiation, collagen production and matrix formation, and increases apoptotic sensitivity (Willey et al., 2011). Total body irradiation is also associated with a decrease in viable osteocytes and hypogonadism, which can cause osteoporosis (Weilbaecher, 2000), although osteocytes are relatively radioresistant (Willey et al., 2011).

Osteoclast number and activity is rapidly elevated following clinical doses of irradiation, producing increased amounts of TRAP5b as early as 24 hours after irradiation (Willey et al., 2011). Osteoclasts are more active 3-days after radiation exposure, increasing in number and surface and producing more TRAP-5b, but osteoblastic and bone microarchitectural changes are not yet present (Willey et al., 2011; Willey et al., 2008).

Physiochemical processes that dissolve the bone matrix may also contribute to the rapid radiation induced bone loss (Green & Rubin, 2014). The occurrence of bone loss independent of hematopoietic cell availability or repair suggests cell-independent causes of bone loss such as physiochemical erosion are major causes (Green et al., 2012). A decrease in mineral composition of trabecular bone, altered collagen cross linking and altered mineralized matrix have been observed within a week after irradiation (Green & Rubin, 2014), and changes in bone strength may be affected by both architectural and material properties (Willey et al., 2011).

Current Treatments

Current treatments for osteoporosis include antiresorptive agents, nonpharmacologic agents, hormone therapy, and improving healthy lifestyle choices (Green & Rubin, 2014).

For adults, adequate calcium and vitamin D intake (Green et al., 2012; Haddy et al., 2001; McClune et al., 2011; Schimmer et al., 2000; Weilbaecher, 2000), regular weight bearing exercises (Haddy et al., 2001; McClune et al., 2011; Schimmer et al., 2000; Weilbaecher, 2000), avoiding tobacco (Haddy et al., 2001; McClune et al., 2011; Schimmer et al., 2000) and alcohol use (McClune et al., 2011), and avoiding carbonated beverages (Haddy et al., 2001; Schimmer et al., 2000) are all encouraged to improve BMD. Hormone replacement therapy may be appropriate if a hormone imbalance exists (Green et al., 2012; Haddy et al., 2001).

Antiresorptive agents are drugs that inhibit osteoclast activity and decrease bone resorption and thus overall loss (Haddy et al., 2001). However, when remodeling is suppressed, microdamage accumulates because it is not remodeled, and mechanical forces are more likely to cause fractures because increased mineralization and cross-linking make the tissue more brittle (Allen & Burr, 2014). Antiresorptive agents include bisphosphonates, calcitonin, teriparatide, estrogen receptor modulators, and hormone replacement therapy (McClune et al., 2011; Shuler et al., 2012; Weilbaecher, 2000). Raloxifene is an estrogen receptor modulator that is becoming widely used because it increases bone density without stimulating breast or endometrial tissue proliferation (Schimmer et al., 2000). Calcitonin inhibits osteoclasts and bone resorption (Haddy et al., 2001; Schimmer et al., 2000) but has not been shown to prevent bone loss (Schimmer et al., 2000). Only bisphosphonates have been shown to reduce or prevent steroid-induced bone loss (Schimmer et al., 2000; Weilbaecher, 2000). Bisphosphonates are administered for HSCT patients who are on steroids for more than 2 months, and using the lowest allowable dose of glucocorticoids with the shortest half-life may also help prevent osteoporosis and osteopenia (Weilbaecher, 2000).

Bisphosphonates are antiresorptive agents and stable analogues of pyrophosphates, which bind to hydroxyapatite crystals to prevent calcification (Sebestyen et al., 2012). Bisphosphonates reduce bone turnover by decreasing osteoclast activity, inhibiting osteoclast recruitment, and inducing osteoclast apoptosis (Green & Rubin, 2014; Schimmer et al., 2000; Sebestyen et al., 2012; Weilbaecher, 2000). They can also decrease bone formation by inhibiting calcification and hydroxyapatite breakdown, reducing overall bone turnover (Green & Rubin, 2014; Sebestyen et al., 2012). Less than 5% of orally administered bisphosphonates are absorbed by the body, but may last several years in the bone depending on the rate of bone remodeling (Sebestyen et al., 2012). They are generally well tolerated, but adverse effects include gastrointestinal reflux and development of flu-like symptoms (Sebestyen et al., 2012). Bisphosphonates include etidronate, alendronate, risedronate, and zoledronate (Haddy et al., 2001; Sebestyen et al., 2012). Zoledronic acid (zoledronate) increases bone density but does not maintain bone mechanical properties (Green & Rubin, 2014), and risedronate can prevent radiation-induced bone loss (Green & Rubin, 2014; Willey et al., 2010).

Anabolic pharmacological agents (parathyroid hormone) enhance the production of bone mass (Shuler et al., 2012). Parathyroid hormone (PTH) increases bone resorption by stimulating osteoblasts to produce RANKL (Green & Rubin, 2014). PTH and zoledronic acid can increase BMD better than the bisphosphonate alone (Green & Rubin, 2014). PTH and vitamin D (calcitriol) regulate calcium balance by stimulating bone resorption and intestinal and renal calcium absorption (Putman & Gordon, 2014).

Nonpharmacologic interventions include fall prevention, balance and exercise programs, avoidance of tobacco and alcohol, and vitamin D and calcium supplements (Shuler

et al., 2012). Approximately 25% of the calcium ingested is absorbed (Putman & Gordon, 2014), so maintaining calcium intake of at least 1500 mg per day and vitamin D levels at high normal limits are major treatments for bone loss (Weilbaecher, 2000). Vitamin D is a prohormone whose metabolite calcitriol regulates calcium homeostasis (Putman & Gordon, 2014), and deficiencies in vitamin D and calcium increase parathyroid hormone production and bone loss (Schimmer et al., 2000).

Pediatric Treatments

As of 2007, there were no recommended guidelines for screening bone densitometry or treating low bone mass in children (von Scheven, 2007). There may be a correlation between BMD and bone fragility in children, but since DXA measurements are dependent on bone size, Z-scores may only be indicative of low bone density for chronologic age, not necessarily osteoporosis or osteopenia (von Scheven, 2007).

Current preventative measures and treatments include radiation dose reduction, calcium and vitamin D supplementation, and bisphosphonate use. Weight bearing exercise and whole body vibration can also increase bone mineral content, although no optimal exercise programs currently exist (von Scheven, 2007). Teriparatide (recombinant human parathyroid hormone) is not recommended for use in children (McClune et al., 2011; von Scheven, 2007), as it may cause osteosarcoma (von Scheven, 2007).

Children are more vulnerable to radiation-induced biological effects than adults, making dose optimization an important goal even for low radiation doses and densitometry screenings (Damilakis et al., 2010). The use of adult radiation protocols on children results in pediatric radiation overexposure, as a spine and hip DXA scan in a child can give a two to three times higher dose of radiation than in an adult (Damilakis et al., 2010). Pediatric doses

can be minimized by reducing image lengths to fit the child's body, preventing exposure to radiosensitive organs, and using automatic exposure controls (Damilakis et al., 2010).

Calcium and vitamin D are considered safe agents, and supplementation is often a first step toward correcting reversible low BMD in children (von Scheven, 2007). Calcium supplements are most commonly available as calcium carbonate, with oral amounts limited to 500mg doses due to absorption limits (Putman & Gordon, 2014). The recommended daily calcium intake for infants less than 1 year is 260mg, for children age 1-5 years is 800mg, up to 1200mg for ages 6 to 10, and 1500mg over ten years old (von Scheven, 2007), with an upper limit of 3000 mg/day (Putman & Gordon, 2014). Vitamin D is also available as oral supplements (Putman & Gordon, 2014), and the recommended daily intake for children is 400-600 IU (Putman & Gordon, 2014; von Scheven, 2007). An inverse relationship between calcium intake and childhood bone fracture has been suggested in epidemiologic studies, and a direct relationship between serum vitamin D levels and bone mineral content or BMD has also been suggested (Putman & Gordon, 2014).

Oral bisphosphonates are an aggressive treatment in children (von Scheven, 2007) and are increasingly used to treat severely low BMD and osteoporosis, although there is no long-term safety and efficacy data (Ooi et al., 2012; von Scheven, 2007). They have been shown to substantially increase BMD, trabecular number (von Scheven, 2007), and reduce fracture rates (Ooi et al., 2012; von Scheven, 2007), preserve trabecular bone, and increase cortical area and thickness in children (Ooi et al., 2012). There are concerns that bisphosphonate use in children may potentially inhibit growth of the patient and offspring, although current data do not support this claim (Sebestyen et al., 2012; von Scheven, 2007), and have been found to improve growth in children (Sebestyen et al., 2012).

CHAPTER 4: ALL AND RADIATION THERAPY

Introduction

Leukemia is an uncontrolled expansion or proliferation of hematopoietic cells that cannot differentiate into mature blood cells (Sawyers et al., 1991). Acute leukemias are characterized by white blood cells that mature and function abnormally, and have high numbers in circulation (Sawyers et al., 1991). Therefore, blood cells must be destroyed, but it is nearly impossible as of yet to only eliminate cancer cells. Currently, treatment is to pretreat the patient with chemotherapeutic agents and irradiation (TBI) to completely destroy blood and bone marrow tissues (myeloablation) before stem cell transplantation (BMT, or HSCT) to replenish blood and immune cells (Domen et al., 2011). Acute lymphoblastic leukemia is the most common childhood cancer (Campana & Pui, 2014; Tucci & Aricò, 2008) and has a cure rate around 80%, or upwards of 1500 new child survivors in the U.S. each year (Haddy et al., 2001).

Acute Lymphoblastic Leukemia

Leukemias are cancers of the blood cells. They are characterized by a malignant proliferation of abnormal and immature white blood cells, especially leukocyte precursors (Campana & Pui, 2014; Imbach, 2011b; Saha & Lilleyman, 1998; Tucci & Aricò, 2008). The cause of leukemia is unknown (Imbach, 2011b; Pui et al., 2008). Less than 5% of cases are associated with inherited conditions, or exposure to ionizing radiation or chemotherapeutic drugs (Campana & Pui, 2014; Pui et al., 2008). However, it is known that leukemia

originates in the bone marrow (Imbach, 2011b), and some may develop prenatally (Pui et al., 2008). They derive from hematopoietic stem cells or progenitor cells (Domen et al., 2011; O'Brien & Lacayo, 2008) and include tumorigenic genetic and epigenetic changes that give rise to cancer cell characteristics such as loss of programmed cell death, retention of telomeres, and evasion of immune cells (Domen et al., 2011). Mutations for self-renewal and stage-specific developmental arrest occur in progenitor cells committed to the B- or T-cell lineages (Pui et al., 2008).

ALL in particular is a malignant disorder of lymphoid progenitor cells (Pui et al., 2008), and the most common childhood cancer (Campana & Pui, 2014; Tucci & Aricò, 2008). There are three main types of ALL, each with specific cell surface markers and defining chromosomal translocations (

Table 2). B-cell precursor ALL affects 70-80% of ALL patients and expresses cell surface markers CD10 and CD19 (Campana & Pui, 2014; O'Brien & Lacayo, 2008). It is characterized by a higher than normal number of chromosomes (hyperdiploidy) and a TEL-AML1 fusion gene translocation in up to 25% of cases, which combines the hematopoietic-cell development gene *Tel* with the embryonic hematopoietic differentiation gene *Aml1*, and is associated with a good prognosis (Campana & Pui, 2014; O'Brien & Lacayo, 2008; Pui & Evans, 2006; Pui et al., 2008; Tucci & Aricò, 2008). Mature B-cell ALL affects 2-5% of ALL patients and expresses CD22 in addition to CD10, CD19, and CD20 (Campana & Pui, 2014; O'Brien & Lacayo, 2008). It is characterized by a translocation between chromosome 8 and an immunoglobulin gene (Campana & Pui, 2014; O'Brien & Lacayo, 2008). Lastly, T-cell ALL affects about 15% of ALL patients, and over 50% of these cases have gain-of-function Notch-1 mutations, which regulate normal development (O'Brien & Lacayo, 2008; Pui & Evans, 2006; Pui et al., 2008; Tucci & Aricò, 2008). T-cell ALL lymphoblasts express

CD2-5, CD7, and CD8, and are associated with a good prognosis (Campana & Pui, 2014; O'Brien & Lacayo, 2008; Pui & Evans, 2006).

Table 2: Three types of ALL, their percentages of total ALL patients, and characteristics. (Compiled from Campana & Pui, 2014; O'Brien & Lacayo, 2008; Pui & Evans, 2006; Pui et al., 2008; Tucci & Aricò, 2008)

	B-Cell Precursor	**Mature B-Cell**	**T-Cell**
ALL Patient Prevalence	70-80%	2-5%	15%
Cell Surface Markers	CD10, CD19	CD10, CD 19, CD 20, CD22	CD2-5, CD7, CD8
Translocation or Mutation	TEL-AML1 translocation	chromosome 8 and immunoglobulin	Notch-1 mutation

Other structural rearrangements, such as point mutations, deletions, and amplifications, are required in addition to chromosomal abnormalities to develop into leukemia (Pui et al., 2008). The PAX5 gene is commonly mutated in B-cell precursors, and deletions in developmental genes such as EBF and Ikaros have also been found (Pui et al., 2008). Clonal rearrangements in immunoglobulin and T-cell receptor genes are also common (Pui et al., 2008).

There are about 3250 new cases of leukemia diagnosed annually in the United States (O'Brien & Lacayo, 2008), accounting for about 33% of all childhood cancer diagnoses (Imbach, 2011b; Saha & Lilleyman, 1998). 75-80% of children diagnosed with leukemia have ALL, or about 2500 cases per year in the U.S. alone (Campana & Pui, 2014; Imbach, 2011a; O'Brien & Lacayo, 2008). Most leukemia and ALL diagnoses occur between 2 and 5 years of age (Campana & Pui, 2014; Imbach, 2011a; Imbach, 2011b; Pui et al., 2008). 88% of children between 1 and 9 years remain event-free after 5 years (Campana & Pui, 2014; Pui et al., 2008), and 80% of children diagnosed with ALL are still in remission a decade later

(Imbach, 2011a; O'Brien & Lacayo, 2008; Pui et al., 2008). Quality of life may be slightly impaired after bone marrow transplantation, but improves in long-term survivors (Barrett, 1999).

Treatment

Treatment for ALL typically occurs in four phases: remission-induction, intensification or consolidation, interim maintenance, and continuation therapy (Campana & Pui, 2014; O'Brien & Lacayo, 2008; Pui & Evans, 2006; Pui et al., 2008; Tucci & Aricò, 2008) (Table 3). Remission-induction is first undertaken to eliminate over 99% of the existing leukemic cells and restore normal hematopoiesis by administering a combination of a glucocorticoid, vincristine, and either asparaginase or anthracycline (Campana & Pui, 2014; O'Brien & Lacayo, 2008; Pui & Evans, 2006; Pui et al., 2008; Tucci & Aricò, 2008). It lasts about 4 weeks and has a 96-99% success rate in children (Campana & Pui, 2014; O'Brien & Lacayo, 2008; Pui & Evans, 2006; Pui et al., 2008; Tucci & Aricò, 2008), but continued treatment is required to prevent reappearance of leukemic cells (Imbach, 2011a). Consolidation treatment targets drug resistant leukemic cells and lasts 4-8 weeks, often involving high doses of vincristine, asparaginase, and/or methotrexate (O'Brien & Lacayo, 2008; Pui & Evans, 2006; Pui et al., 2008). Interim maintenance involves daily mercaptopurine and weekly methotrexate with intermittent vincristine, and lasts 8 weeks (O'Brien & Lacayo, 2008). Continuation therapy is needed to prevent relapse and usually consists of daily doses of mercaptopurine, weekly doses of methotrexate, and monthly doses of vincristine for 2 to 3 years (Imbach, 2011a; O'Brien & Lacayo, 2008; Pui & Evans, 2006; Pui et al., 2008; Tucci & Aricò, 2008).

Table 3: ALL Treatment phases, durations, agents used, and purpose. Abbreviations: vincristine (VCR), methotrexate (MTX), mercaptopurine (6-MP). (Compiled from Campana & Pui, 2014; Imbach, 2011a; O'Brien & Lacayo, 2008; Pui & Evans, 2006; Pui et al., 2008; Tucci & Aricò, 2008)

	Remission-Induction	**Intensification / Consolidation**	**Interim Maintenance**	**Continuation**
Duration	4 weeks	4-8 weeks	8 weeks	2-3 years
Agents used	Glucocorticoid, VCR, asparaginase or anthracycline	high dose VCR, asparaginase, and/or MTX	daily 6-MP, weekly MTX	daily 6-MP, weekly MTX, monthly VCR
Purpose	Eliminate majority of leukemic cells, restore normal hematopoiesis	Targets drug-resistant leukemic cells	Therapy transition	Prevent relapse

While bone marrow ablation and transplantation are used widely to treat acute myeloid leukemia (AML) (O'Brien & Lacayo, 2008), in ALL they are reserved for the most severe or unresponsive cases (Mogul, 2002; Tucci & Aricò, 2008). Irradiation is used for patients with very high white blood cell counts, those with central nervous system (CNS) leukemia at diagnosis (Saha & Lilleyman, 1998), and testicular leukemia (Tucci & Aricò, 2008). Most of the approximately 20% of ALL patients who relapse undergo bone marrow transplants and increased intensive therapy (Saha & Lilleyman, 1998).

Chemotherapy

The major chemotherapeutic drugs used to treat acute leukemias are glucocorticoids, vincristine, asparaginase, methotrexate, and mercaptopurine. Cyclophosphamide and busulfan are commonly used during radiation treatment and stem cell transplantation.

Glucocorticoids are used in the remission-induction phase of treatment, with prednisone and dexamethasone used most widely (Pui et al., 2008). Prednisone is a steroid hormone with anti-inflammatory effects (Hyman & Sturgeon, 1956). Dexamethasone has a

longer half-life and greater penetration in the CNS than prednisone or prednisolone (Pui & Evans, 2006; Pui et al., 2008).

Vincristine (VCR) is an alkaloid from the periwinkle plant (BMJ, 1968). It is an anticancer lipophilic amine that causes cell cycle arrest in the M-phase and apoptosis by binding to tubulin and causing microtubule depolymerization that affects cellular transport processes (Raj et al., 2013). It has a high cytotoxicity and neurotoxicity that can result in autonomic and peripheral sensory-motor neuropathy, limiting the dosage amounts that can be given (BMJ, 1968; Raj et al., 2013).

Asparaginase is an enzyme that breaks down the amino acid L-asparagine, which is needed by cells but which some malignant cells cannot synthesize (BMJ, 1969). It can be harvested from E. coli, and has a potent effect on protein synthesis (BMJ, 1968; BMJ, 1969).

Methotrexate (MTX) is a folic acid agent antagonist (BMJ, 1968) with reliable absorption (Jonsson & Kamen, 1991) that inhibits folate reductase needed for purine synthesis (de Beaumais et al., 2011). It is a highly ionized, lipid-insoluble antineoplastic drug with high cytotoxic effects (Jonsson & Kamen, 1991; Kim et al., 2011) and can diffuse into the CNS, thus providing treatment where other agents cannot access (Tucci & Aricò, 2008).

Mercaptopurine (6-MP) is a thiopurine hypoxanthine analog that exerts antineoplastic and cytotoxic effects when metabolized by the cell (de Beaumais & Jacqz-Aigrain, 2012). It is a purine antagonist (BMJ, 1968) that inhibits de novo purine synthesis (de Beaumais et al., 2011).

Cyclophosphamide (CY) is an alkylating agent (BMJ, 1968) that is poorly tolerated by patients (Pui & Evans, 2006). High-dose cyclophosphamide with other chemotherapy agents such as busulfan or total body irradiation is used most frequently for patients with

malignancies (Barrett, 1999; Sanders, 1990) and in preparation for bone marrow transplantation (Mogul, 2002). It is often used with asparaginase in patients with T-cell ALL (Pui et al., 2008).

Radiation Therapy

It is estimated that 50-60% of all cancer cases need radiation therapy during treatment (Beyzadeoglu et al., 2010; Zeman et al., 2014). Due to toxicity, radiation treatment for ALL is generally reserved for the most severe or unresponsive cases of leukemia (Pui & Evans, 2006; Tucci & Aricò, 2008). Irradiation, especially cranial irradiation for the CNS, is recommended for patients with very high risk of relapse, leukemia of the CNS, T-cell ALL, and very high leukocyte counts (Pui & Evans, 2006). High risk of relapse includes patients who do not remit by day 28 of therapy, who have Ph+ cells or biphenotypic leukemia, infants with MLL gene rearrangements, and patients who have high hazard scores (Barrett, 1999).

Radiation is used for immunosuppression, marrow ablation, eradication of malignant cells, and clearing space for bone marrow transplantation to improve engraftment (Barrett, 1999; Beyzadeoglu et al., 2010; Chou et al., 1996; Girinsky et al., 1997; Green & Rubin, 2014; Mogul, 2002). TBI and increased immune suppression is useful after rejection of a first graft or with less than ideal HLA matching (Barrett, 1999). Bone marrow ablation can be achieved at 6 to 15 Gy doses of total body irradiation (Barrett, 1999). Unlike most chemotherapeutic agents, radiation is both immunosuppressive and antineoplastic, and does not cross-resist chemotherapy drugs (Mogul, 2002). Most preparative regimens combine TBI with cyclophosphamide (Mogul, 2002), and bone marrow transplantation is used to rescue the patient from bone marrow toxicity (Barrett, 1999).

External beam fractionated radiotherapy is the most commonly used clinical technique (Zeman et al., 2014). Radiation treatment is typically administered in small doses (fractionated) to prevent toxicity and increase the maximum tolerated dose (Mogul, 2002). Dose fractions may be administered two or three times daily, for a total dose of 12 - 18 Gy (Girinsky et al., 1997; Green & Rubin, 2014; Pui & Evans, 2006). Most machines used for TBI use either cobalt or linear accelerators (4-18MV protons or X rays) mounted on a rotating gantry (Barrett, 1999; Girinsky et al., 1997; Zeman et al., 2014). Dose distributions, depth dose, scatter, and beam flatness are obtained (Barrett, 1999; Zeman et al., 2014), and dosimetry can be monitored in vivo (Barrett, 1999; Girinsky et al., 1997). Radiation beams are chosen and a dose strategy is devised to administer desired levels to the target volume while remaining within acceptable limits in normal tissues (Zeman et al., 2014), with a goal to obtain as homogenous a dose as possible (Barrett, 1999). To administer a dose fraction, the patient is immobilized, and a contrast agent may be administered (Beyzadeoglu et al., 2010). The lungs are partially shielded to prevent toxicity (Girinsky et al., 1997). The patient may be positioned supine or on their side at approximately 4 meters from the source (Barrett, 1999; Girinsky et al., 1997) with Perspex to absorb backscatter and prevent burns, or treated with multiple angle postero-anterior and antero-posterior fields (Barrett, 1999; Zeman et al., 2014).

The acute tolerance of normal tissues limits the dose that can be given, usually the lung at 9 - 10 Gy or 14 - 15 Gy with fractionation (Barrett, 1999). Small dose fractions work best because they allow normal tissues to recover from radiation damage while accumulating damage in stem and leukemic cells (Barrett, 1999; Green & Rubin, 2014). Bone marrow stem cells are radiosensitive and cannot completely repair sub-lethal damage, regardless of dose

rate or fractionation (Barrett, 1999). Leukemic cells are highly radiosensitive and can only repair low amounts of sub-lethal damage (Barrett, 1999).

Allogeneic Hematopoietic Stem Cell Transplantation

HSCT is reserved for life-threatening disease (mostly malignancies) and is a last resort because of its significant morbidity and mortality (Bashie & Champlin, 2014). Bone marrow transplants are performed to replace defective bone marrow stem cells with functioning cells, in cases of malignant cancers such as leukemias that require TBI to eradicate cancer cells, and to treat systemic metabolic diseases (Bashie & Champlin, 2014; Mogul, 2002). BMT can improve disease-free survival, and can achieve up to 75% long-term survival in adults (Chou et al., 1996; Pui & Evans, 2006). It presents a treatment option for individuals who fail conventional therapy (Campana & Pui, 2014; Chou et al., 1996; Tucci & Aricò, 2008), who have persistent or high (>1%) levels of minimal residual disease, T-cell ALL or poor early response, severe hypoploidy, or early hematologic relapse (Bashie & Champlin, 2014; Campana & Pui, 2014). Currently, the only known treatment for hematopoietic failure after TBI is BMT or HSCT to regenerate the hematopoietic system (Domen et al., 2011).

Stem cell transplantations can be either autologous or allogeneic. Autologous transplants use the patient's own tissue, while allogeneic transplants use tissues from a related or unrelated donor (Bashie & Champlin, 2014; Domen et al., 2011; Mogul, 2002). Syngeneic transplants are a type of allogeneic transplant that uses blood from a genetically identical twin donor (Bashie & Champlin, 2014; Mogul, 2002). Autologous transplants will not develop GVHD, a condition in which the body identifies the transplanted cells as foreign and attacks them (Domen et al., 2011). Allogeneic transplants are the most widely used, with

a histocompatible (HLA-matched) sibling as the most common and most promising donor (Barrett, 1999; Mogul, 2002). Allogeneic transplants are effective against ALL but run the risk of GVHD (Bashie & Champlin, 2014), although they may develop graft-versus-leukemia (GVL) or graft-versus-tumor (GVT) responses in which the donor immune cells further combat any remaining leukemia or tumor cells in the patient (Domen et al., 2011).

Pluripotent hematopoietic stem cells are found in the bone marrow and are known to express cell surface marker CD34 (Bashie & Champlin, 2014; Sawyers et al., 1991). They can be harvested through bone marrow, umbilical cord blood, or mobilized peripheral blood (MPB) (Barrett, 1999; Bashie & Champlin, 2014; Domen et al., 2011; Staal et al., 2011). Harvesting from bone marrow is invasive and requires local anesthesia (Domen et al., 2011; Mogul, 2002). About 300 million nucleated bone marrow cells per kilogram of body weight of the recipient are taken through aspirations of both posterior iliac crests (Mogul, 2002). It is pooled with culture medium and heparin, and filtered to remove fat, clotted material, and bone spicules (Mogul, 2002). Stem cell mobilization to the peripheral blood can be accomplished by administration of granulocyte colony stimulating factor (G-CSF) (Staal et al., 2011). Harvesting through mobilized peripheral blood is less invasive (Domen et al., 2011; Mogul, 2002). Cytokine mobilization of HSCs results in more HSCs and hematopoietic progenitors in the blood (Domen et al., 2011). A device enriches cells that express CD34, and the resulting mixture of HSCs, hematopoietic progenitors, and contaminants is infused back into the patient (Domen et al., 2011). Almost all autologous HSCTs use peripheral blood progenitor cells because they contain large numbers of CD34+ cells and accelerate hematopoietic recovery (Bashie & Champlin, 2014). Umbilical cord

blood is less likely to produce GVHD but has less stem cells, resulting in slower hematopoietic and immune recovery (Bashie & Champlin, 2014).

Treatment Effects

It is estimated that about two-thirds of long-term childhood cancer survivors suffer from one or more psychological or physical late effect from treatment (Rueegg et al., 2013). Chronic health problems decrease quality of life (Rueegg et al., 2013), and survivors report significantly lower quality of life in areas such as physical functioning and general health perception than their unaffected siblings (Rueegg et al., 2013). We will briefly touch on some general effects of ALL treatment, and highlight some of the more significant effects on bone.

General Effects of ALL Treatment

There are a number of short and long term effects from treatment with radiation, chemotherapy, and stem cell transplantation. Major side effects of preparative radiation therapy are nausea, fever, diarrhea, fatigue, and acute fluid shifts (Barrett, 1999; Mogul, 2002). Patients undergoing HSCT are susceptible to bacterial, fungal, and viral infections (Bashie & Champlin, 2014). A large increase in granulocyte numbers occurs in the peripheral blood as they are released from the bone marrow (Girinsky et al., 1997). Increases in IL-6 and TNF are also observed in the blood (Girinsky et al., 1997).

Chronic health conditions afflict almost 75% of childhood cancer survivors within 30 years of diagnosis (Oeffinger et al., 2006). Hypothyroidism, cataracts, decreased growth rates, and delayed onset of puberty may occur from radiation exposure (Sanders, 1990). Interstitial pneumonitis, renal failure, and liver damage may be observed long-term from chemotherapy and radiation treatments together (Barrett, 1999; Bashie & Champlin, 2014; Haddy et al., 2001). Patients who have had HSCT are at a higher risk of secondary

malignancies, particularly of the skin (Bashie & Champlin, 2014). Compared to their siblings, childhood cancer survivors have a 54 times increased risk of major joint replacement, 15 times increased risk of congestive heart failure, 10 times increased risk of coronary artery disease (Oeffinger et al., 2006), and 14 times increased risk of developing a second malignant neoplasm (Armenian et al., 2011; Oeffinger et al., 2006). The risk of developing a second tumor is directly related to time since treatment, original tumor type, and dose of radiation, but inversely proportional to the age at the time of bone marrow transplantation (Barrett, 1999). Ovarian insufficiency also occurs in over 90% of women after TBI and high dose chemotherapy (Weilbaecher, 2000).

Ionizing radiation kills cells through reproductive inhibition and by inducing apoptosis (Girinsky et al., 1997). Irradiation causes cells to sense damage, mobilize DNA repair proteins, repair DNA damage, trigger cell cycle check points, and initiate cell death (Zeman et al., 2014). Extrinsic environmental factors such as the availability of nutrients and oxygen, the ability to eliminate waste, and the presence or absence of cytokines, growth factors, and other signaling molecules influence cellular radiosensitivity (Zeman et al., 2014). Cells are most radiosensitive in the G2 and M cell cycle phases, and radioresistant in the S phase (Zeman et al., 2014). Well oxygenated cells are up to three times more radiosensitive than severely hypoxic cells (Zeman et al., 2014).

GVHD is a clinicopathological syndrome and a major complication of allogeneic HSCT (Bashie & Champlin, 2014) that occurs in 25 – 75% of HLA-matched transplant patients (Mogul, 2002). Donor T-cells react against histocompatibility antigens in recipient tissues, resulting in cytokine- and cell-mediated tissue injury (Bashie & Champlin, 2014). The incidence and severity of GVHD increases with the number of genetic differences

between the patient and donor's human leukocyte antigens (Bashie & Champlin, 2014). Acute GVHD occurs within the first 100 days after BMT (Bashie & Champlin, 2014; Mogul, 2002) and most commonly affects the gastrointestinal tract and the liver (Mogul, 2002). It is characterized by diarrhea, mucosal ulcerations, single-cell necrosis, hepatocellular necrosis, and damaged bile duct epithelium (Mogul, 2002). Chronic GVHD is often a continuation of acute GVHD and most commonly affects the esophagus, liver, and eyes (Mogul, 2002). It presents as cataract formation, insufficient tear production, dysphagia, pain and partial occlusion of the esophagus, and varying degrees of chronic liver disease (Mogul, 2002). Immune recovery is also delayed until GVHD has subsided (Mogul, 2002).

Treatment Effects on Bone

Osteoporosis is a late effect in childhood cancer survivors (Haddy et al., 2001). Children treated for ALL are particularly at risk (Weilbaecher, 2000), with immunosuppressants, irradiation, physical inactivity, and nutritional deficiencies acknowledged as the main causes of bone loss associated with ALL treatment (Mussa et al., 2010). Reduced bone turnover and BMD have been observed during ALL treatment, and reduced BMD has been observed long-term (van der Sluis et al., 2002). An almost doubled fracture risk has been observed in ALL survivors compared to healthy controls (Mussa et al., 2010; van der Sluis et al., 2002), and ALL itself may cause osteopenia, as some children have been found to have reduced BMD at diagnosis (van der Sluis et al., 2002). Childhood cancer survivors with musculoskeletal problems also report a significantly lower quality of life compared to their siblings (Rueegg et al., 2013).

A side effect of cancer and its treatment is decreased BMD (Haddy et al., 2001; Mandel et al., 2004), which can lead to fractures, deformity, kyphosis, lordosis, growth

failure, and musculoskeletal pain (Haddy et al., 2001). 65% of children treated for ALL experienced decreased bone mass during therapy (Mandel et al., 2004). 21-59% of children experience musculoskeletal pain (Haddy et al., 2001). 39% of children with ALL had at least one fracture by the end of therapy (Haddy et al., 2001; Mandel et al., 2004), with vertebral fractures commonly reported (Mandel et al., 2004).

In ALL patients, the most prominent bone loss occurs during therapy (Mussa et al., 2010). Within 1-2 weeks, radiation therapy causes bone marrow hemorrhage and edema (Guillerman, 2013). Hematopoietic red marrow is replaced by fat and fibrosis in the following months, although some hematopoietic marrow can regenerate, before complete replacement by yellow marrow (Guillerman, 2013). Bone deterioration occurs within the first 6 months of treatment and continues throughout therapy (McClune et al., 2011; Mussa et al., 2010). Bone properties uncouple and BMD and cortical thickness are both rapidly reduced, but cortical thickness later recovers (Mussa et al., 2010). This may be suggestive of endosteal loss (Mussa et al., 2010). Bone mass may recover after treatment has finished (Mussa et al., 2010), and BMD has been observed to increase with increasing time after completion of therapy (Mandel et al., 2004). The majority of children treated for ALL recover normal bone mass within one decade of diagnosis (Mandel et al., 2004).

Radiation Effects on Bone

Individuals who received radiation therapy have been observed to suffer from bone loss and increased fracture risk (Green & Rubin, 2014). It has been shown that most ALL patients who experience reduced BMD received radiation as part of their treatment, and chemotherapy in this group contributed only a small amount of bone loss (Weilbaecher, 2000). Patients who received TBI as part of a conditioning regimen for HSCT had a 76%

higher risk of developing musculoskeletal abnormalities and impairment than their siblings (Armenian et al., 2011). An increase in adipose tissue in the bone marrow, reduction of trabecular bone, and an increase in osteoclast activity are known to occur after irradiation (Green & Rubin, 2014). TBI can also cause hypogonadism and associated bone loss (McClune et al., 2011).

TBI can induce bone changes that mainly affect the epiphyseal and metaphyseal regions (Miyazaki et al., 2009), and exposure to ionizing radiation can cause a 20-40% reduction in trabecular bone and a minor reduction of cortical bone (Green & Rubin, 2014). Radiation exposure to growing bones causes epiphyseal, metaphyseal, and diaphyseal injury and reduces bone growth, with increasing severity for larger doses, longer time after exposure, and younger age at exposure (Miyazaki et al., 2009; Sanders, 1990). Abnormal epiphyseal ossification, metaphyseal fraying, longitudinal metaphyseal striations, fragile growth plates, and irregular metaphyseal sclerosis has been observed in children with TBI-induced skeletal changes (Miyazaki et al., 2009). Short stature and scoliosis are also known to result from TBI and high dose radiation therapy (Miyazaki et al., 2009).

BMT Effects on Bone

Osteoporosis is a side effect of organ and marrow transplantation, largely caused by immunosuppressive therapy (Weilbaecher, 2000), with a 48% prevalence reported among individuals who have undergone HSCT for cancer treatment (McClune et al., 2011). HSCT can cause bone loss from toxic effects of radiation, chemo, and steroid therapies and their effects on gonadal and pituitary hormone secretion (Weilbaecher, 2000). Lower BMD values have been reported in patients treated with and without HSCT for cancer than healthy individuals (McClune et al., 2011). Up to a 10% decrease in bone density has been observed

in allogeneic transplantation patients 1 year after BMT and correlated with cyclosporine and prednisone use (Schimmer et al., 2000). BMT can also produce additional morbidities such as gonadal dysfunction, hypothyroidism, and secondary malignancies (Miyazaki et al., 2009).

Chemotherapy Effects on Bone

Chemotherapy is known to reduce BMD. BMD in the lumbar spine is significantly reduced at ALL diagnosis and during chemotherapy (van der Sluis et al., 2002). High dose methotrexate and high doses of corticosteroids are known to affect bone metabolism (Mandel et al., 2004) and impair bone mineralization (van der Sluis et al., 2002), and are associated with a higher risk of bone loss (Haddy et al., 2001) and failing to recover normal bone mass (Mandel et al., 2004) and BMD (McClune et al., 2011). Patients with reduced femoral BMD a decade after treatment were more than twice as likely to have received higher dose corticosteroids as survivors with normal BMDs (Mandel et al., 2004). Additionally, up to 50% of patients taking high-dose steroids for more than 6 months will experience an osteoporosis related fracture (Weilbaecher, 2000).

Chemotherapeutic agents themselves are known to be toxic. Methotrexate is particularly toxic to bones and induces osteopenia (Weilbaecher, 2000). Mercaptopurine causes bone marrow aplasia (BMJ, 1968). Bone marrow suppression can be caused by methotrexate and cyclophosphamide (BMJ, 1968). Cyclophosphamide effectively destroys all bone marrow cells except the most ‘primitive’ (Staal et al., 2011), and can induce cardiac tumors (Barrett, 1999). Cyclosporine reduces BMD by decreasing magnesium stores (Schimmer et al., 2000), and cortisol and related steroids accelerate bone loss (Haddy et al., 2001). Glucocorticoids may decelerate growth rates and present an early but transient

increase in bone resorption (Bellido et al., 2014), and are associated with decreased total body calcium in young children (van der Sluis et al., 2002; Weilbaecher, 2000).

Various mechanisms are responsible for chemotherapy induced bone loss. Osteoblast differentiation and function is inhibited by glucocorticoids (Marie, 1998; Weilbaecher, 2000), methotrexate (Mandel et al., 2004; Weilbaecher, 2000), and steroids (Mandel et al., 2004; Schimmer et al., 2000). Osteoblast and osteocyte apoptosis is promoted by glucocorticoids (Bellido et al., 2014; Weilbaecher, 2000) and steroids (McClune et al., 2011). Osteoclast lifespan is prolonged by glucocorticoids (Bellido et al., 2014). Osteoclast recruitment and bone resorption is stimulated by methotrexate (Mandel et al., 2004; Weilbaecher, 2000) and steroid use (Schimmer et al., 2000). Chemotherapy also causes hypogonadism and an associated decrease in estrogen and testosterone and increased bone loss (McClune et al., 2011; Weilbaecher, 2000).

CHAPTER 5: THE ACUTE RESPONSE OF BONE TO A MARROW ABLATING DOSE OF IONIZING RADIATION IN YOUNG SUBJECTS

Introduction

Acute lymphoblastic leukemia (ALL) is the most common type of childhood cancer and has over an 80% cure rate (Pui et al., 2008). 75% of survivors experience long-term side effects of treatment (Oeffinger et al., 2006), including osteoporosis and an almost doubled fracture risk (Mussa et al., 2010). With increasing numbers of survivors, reducing long term complications and improving quality of life are important goals.

Treatment for ALL includes radiation, bone marrow transplantation, and chemotherapies. Radiation is known to contribute to most of the bone loss observed during treatment, and this loss has been documented in the clinical setting. In research, bone loss due to radiation exposure is also well documented, although few studies analyze bone loss in young subjects due to a high dose of radiation, which occurs during ALL treatment. Therefore, the goal of this study is to characterize the response of bone to a marrow ablating dose of radiation in young subjects and model the human condition. Understanding this response will allow preventative measures to be developed and implemented in clinical practice, reducing long term skeletal complications from radiation exposure and improving survivor quality of life.

Metrics and Motivation

To assess trabecular microarchitecture to understand the response of bone to radiation, we quantified 6 parameters using microcomputed tomography (μCT):

BV/TV, vBMD, trabecular thickness (TbTh), trabecular number (TbN), trabecular separation (TbSp), and connectivity density (ConnD). BV/TV is the portion of the total volume analyzed that contains bone (as opposed to bone marrow) (Yumoto et al., 2010). A measure of bone density, vBMD is dependent on mineralization and the amount of bone present, and cannot differentiate between changes in density due to changes in either factor (Allen & Burr, 2014). TbN, TbTh, and TbSp are characteristics of trabecular bone and denote number, thickness, and separation, respectively. ConnD is the number of trabecular connections and an indicator of bone quality (Yumoto et al., 2010). Several groups have used μCT to analyze morphological parameters of bone in response to radiation (Wernle et al., 2010; Willey et al., 2008; Yumoto et al., 2010); thus we can compare our results to those established in literature.

To detect bone turnover and osteoblast and osteoclast activity, we analyzed blood serum for concentrations of osteocalcin (OC) and TRAP-5b. Osteocalcin is a marker of bone formation produced by osteoblasts (Marie, 1998; Olsen et al., 2000; Sebestyen et al., 2012), while TRAP-5b is a marker of bone resorption produced by osteoclasts (Sebestyen et al., 2012). OC and TRAP-5b have both been used to assess osteoblast and osteoclast activity after radiation exposure both in animals (Green et al., 2012; Willey et al., 2008) and humans (Carlson et al., 1994), allowing us to compare and better interpret the results of our study. Both biomarkers can be detected in blood serum (Allen & Burr, 2014; Christenson, 1997), and reference intervals for both have been developed in literature (Huang et al., 2011; Rauchenzauner et al., 2007; Yang & Grey, 2006).

To understand the functional effects of radiation on bone in young subjects, bone volume, stiffness, and efficiency were calculated through a computer simulated compression test using finite element analysis (FEA). Stiffness is a measure of the force the bone can

withstand per unit length. Efficiency indicates the effectiveness of the bone present at bearing the loads applied, or the stiffness of the bone over a given area. It is calculated by dividing the stiffness by the bone volume from FEA. FEA has been used to test compressive strength of bones (Ito et al., 2002; Schwen & Wolfram, 2014) and determine the contributions of cortical and trabecular bone to the mechanical properties of the whole bone (Ito et al., 2002). Finite element models can accurately predict experimental response (Schwen & Wolfram, 2014; Wernle et al., 2010), and this capability has been developed in our lab.

A Word About Animal Models

Several factors should be understood and considered when choosing an animal model and analyzing results. For example, animal models may have different radiation limits, amounts of bone and muscle, and immune cell levels than humans, although trends may be similar. Mice reach skeletal maturity between 4 and 5 months of age (Henderson et al., 2011), while humans achieve peak bone density around 18-22 years of age (Beamer et al., 1996). Humans exhibit intracortical remodeling, while rodents do not (Turner, 2011). The median lethal dose of radiation for humans within 60 days is between 2.5 and 5 Gy (Green & Rubin, 2014), but the median lethal dose for C57BL/6 mice within 30 days is about 8 Gy (Green & Rubin, 2014).

Animals are also different among each other. Mice commonly exhibit differences in BMD, cortical width, and trabecular architecture between males and females (Henderson et al., 2011), among other phenotypic parameters. For example, female B6 mice have higher red blood cell counts than males or BALB/c mice, and female C57BL/6 and BALB/c mice overall have higher white blood cell counts than their male counterparts (The Jackson Laboratory, 2006b). In muscle, male C57BL/6 mice attain higher grip strength than female

B6 mice or BALB/c mice of either gender (Crabbe et al., 2003). In bone, female C57BL/6 mice attain higher BMD than males or BALB/c mice of either gender (The Jackson Laboratory, 2006a). Cortical thickness is much greater in C3H/HeJ mice than C57BL/6, and cortical thickness in BALB/c mice is only slightly thicker than C57BL/6 mice (Beamer et al., 1996).

It is important to be aware of these and other confounding factors between animal models and humans for correct interpretation and validation of experimental animal studies of human conditions. Nevertheless, mice are commonly used to study radiation effects on bone, and are attractive options for many experiments due to their small size, similar response as humans, and qualitatively similar phenotype to humans in areas such as bone.

Hypotheses and Goals

This project aims to characterize the consequences to the skeletal structure of a marrow-ablating dose of ionizing radiation exposure on young mice. It is a first step in developing a murine model of treatment related bone loss in ALL patients from radiation therapy, chemotherapy, and bone marrow transplantation. In this section, the overall goals of the completed model are presented first, followed by the goals of this portion of the project, which focuses on the osteoporotic effects of a marrow ablating dose of radiation.

Overall Goals

The overall goal of this research is to develop a model to characterize bone loss after radiation therapy and bone marrow transplantation in young mice. The completed model will:

- Quantify the amount of bone loss that can be attributed to each factor (radiation, chemotherapy, and bone marrow transplantation) independently and combined,
- Identify the mechanisms of radiation induced bone loss for treatment development and prevention,
- Identify the optimal time to initiate bone loss prevention procedures, and
- Provide insight of possible vantage points for bone loss prevention or treatment.

Marrow-ablating radiation therapy is a standard part of preparative treatment before bone marrow transplantation for leukemia. Patients receive bone marrow transplants to restore stem cells and immune cells, but treatment-related bone loss still occurs. Identifying the timing of osteoblast and osteoclast activation can locate an appropriate time to intervene to prevent future bone loss. Identifying the mechanisms of this loss provides different pathways and vantage points to use to develop treatments.

The finished model will take into account radiation, chemotherapy, and bone marrow transplantation, and characterize typical bone loss when they are applied together in the clinical setting. The model will be correlated to clinical observations, so that the finished model can be used to test preventative measures and treatments and provide the correct understanding of their effects and benefits.

Goals of the Radiation Therapy Model

Toward the overall goal, this study will characterize bone loss in young subjects due to a clinical dose of radiation. The outcomes will:

- Quantify the amount of bone loss due to a marrow ablating dose of radiation,
- Quantify changes in mechanical properties of whole bone, and cortical and trabecular sections,
- Provide evidence of the cellular role of osteoblasts and osteoclasts after radiation exposure, and
- Suggest an opportune time frame for intervention.

We hypothesize that a marrow ablating dose of radiation will cause significant amounts of bone loss observable within days of radiation exposure due to elevated osteoclast activity and resorption, and that this loss will have significant functional effects on the mechanical properties of bone. Although these effects have been observed in the literature after radiation exposure, there is no characterization of the effects of radiation exposure and bone marrow transplantation in children for ALL treatment, particularly cellular and microarchitectural changes in young subjects.

We expect to observe severe, irreversible bone loss in less than one week after radiation exposure in young subjects. Rapid bone loss has already been observed in animal models with subclinical doses of radiation within one week of radiation exposure (Willey et al., 2011). In children, Mussa et al found that within the first 6 months of ALL treatment, skeletal deterioration can be detected using quantitative ultrasound (QUS), and can accurately identify patients with skeletal complications (Mussa et al., 2010). They concluded that bone properties uncouple and deterioration begins early and persists throughout ALL treatment (Mussa et al., 2010).

We expect osteoclast activity to be elevated as the cellular mechanism of bone loss. Osteoclast number and surface are greatly elevated 3-days after radiation exposure (Willey et al., 2008). TRAP5b levels are elevated as early as 24 hours after irradiation (Willey et al., 2011), and remain heightened for at least 3 days (Willey et al., 2008). A reduction in the overall number of osteoblasts is also known to follow irradiation (Willey et al., 2011).

We expect our observed structural consequences of radiation exposure in young subjects to agree with functional losses already present in the literature. Functional bone loss has been observed as early as 3 days after radiation exposure with a dose of 2 Gy (Kondo et al., 2009). Hamilton et al and other groups have observed significant reductions in trabecular volume fraction and connectivity density and increases in trabecular thickness and spacing from 2 Gy doses of various types of ionizing radiation (Hamilton et al., 2006; Willey et al., 2010). FEA was able to predict bone strength in mice, noting an increase in bone volume and bone strength at 2 weeks post-irradiation, but a loss of strength with further increase in bone volume at 12 weeks (Wernle et al., 2010).

Methods

To characterize the acute effects of a marrow-ablating dose of radiation, the tibiae of mice were studied at 2, 4, and 6 days after irradiation in irradiated (IRR) and non-irradiated (NR) groups using micro-computed tomography (μCT) and FEA. Serum chemistry was also analyzed for bone formation and resorption markers using enzyme-linked immunosorbent assays (ELISA).

Sixty female five-week-old C57BL/6 mice were obtained from Charles River Laboratories International, Inc. (Morrisville, NC) to model the acute response to radiation in the immature skeleton. Mice were weighed at the beginning of the study and each day of the

study as a monitor of general health. Mice were removed from the study if they exhibited a decline of 20% or more from their original mass before the day of sacrifice. Mice were housed 5 per cage, and cages were paired to normalize weights among 6 different groups. The pairs were then assigned a radiation group and day to indicate experimental group and time point. The groups were 2, 4, and 6 day NR and IRR (n = 10 per group), with all days counted from the time of irradiation.

The irradiated cage pairs were exposed to a singular 8 Gy whole-body dose of X rays (X-RAD 320, Precision X-Ray, North Branford, CT) on Day 0. Non-irradiated cage pairs were placed in the x-ray irradiator but not irradiated as a sham operation. At each time point (2, 4, and 6 days post-irradiation), the designated cage pairs were euthanized humanely using cardiac puncture and exsanguination to collect blood serum samples. Right tibiae were harvested and fixed in formalin for 48 hours before being stored in 70% ethanol.

Right tibiae were then analyzed in a 1 mm region of the metaphysis just below the growth plate using μCT (μCT 80, SCANCO Medical AG, Bassersdorf, Switzerland) at high energy (7000V) with the lower threshold set to 185 to obtain six microarchitectural parameters: BV/TV, vBMD, ConnD, TbTh, TbSp, and TbN.

Finite element analysis was also performed on the same region using SCANCO software (SCANCO Medical FE-software, SCANCO Medical AG, Bassersdorf, Switzerland) to obtain whole and cortical bone volume and stiffness as measures of structural properties. The inferior surface was fixed and a 5% downward displacement was applied to the superior surface to simulate axial compression. The material was considered isotropic with a Young's modulus of 10 GPa and a Poisson's ratio of 0.3. Trabecular bone volume and stiffness were calculated by subtracting cortical values of individual samples from their corresponding

whole bone values. Efficiencies were calculated by dividing stiffness by bone volume from FEA. Images were rendered in Abaqus (Abaqus/CAE 6.9-EF1, Dassault Systems Simulia Corp, Providence, RI).

ELISAs were used to analyze blood serum levels of bone formation marker osteocalcin (OC) (Biomedical Technologies Inc., Stoughton, MA) and bone resorption marker TRAP-5b (ImmunoDiagnostic Systems Inc., Scottsdale, AZ) to characterize bone turnover. ELISAs were performed according to the protocols provided by the manufacturers.

Statistical significance was determined using SigmaPlot 12.0 (Systat Software Inc., San Jose, CA). Two-way ANOVAs were performed to determine differences between irradiated and non-irradiated groups on each day of interest. P-values less than 0.05 were considered significantly different. Outliers were defined as data points that were more than three standard deviations from the mean in either direction.

Results

This section contains the results of the experiment. Group body mass data throughout the experiment is presented, as well as structural and microarchitectural properties from μCT and FEA, and bone turnover biomarker analysis ELISA data. For completeness, tables of average values and standard deviations for the data presented are included in Appendix A. No outliers were detected in any parameter.

Body Mass

Body mass was monitored each day of the study as a measure of general health. No significant differences among groups were measured at Day 0, but significant differences were present after irradiation (Figure 17). IRR groups had less mass than non-irradiated controls at each time point. No differences were found among the non-irradiated groups,

while the average mass of the 6 IRR group was statistically different from the other irradiated averages. Two mice in the 6 IRR group were removed from the study on Day 5 due to loss of mass greater than 20% of their original individual masses.

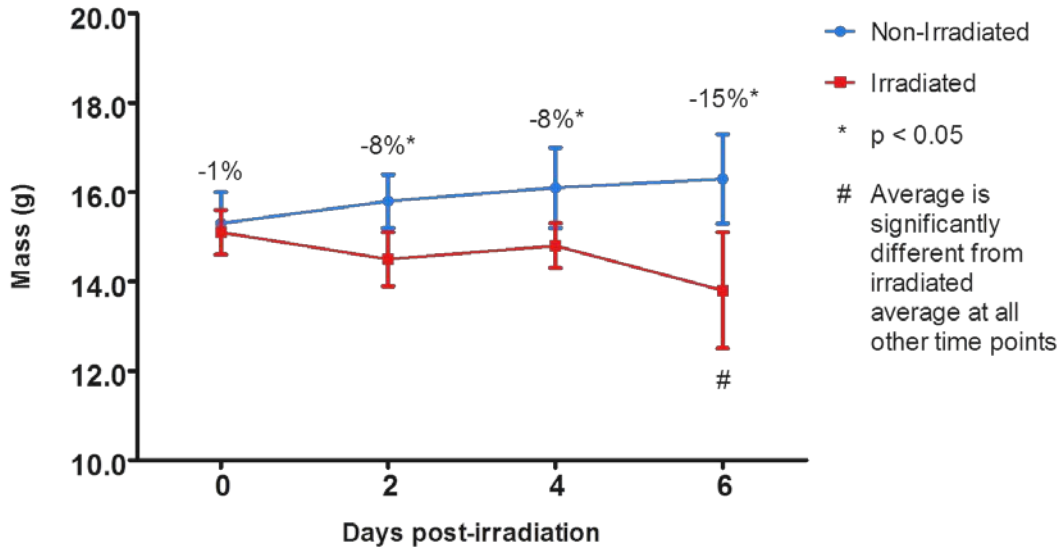

Figure 17: Body mass of irradiated and non-irradiated groups at 2, 4, and 6 days post-irradiation.

Cortical Bone Microarchitecture

Microarchitectural properties of the cortical bone were analyzed in the metaphysis of the proximal tibia using µCT. Figure 18 gives a visual representation of a typical µCT image of a trabecular section from each group at each time point, with visible cortical porosity. Cortical bone volume (CtBV), cortical thickness (CtTh), cortical porosity (CtPo), and polar moment of inertia (pMOI) were calculated at each time point to quantify bone loss.

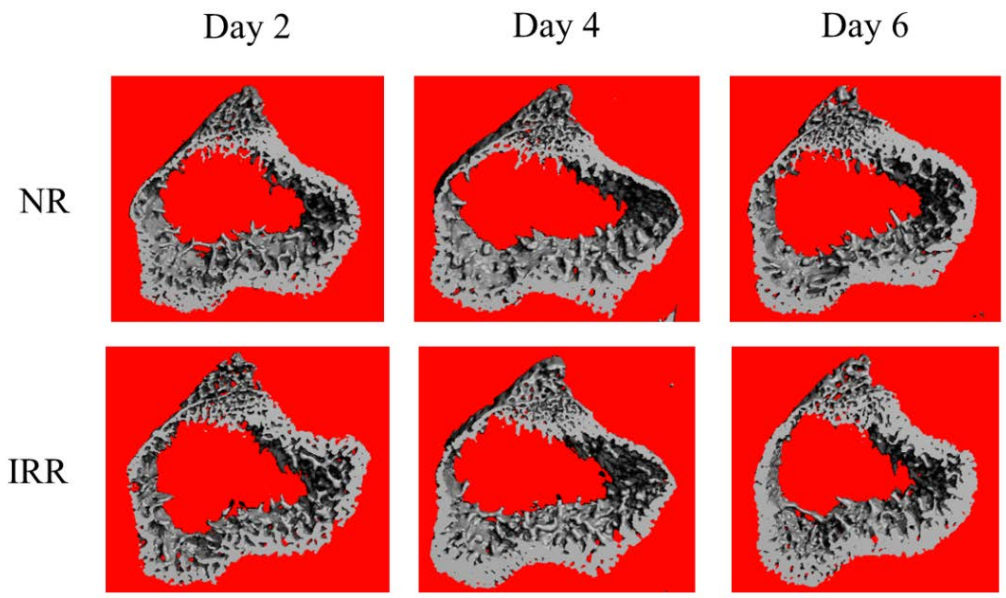

Figure 18: µCT images of cortical bone from the proximal tibia of female C57BL/6 mice 2, 4, and 6 days post-irradiation. The top row shows representative images from average non-irradiated (NR) bones, while the bottom row shows images from average irradiated (IRR) bones. Note the visible porosity. Images are not scaled.

Cortical bone volume was significantly greater in the irradiated group than the non-irradiated group at 6 days (Figure 19). Irradiated averages were not significantly different from each other on any day of the study, but the 6 NR average was significantly lower than the 2 NR average.

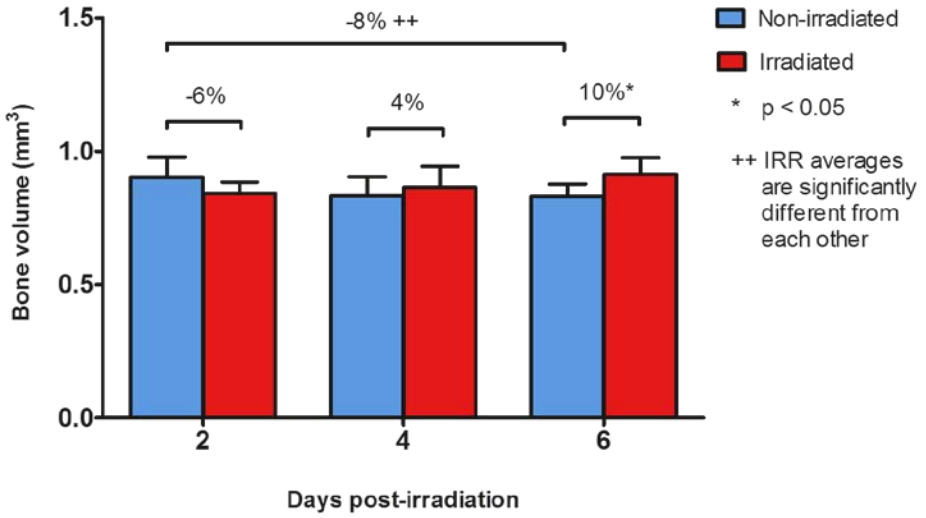

Figure 19: Cortical bone volume of irradiated and non-irradiated groups at 2, 4, and 6 days after exposure to an 8 Gy dose of X rays.

Cortical thickness was not significantly different between the irradiated and non-irradiated group on any day, although the 6 IRR average was significantly greater than the 2 IRR average (Figure 20).

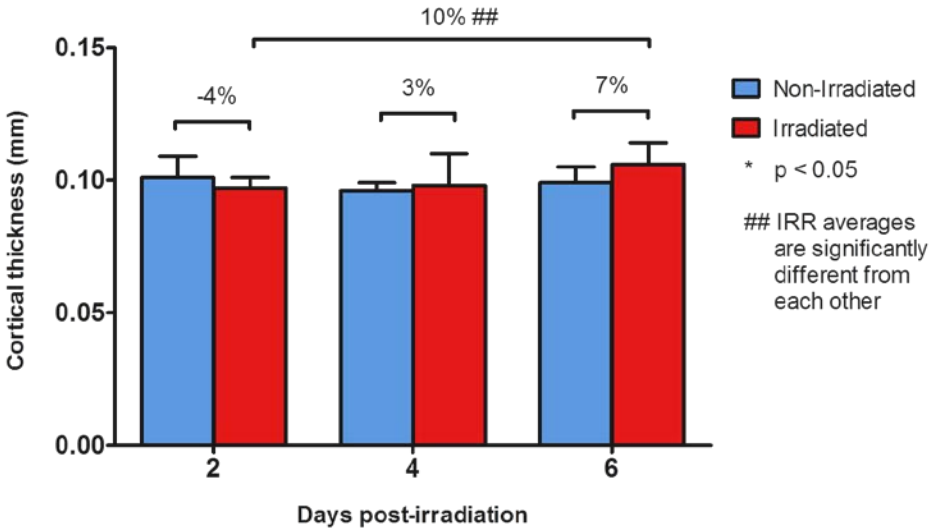

Figure 20: Cortical thickness of irradiated and non-irradiated groups at 2, 4, and 6 days after exposure to an 8 Gy dose of X rays.

Cortical porosity was lower in the irradiated group than the non-irradiated group at 6 days (Figure 21). The non-irradiated average was also significantly lower at 2 days than 4 or 6 days.

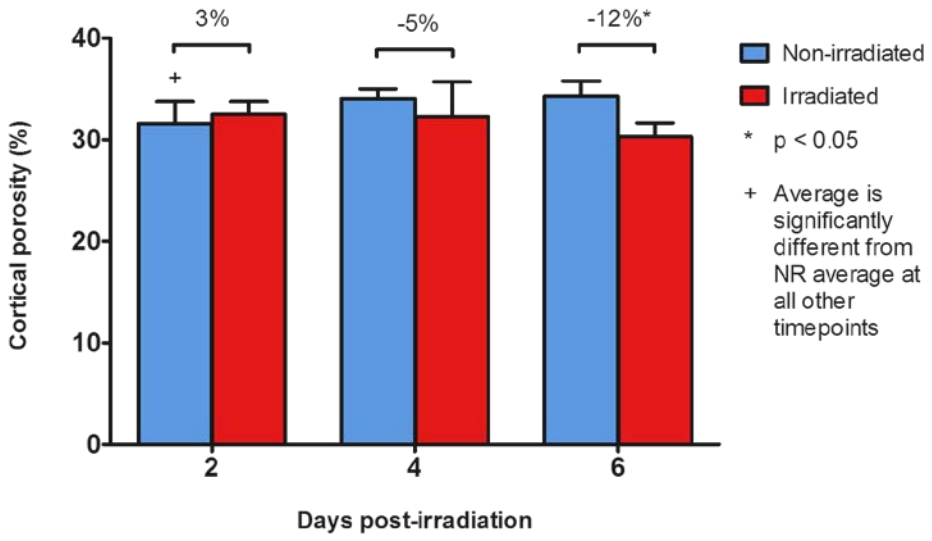

Figure 21: Cortical porosity of irradiated and non-irradiated groups at 2, 4, and 6 days after exposure to an 8 Gy dose of X rays.

The polar moment of inertia, or the resistance to torsion, was higher in the non-irradiated group than the irradiated group at 2 days, but no significant differences were observed at 4 or 6 days (Figure 22).

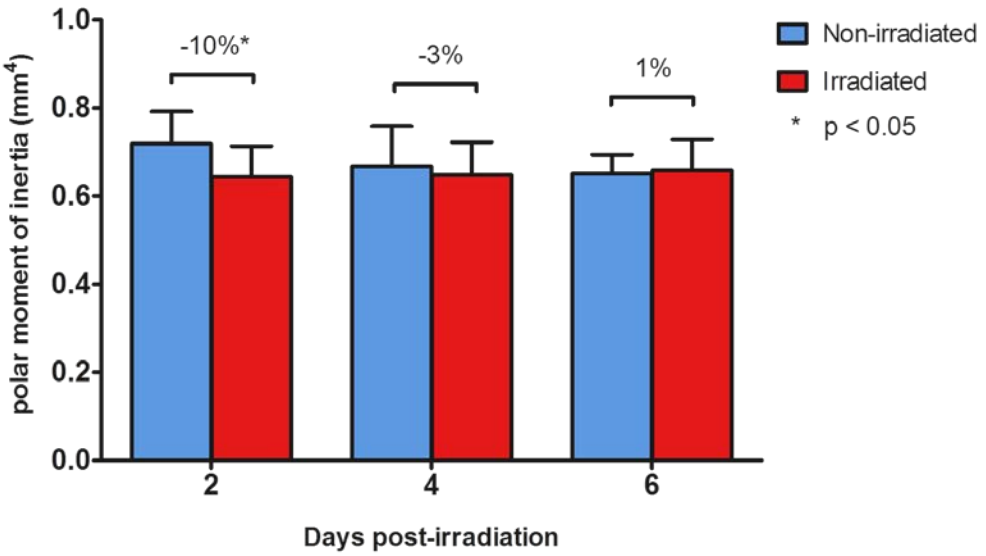

Figure 22: Polar moment of inertia of irradiated and non-irradiated groups at 2, 4, and 6 days after exposure to an 8 Gy dose of X rays.

Trabecular Bone Microarchitecture

Microarchitectural properties of the trabecular region of the metaphysis were also analyzed using µCT. Figure 23 gives a visual representation of a typical µCT image of a trabecular section from each group at each time point. Bone loss is clearly visible in the 6 day irradiated group. BV/TV, vBMD, TbTh, TbN, TbSp, and ConnD were calculated at each time point to quantify bone loss.

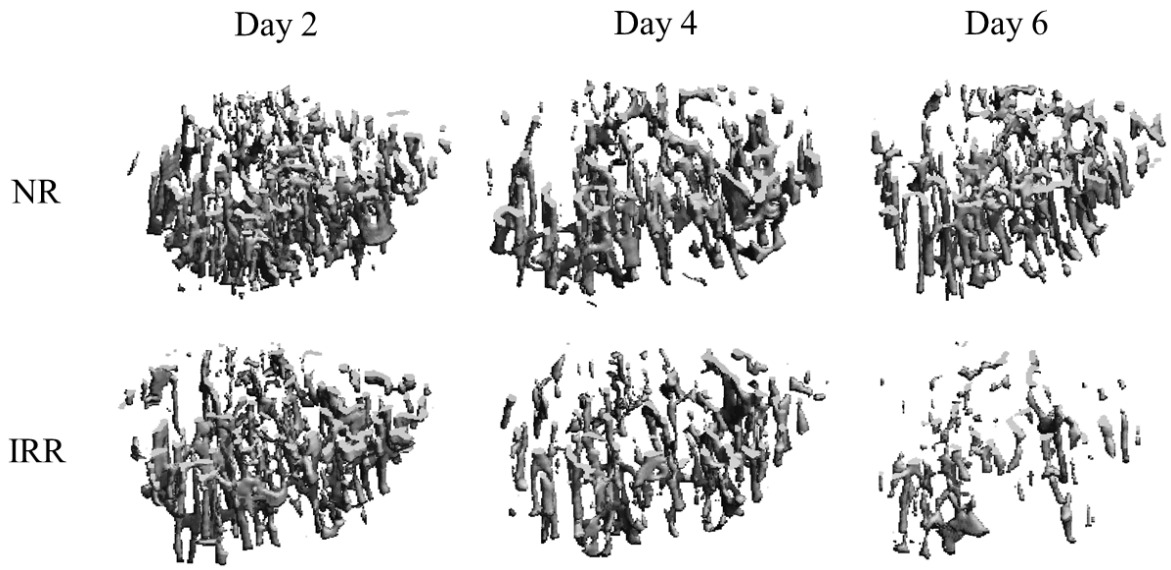

Figure 23: μCT images of trabecular bone from the proximal tibia of female C57BL/6 mice 2, 4, and 6 days post-irradiation. The top row shows representative images from average non-irradiated (NR) bones, while the bottom row shows images from average irradiated (IRR) bones. Images are not scaled.

Trabecular bone volume fraction shows a 16% increase in BV/TV at 2 days in the irradiated group compared to non-irradiated controls, followed by a steady decline to 70% less than controls by 6 days (Figure 24). All irradiated values are significantly different from each other, while none of the non-irradiated averages are significantly different.

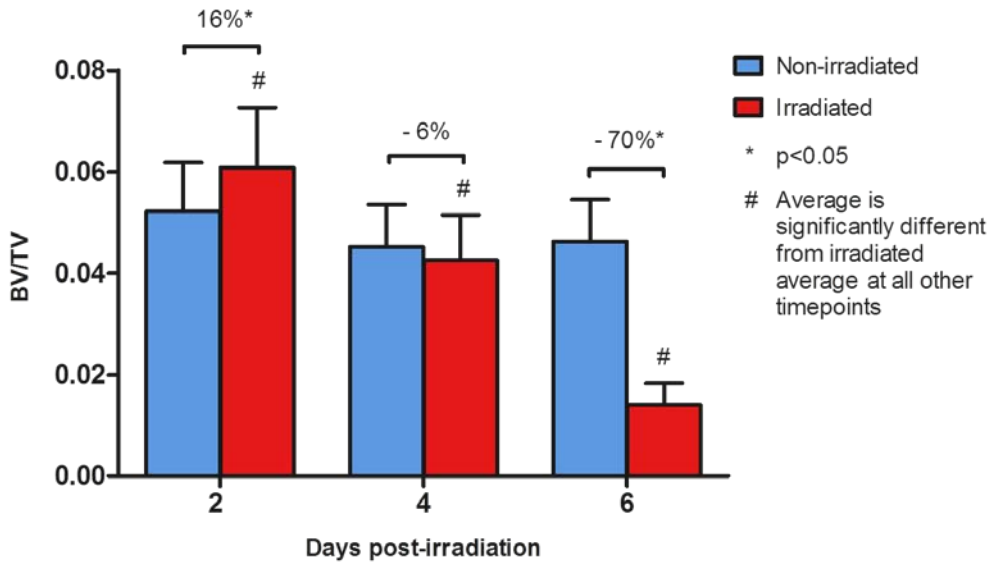

Figure 24: Trabecular bone volume fraction of irradiated and non-irradiated groups at 2, 4, and 6 days after exposure to an 8 Gy dose of X rays.

Volumetric bone mineral density followed a similar trend to BV/TV with an increase in the irradiated group over controls at 2 days and over a 70% decline by 6 days, although the increase at 2 days was not statistically significant (Figure 25). None of the non-irradiated averages were significantly different from each other, but all of the irradiated values were significantly different from each other.

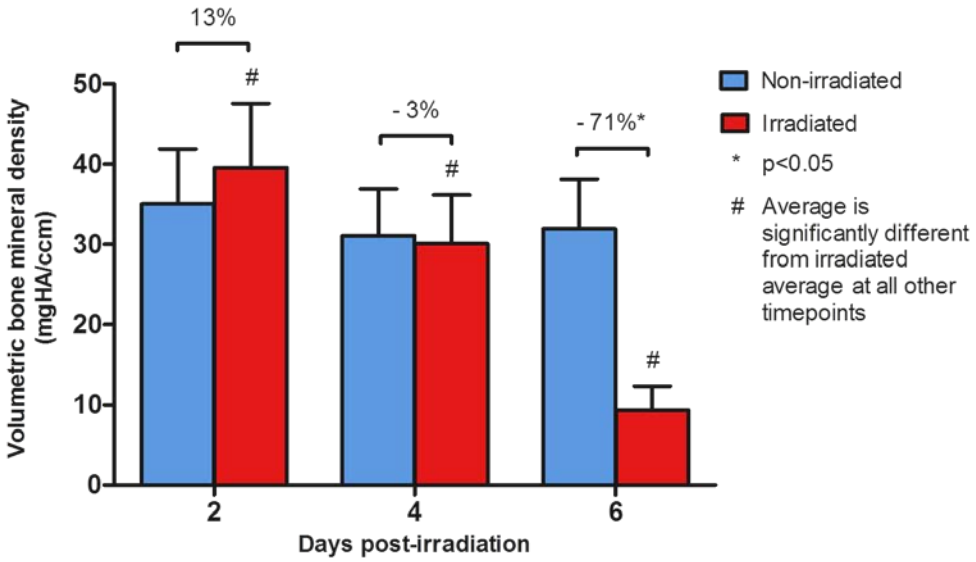

Figure 25: Volumetric bone mineral density of irradiated and non-irradiated groups at 2, 4, and 6 days after exposure to an 8 Gy dose of X rays.

Trabecular thickness was 7% and 9% higher than controls in the irradiated group at 2 and 4 days, respectively, but not significantly different than controls at 6 days (Figure 26). None of the non-irradiated values are significantly different from each other, while 4 IRR is significantly different from 2 IRR and 6 IRR.

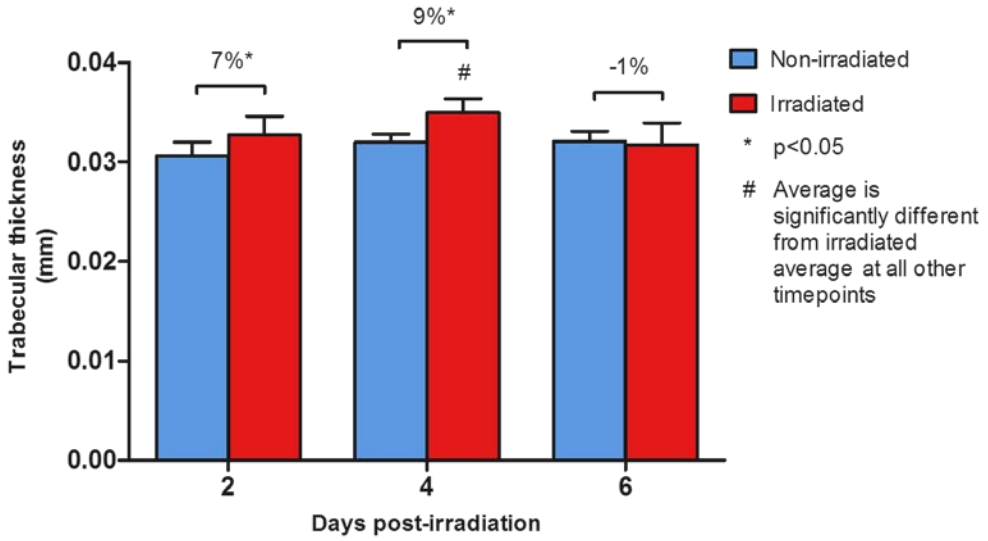

Figure 26: Trabecular thickness of irradiated and non-irradiated groups at 2, 4, and 6 days after exposure to an 8 Gy dose of X rays.

The number of trabeculae was significantly elevated above controls in the irradiated group at 8% at 2 days, and decreased to 37% below controls by 6 days (Figure 27). The non-irradiated values were not significantly different from each other, while the irradiated values show a steady, significant decline at each time point.

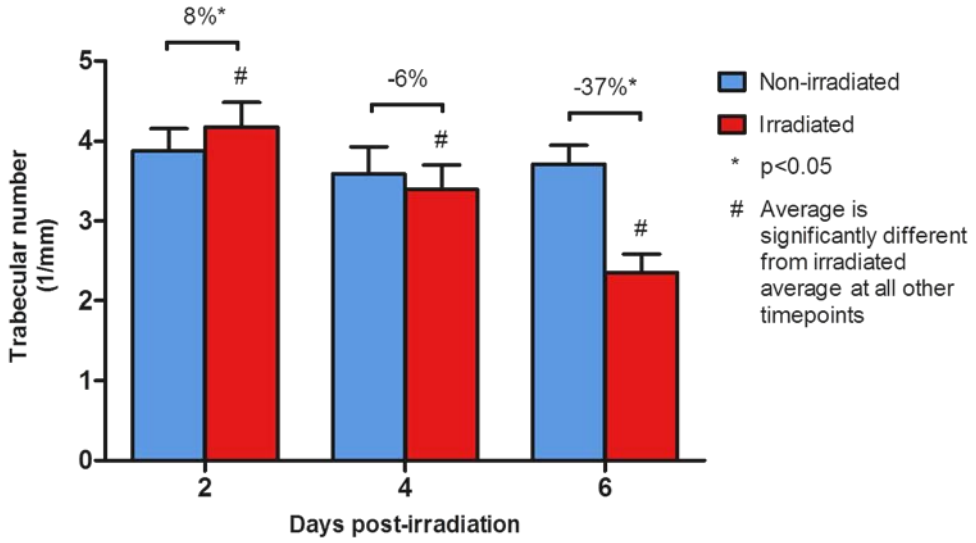

Figure 27: Trabecular number of irradiated and non-irradiated groups 2, 4, and 6 days after exposure to an 8 Gy dose of X rays.

Trabecular separation was only significantly different between control and irradiated groups at 6 days post-irradiation, with a 63% increase in separation in the irradiated group (Figure 28). Trabecular separation in the irradiated group increased significantly at each time point, while non-irradiated values were all similar to each other.

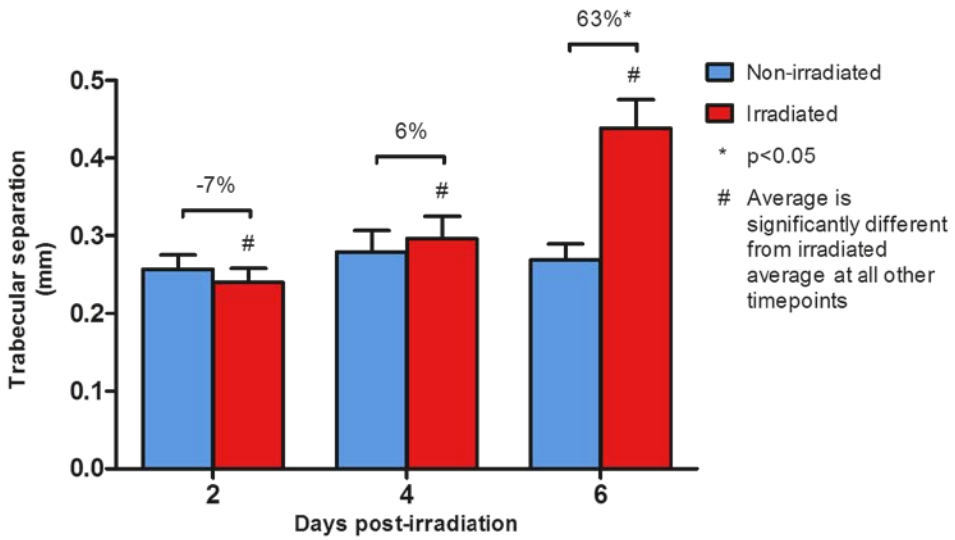

Figure 28: Trabecular separation of irradiated and non-irradiated groups at 2, 4, and 6 days after exposure to an 8 Gy dose of X rays.

Connectivity density appeared inversely related to trabecular separation, decreasing to 94% below control levels at 6 days post-irradiation (Figure 29). The non-irradiated averages are all similar, while the irradiated average at 2 days is significantly higher than the irradiated values at 4 and 6 days. No outliers were detected.

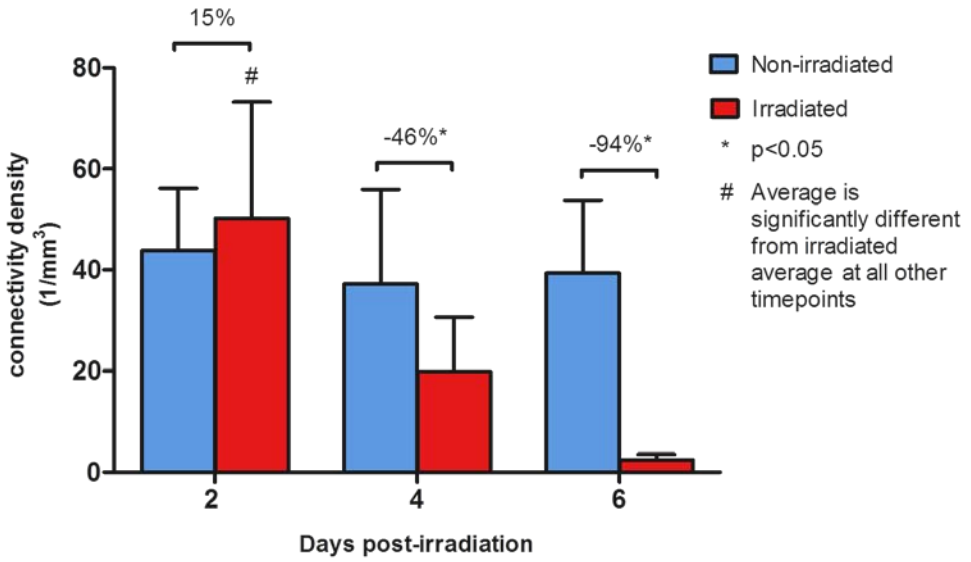

Figure 29: Connectivity density of irradiated and non-irradiated groups 2, 4, and 6 days after exposure to an 8 Gy dose of X rays.

In summary, BV/TV, TbTh, TbN were significantly elevated in the irradiated group over non-irradiated controls at 2 days post-irradiation, and BV/TV, vBMD, TbN and ConnD were all reduced and TbSp increased by 6 days post-irradiation. ConnD and vBMD were elevated at 2 days, but this was not statistically significant in either case. None of the non-irradiated averages are different from each other in any parameter.

Biomarkers of Bone Turnover

Serum chemistry was analyzed using ELISAs for bone formation marker osteocalcin (OC) (Figure 30) and bone resorption marker TRAP-5b (Figure 31).

Serum osteocalcin levels were elevated by a significant 17% over controls in the irradiated group at 2 days post-irradiation (Figure 30). There were no significant differences between irradiated and non-irradiated groups at any other day, nor were any of the irradiated averages significantly different from each other. The 2 day non-irradiated average was significantly lower than the 4- and 6-day non-irradiated values.

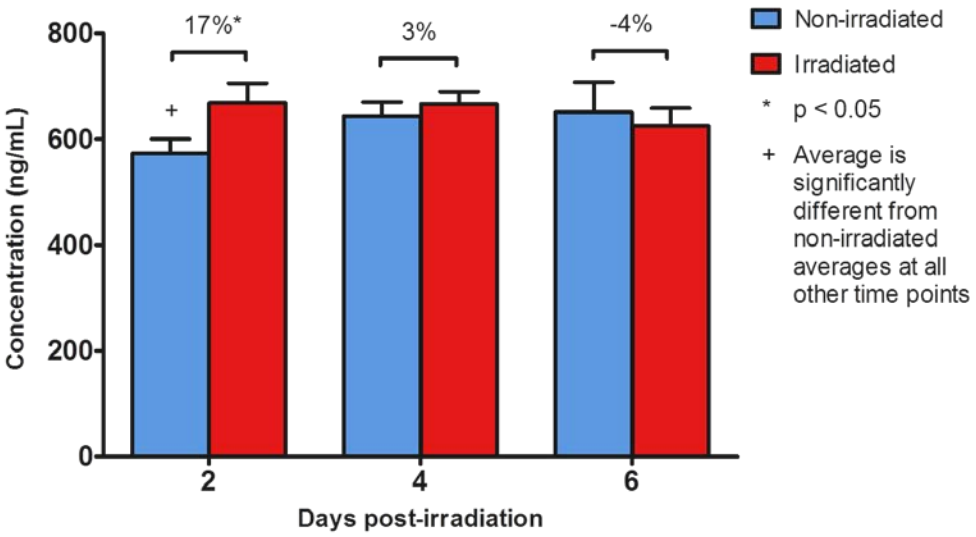

Figure 30: Serum osteocalcin levels of irradiated and non-irradiated groups 2, 4 and 6 day after exposure to an 8 Gy dose of X rays.

The serum concentration of TRAP5b was significantly higher in irradiated mice than controls at 6 days, but not at 2 or 4 days (Figure 31). There were no differences in the non-irradiated values, and no outliers were detected.

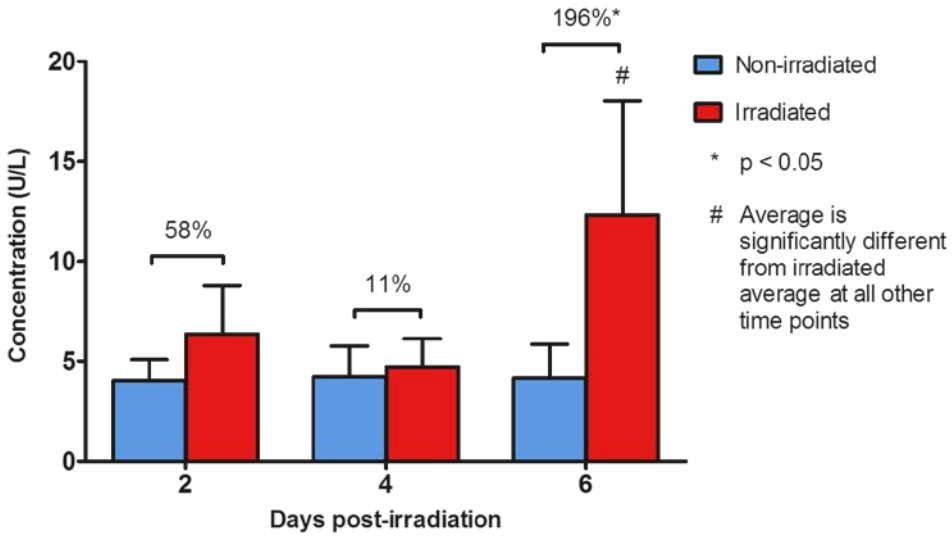

Figure 31: Serum TRAP-5b concentrations in irradiated and non-irradiated groups 2, 4, and 6 days after exposure to an 8 Gy dose of X rays.

Finite Element Analysis

FEA was performed to analyze the mechanical properties of bone non-destructively through computer simulation. Figure 32 below shows representative images of FEA compression test results for a whole bone and cortical section for an irradiated and non-irradiated bone. The stresses throughout the structure were used to quantify stiffness and efficiency, with lighter colors indicating higher stress. Also note the visible porosity in the cortex. Stiffness and efficiency of the whole bone, cortical bone only, and trabecular bone only as determined through FEA modeling are presented in this section.

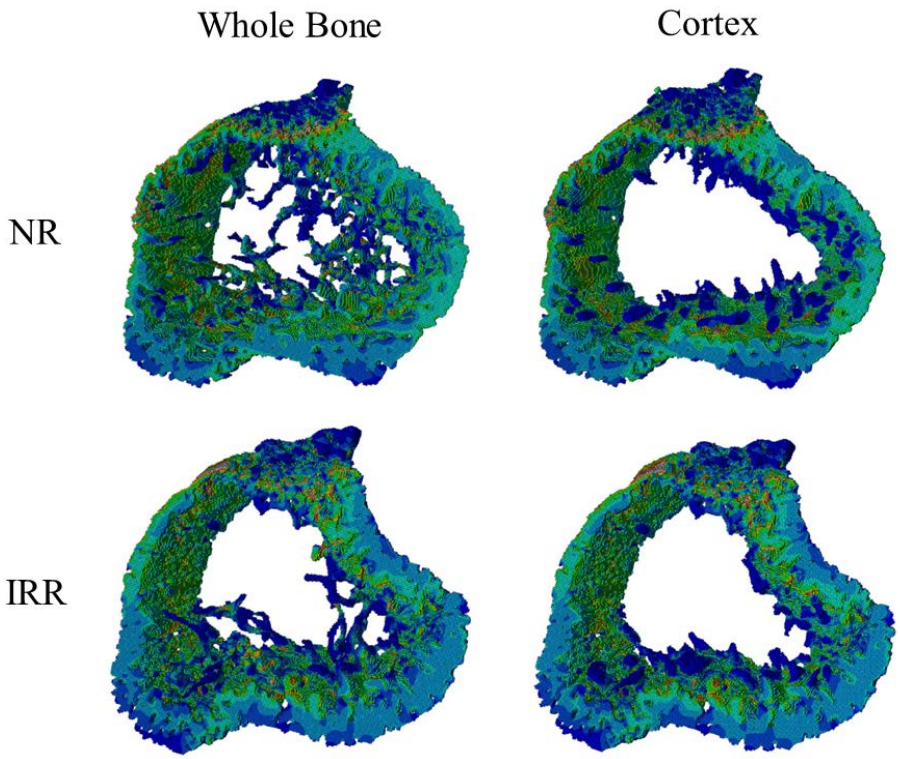

Figure 32: Finite element images of whole bone (left) and cortical bone (right) showing stress distributions after modeling a fixed displacement. The top row represents non-irradiated mice (NR) 6 days post-irradiation, while the bottom row shows an example from an irradiated mouse (IRR) at 6 days. Lighter colors indicate higher stress. Note the visible cortical porosity.

FEA determination of whole bone volume did not show any differences between irradiated and non-irradiated groups on any day (Figure 33). The volume of the irradiated groups did not significantly change throughout the study, but the 2 day non-irradiated group had more volume than the 4- and 6-day non-irradiated groups.

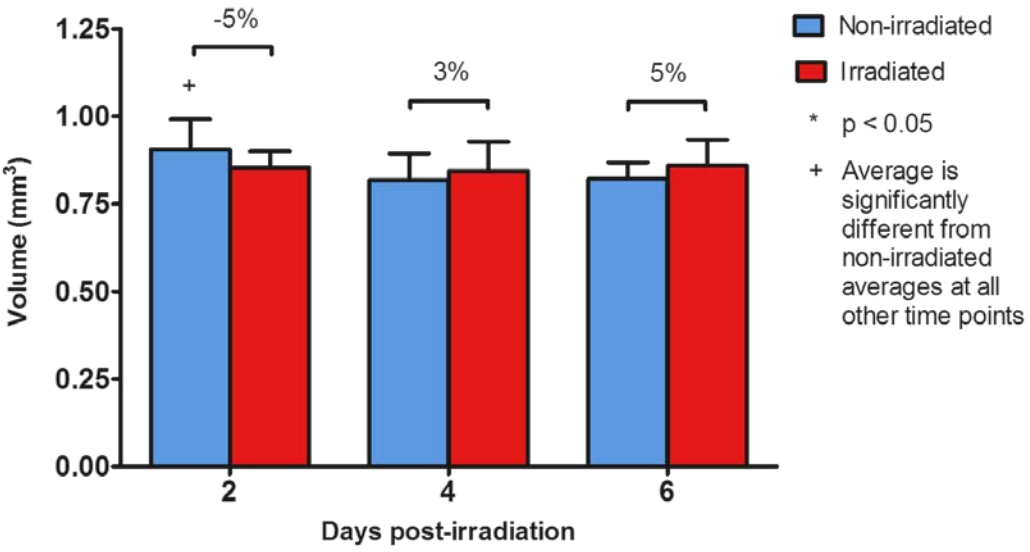

Figure 33: Whole bone volume as determined by FEA in irradiated and non-irradiated groups 2, 4, and 6 days after exposure to an 8 Gy dose of X rays.

Whole bone stiffness determined by FEA also did not show any statistically significant differences between irradiated and non-irradiated groups on any day, or between either group on different days (Figure 34).

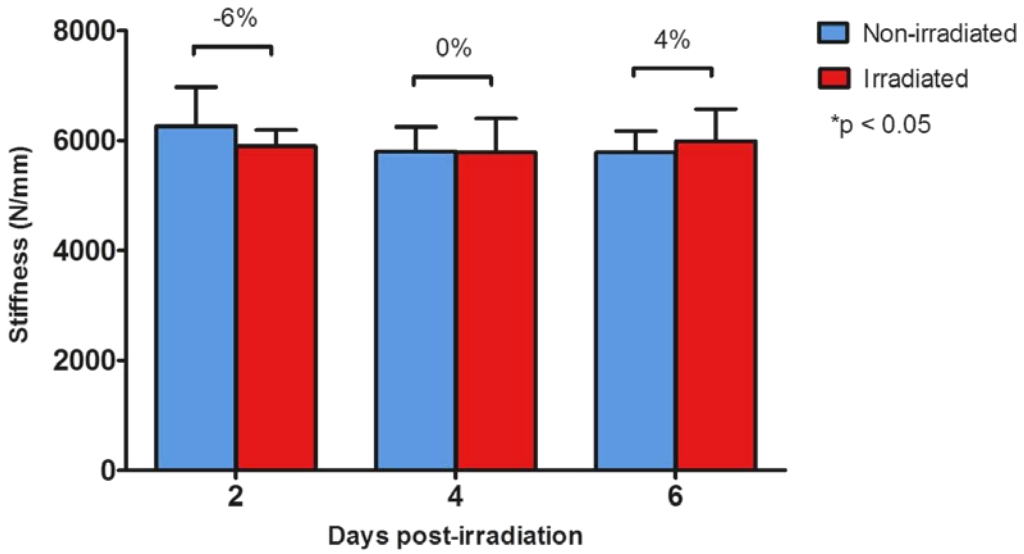

Figure 34: Whole bone stiffness as determined by FEA in irradiated and non-irradiated groups 2, 4, and 6 days after exposure to an 8 Gy dose of X rays.

Whole bone efficiency does not show any significant differences between irradiated and non-irradiated groups at any day (Figure 35). Likewise, efficiency of each group does not change from 2 to 6 days.

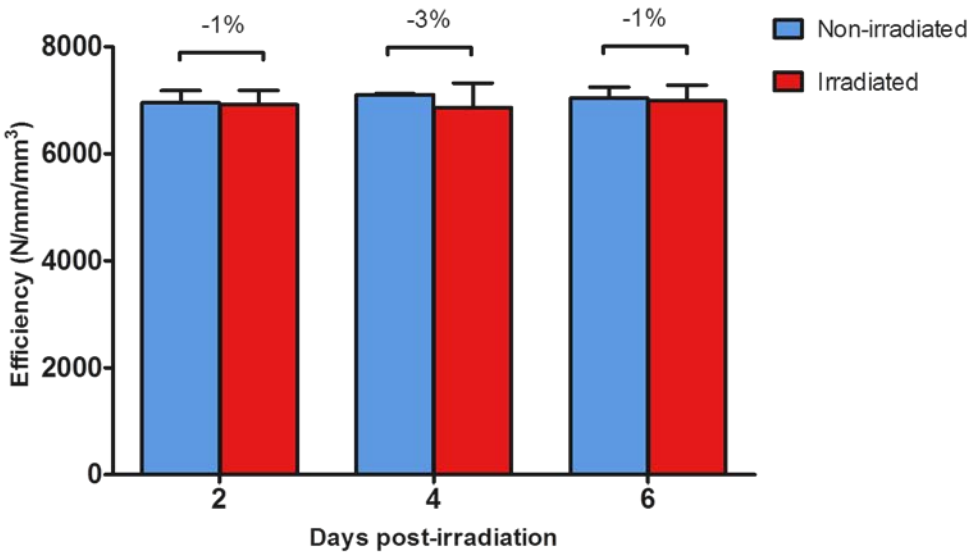

Figure 35: Whole bone efficiency as determined by FEA in irradiated and non-irradiated groups 2, 4, and 6 days after exposure to an 8 Gy dose of X rays.

Cortical bone volume was significantly greater in the irradiated group than non-irradiated controls at 6 days post-irradiation (Figure 36). The 2 day irradiated group was significantly larger than all other non-irradiated groups, while there was no significant difference among different values of IRR.

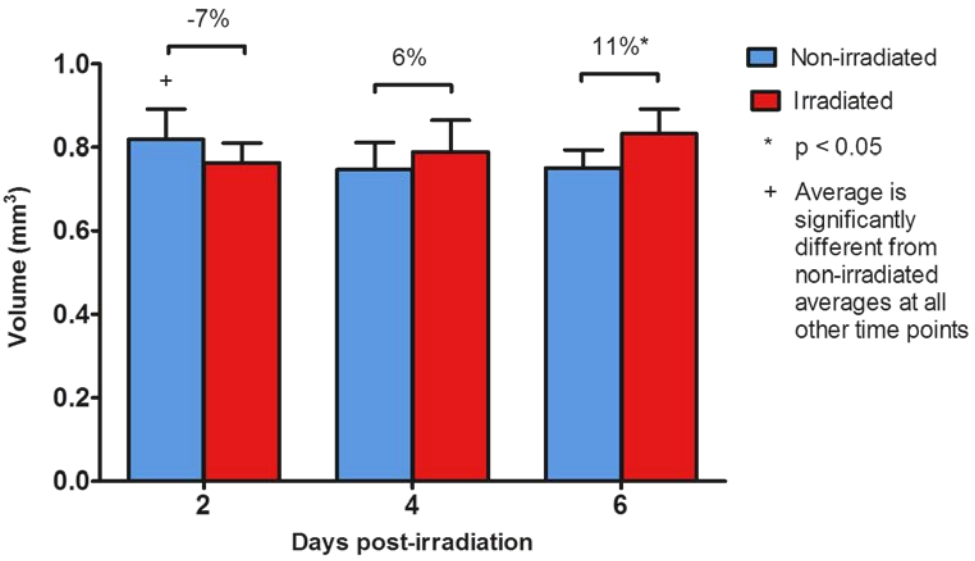

Figure 36: Cortical bone volume as determined by FEA in irradiated and non-irradiated groups 2, 4, and 6 days after exposure to an 8 Gy dose of X rays.

Cortical stiffness was significantly greater in irradiated mice than non-irradiated controls at 6 days post-irradiation (Figure 37). There were no significant differences between the values of NR or IRR across time points.

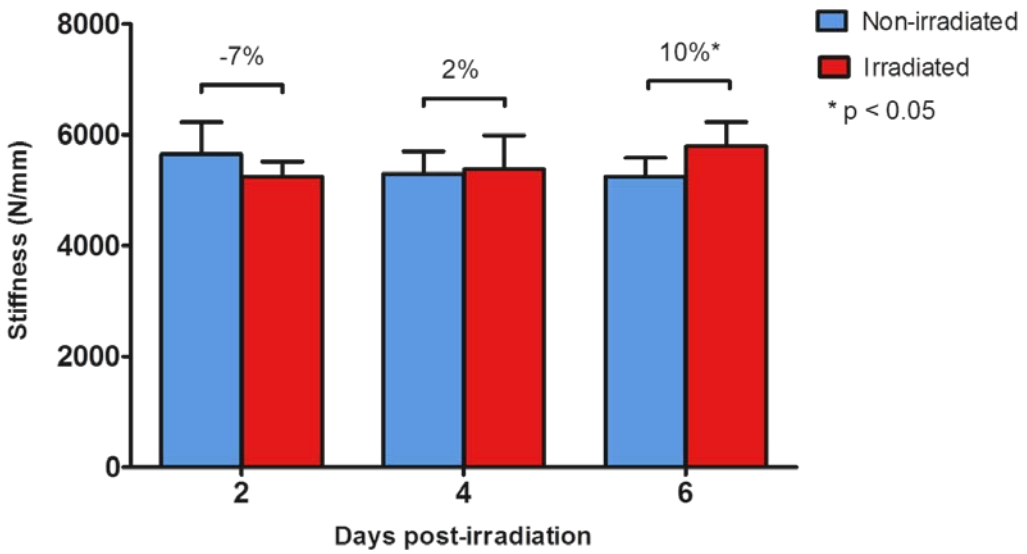

Figure 37: Cortical stiffness as determined by FEA in irradiated and non-irradiated groups 2, 4, and 6 days after exposure to an 8 Gy dose of X rays.

There were no significant differences in cortical efficiency among either radiation group (irradiated or non-irradiated) over different days, nor were there any differences observed between irradiated and non-irradiated groups (Figure 38).

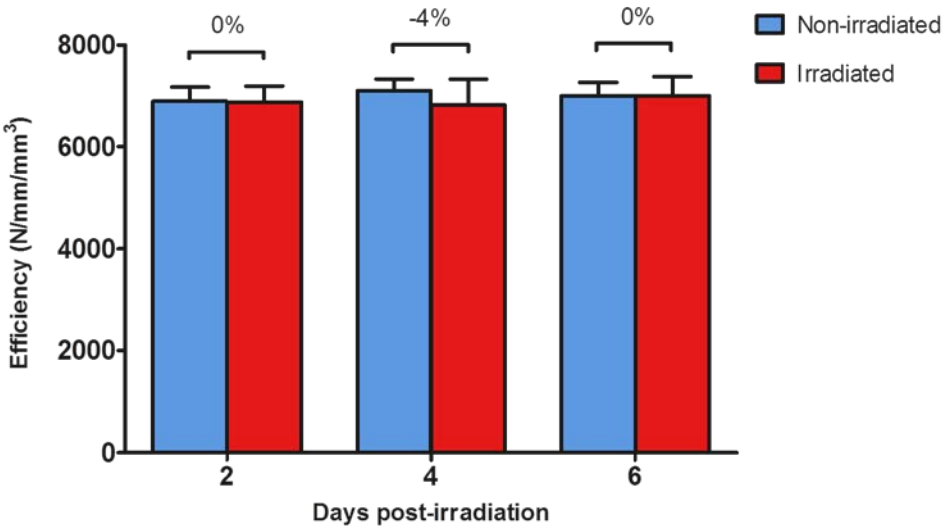

Figure 38: Cortical efficiency as determined by FEA in irradiated and non-irradiated groups 2, 4, and 6 days after exposure to an 8 Gy dose of X rays.

Trabecular bone volume was reduced by 77% in the irradiated group at 6 days post-irradiation (Figure 39). An increase in the irradiated group over controls was observed at 2 days, but was not statistically significant. No outliers were detected. Non-irradiated averages were similar across all time points, while irradiated averages exhibited a significant, steady decline at each day.

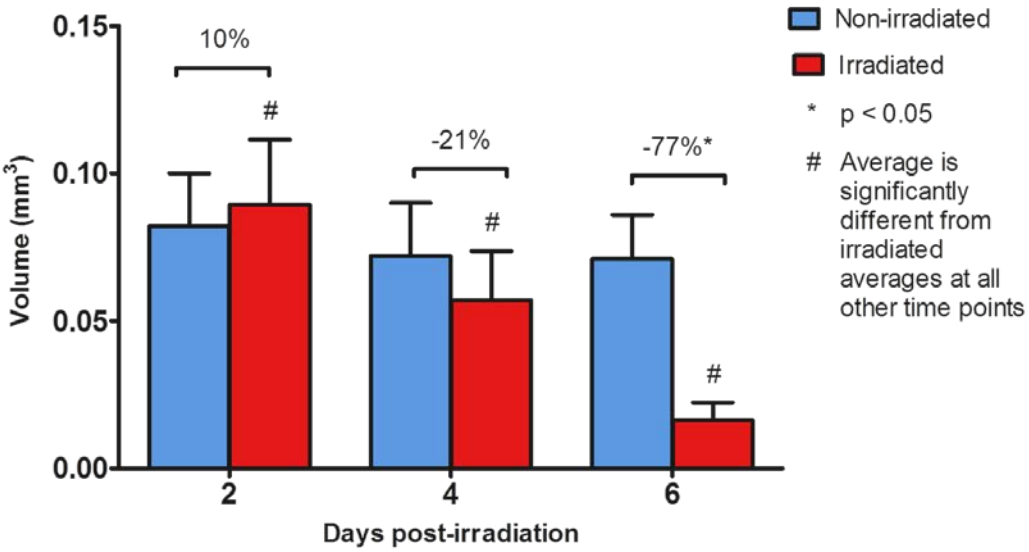

Figure 39: Trabecular bone volume as determined by FEA in irradiated and non-irradiated groups 2, 4, and 6 days after exposure to an 8 Gy dose of X rays.

Trabecular stiffness decreased dramatically in the irradiated group to 77% below control values at Day 6 post-irradiation (Figure 40). Non-irradiated averages were similar across all time points, while irradiated averages exhibited a significant, steady decline at each day.

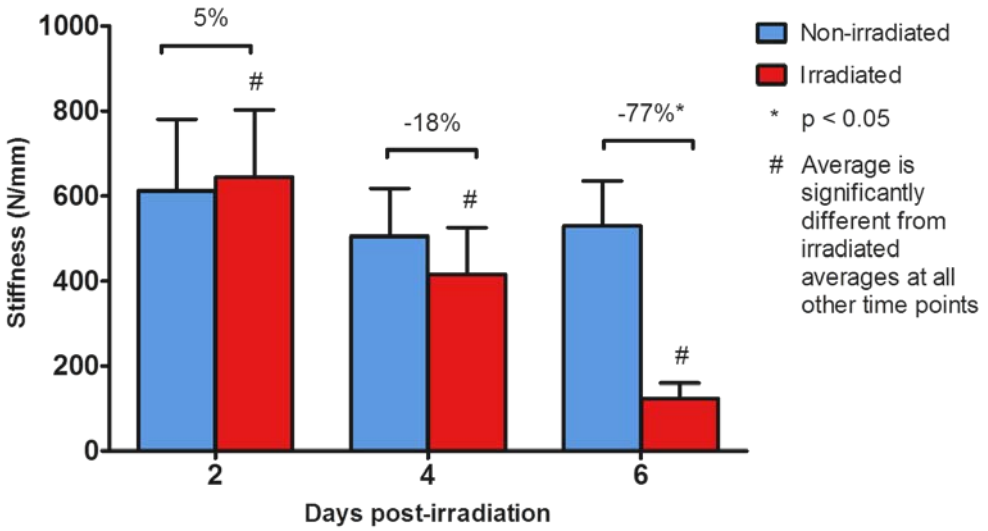

Figure 40: Trabecular stiffness as determined by FEA in irradiated and non-irradiated groups 2, 4, and 6 days after exposure to an 8 Gy dose of X rays.

There were no significant differences in trabecular efficiency among either radiation group (irradiated or non-irradiated) over different days, nor were there any differences observed between irradiated and non-irradiated groups (Figure 41).

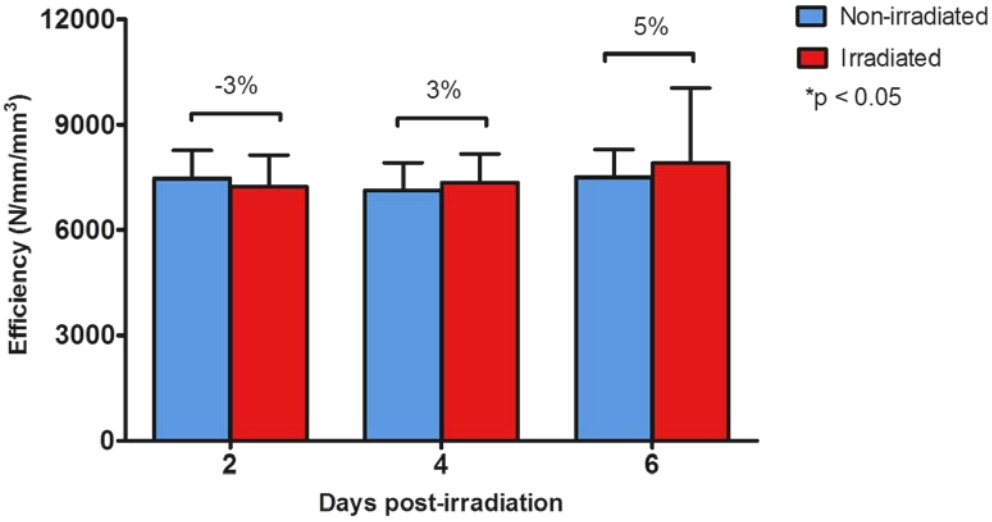

Figure 41: Trabecular efficiency as determined by FEA in irradiated and non-irradiated groups 2, 4, and 6 days after exposure to an 8 Gy dose of X rays.

Discussion

An increase in trabecular bone volume fraction was observed in irradiated mice at 2 days post-irradiation with an increase in serum osteocalcin levels, a biomarker of bone formation. By 6 days, this increase became decline and bone loss, coupled with an elevation in marker of osteoclast activity TRAP-5b. Here we discuss the findings from μCT, serum chemistry, and finite element analyses as they pertain to each other and previous observations in literature. We also present possible causes of the observed increase in BV/TV and subsequent loss, and mention possible sources of variation and literature comparison limitations.

Decreased Body Mass

Body mass declined by 8-15% in the irradiated group compared to non-irradiated controls. With an 8 Gy whole body dose of radiation, we would expect overall body mass to decrease, and death is expected to peak in 10 – 14 days (Storer, 1966); we therefore did not expect any fatalities within 6 days of radiation exposure. The young age of the mice and other side effects of radiation such as nausea and fatigue (Mogul, 2002) may have contributed to the rapid weight loss of the two mice from the irradiated group removed from the study.

Changing Microarchitecture

By 6 days post-irradiation, cortical bone volume was elevated in the irradiated group over control levels and was less porous than controls. Cortical thickness also increased in the irradiated group from 2 to 6 days, suggesting that the increase in cortical bone volume observed in the irradiated group relative to itself was due to cortical thickening and calcification to reduce pores after radiation exposure. Porosity in the non-irradiated control

group was observed to increase from 2 to 6 days, coinciding with a higher bone volume in the control group at 2 days compared to 6 days as well. Therefore, the response of the cortex to radiation exposure appears opposite in irradiated bones compared to non-irradiated bones, that is, cortical porosity normally increases in growing subjects an decreases cortical volume, but irradiated subjects exhibit an increase in cortical volume, thickening of the cortex, and decreased porosity.

In trabecular bone, BV/TV, TbTh, and TbN were all significantly elevated in the irradiated group at 2 days post-irradiation. This indicates that there was a rapid increase in trabecular bone just 2 days after irradiation, and that the additions were primarily due to thickening and increasing numbers of trabeculae. It is known that in skeletally mature subjects, an increase in trabecular number and connections is not possible (Allen & Burr, 2014), and trabecular thickening has been observed after radiation exposure (Willey et al., 2011). However, in young subjects, bone is still forming and thus it is still possible to increase the trabecular number (Buck & Dumanian, 2012). Therefore, it is plausible that a combination of these two phenomena were observed in this study at 2 days: trabecular thickness increased acutely after radiation exposure, and trabecular number increased as an alternative compensation to radiation damage because the mice were skeletally immature. Consistent with these increases, TbSp decreased slightly as would be expected with trabecular thickening and an increase in trabecular number, ConnD increased as expected for an increase in trabecular number, and vBMD also increased as expected with an increase in BV/TV, although none of these values were statistically significant. Nevertheless, they provide further evidence of an increase in bone through thickening of and additional trabeculae at 2 days post-irradiation in young mice.

To my knowledge, no significant increases in BV/TV within 2 days of radiation exposure have been documented yet in young mice. Several authors report no change in BV/TV 3-days after irradiation (Willey et al., 2008; Yumoto et al., 2010) or a decline in BV/TV 3-days after exposure in older mice (Kondo et al., 2009; Yumoto et al., 2010). An increase in BV/TV at 3-days after exposure has been documented in rats, along with an increase in TbTh (Sawajiri & Mizoe, 2003). Willey and Yumoto also reported no change in TbTh and TbN at 3-days, although their mice were skeletally mature (Willey et al., 2008; Yumoto et al., 2010). Consistent with our observations, Willey reports no differences between irradiated mice and controls in ConnD or TbSp at 3-days (Willey et al., 2008), and Yumoto reports either no change or a decline in ConnD relative to controls depending on the radiation dose (Yumoto et al., 2010).

Similar to our findings, Green et al report an increase in BV/TV 2 days after exposure to a 5 Gy whole body dose of gamma rays (Green et al., 2012). However, their mice were older (8 weeks) and exhibited only trabecular thickening, unlike our 5-week-old mice, which showed trabecular thickening with an increase in trabecular number and connectivity. It is likely that the response is similar in mature and growing mice as evidenced by the increase in BV/TV in both cases. However, the differences in cellular response and long term effects due to continuing skeletal maturation after irradiation in the younger mice are still unknown.

At 6 days post-irradiation, we observed the dramatic decline in bone mass expected with radiation exposure. BV/TV and vBMD were 70% lower in the irradiated group compared to controls. Trabecular number and connectivity density were 37% and 94% lower in the irradiated group than controls, respectively, indicating that bone loss was primarily carried out through the destruction and separation of trabeculae. Consistent with this,

trabecular separation was 63% greater in irradiated mice than controls. Trabecular thickness of the irradiated group was significantly reduced from 4 days to 6 days so that it was no different in irradiated or control mice at 6 days, providing further evidence that young mice respond to radiation in a similar fashion as their skeletally mature counterparts by losing trabecular number and connections in the location with the most surface area, and thickening trabeculae as observed at 2 days.

This bone loss response to radiation exposure through loss of trabecular number and connectivity by 6 days is well documented. For instance, Green and Willey both report decreases in BV/TV in irradiated groups with a loss of TbN and ConnD and increases in TbSp (Green et al., 2012; Willey et al., 2010) consistent with our observations. In addition, several other studies also confirm loss of BV/TV after irradiation (Kondo et al., 2009; Wernle et al., 2010), and may parallel one or more other select observations such as the decline in ConnD (Keenawinna et al., 2013; Kondo et al., 2009), increase in TbSp (Keenawinna et al., 2013; Kondo et al., 2009; Wernle et al., 2010), and consistent TbTh (Cao et al., 2011; Keenawinna et al., 2013; Sawajiri & Mizoe, 2003).

Elevated Biomarkers

Serum osteocalcin (a marker of osteoblastic bone formation) levels were significantly elevated in the irradiated group at 2 days compared to controls, but were within the expected range for 5-week old B6 mice (Li et al., 2002) and similar to controls at 4 and 6 days. This suggests that increased osteoblast activity plays a role in the increase in BV/TV observed with μCT at 2 days, but reduced activity is not present and does not impact the subsequent loss. Willey et al also report similar osteocalcin levels between irradiated and non-irradiated groups at 1-week post-irradiation (Willey et al., 2010), although they did not observe the

increase in osteocalcin at 3-days in older mice (Willey et al., 2008). The observed increase in BV/TV in our study suggested from increased osteoblast activity and reduction in BV/TV from increased osteoclast activity is further supported by the serum TRAP-5b analysis.

Serum TRAP-5b (a marker of osteoclastic bone resorption) levels were only significantly elevated at 6 days post-irradiation. This suggests that highly increased osteoclast activity is a significant factor in the bone loss observed at 6 days. Furthermore, a non-statistically significant increase in TRAP-5b levels at 2 days suggests that reduced osteoclast activity is not present and does not contribute to the increase in BV/TV observed at 2 days. It is expected that osteoclast activity is elevated at the onset of bone loss to resorb bone. It is also understood that the areas within bone with the most surface area are most susceptible to bone resorption, which would be the cancellous bone. Thinner trabeculae are at the highest risk of separation and complete resorption due to the mere size of osteoclasts. Thus, it is conceivable that the increase in TbN and ConnD observed at 2 days would stand the greatest risk of bone resorption at 6 days simply because the trabeculae have not had time to fully mineralize. Indeed, we also observed significant reductions in TbN and ConnD at 6 days in the irradiated mice. Trabecular thickness was not spared either, with significant reductions in the thickness of 6 day irradiated bones compared to 4 day irradiated bones, reducing TbTh to near normal levels. This increase in TRAP-5b levels has been observed in other studies within 3-10 days of radiation exposure (Green et al., 2012; Willey et al., 2008; Willey et al., 2010), along with the corresponding microarchitectural losses previously described.

Functional Compensation

Even with radiation exposure, whole bone volume, stiffness, and efficiency did not change among irradiated and non-irradiated groups. This suggests that within 6 days of

radiation exposure, bone as a complete system remains structurally sound. However, analysis of cortical and trabecular sections separately provide more insight. From the μCT analysis, we saw that trabecular bone was significantly affected by radiation exposure. Finite element analysis confirms the loss of BV/TV and vBMD at 6 days, registering a 77% loss each in trabecular bone volume and stiffness. Trabecular bone was no less effective at bearing loads, as indicated by similar values of trabecular efficiency at all days. However, the significant loss of trabecular bone volume present without changes in whole bone properties suggests a compensatory mechanism for loss of trabeculae. Indeed, there were significant increases in cortical volume and stiffness at 6 days that paralleled the loss of trabecular bone.

The cortical shell supports about 10% of a load under uniform stress and about 64% of the load under uniform displacement (Silva et al., 1997). Ito et al suggested that the cortical shell may transfer even more load from the trabeculae if the trabeculae are deteriorated to maintain stability of the entire bone (Ito et al., 2002). It is known that loss of trabecular number or connectivity can reduce bone stiffness and strength up to three times more than reducing trabecular thickness (Burr & Akkus, 2014), and that osteoporotic bones can exhibit up to 10 times higher maximum stress than healthy bones in highly loaded regions (Müller et al., 2014). Also, a strong correlation between cortical yield strength and cortical bone volume has been identified (Ito et al., 2002), suggesting that if trabecular bone is greatly reduced, as occurs with radiation exposure, cortical bone should thicken to maintain overall strength of the bone as a whole. Our study supports these claims, evidenced by the fact that we observed cortical stiffness and volume increase with the reduction of trabecular bone for a net maintenance effect on the whole bone after radiation, as determined through FEA.

FEA is a fairly new method used to analyze structural properties of bone. Most papers at present on the topic focus on the construction of models for use with bone. However, a few groups have used it to gain insight on their studies. Wernle et al observed that irradiated femora were stronger than controls at 2 weeks post irradiation but weaker by 12 weeks and suggested that trabecular architecture and properties of bone structure should be analyzed in addition to the amount of bone present to explain loss of bone strength (Wernle et al., 2010). Our FEA observations that whole bone stiffness and efficiency are unaltered with radiation, but that cortical stiffness increases while trabecular stiffness decreases, support this suggestion by providing evidence of where and how bone loss is occurring after radiation, as detected in cortical and trabecular sections using FEA. Similar to our findings, other groups have also reported a lack of change in compressive strength and whole bone stiffness 4-weeks after irradiation with FEA (Keenawinna et al., 2013; Kondo et al., 2009).

Increased Bone Mass Before Decline

There are several possible explanations for the increase in BV/TV observed in young mice at 2 days post-irradiation. First, our study suggests increased osteoblast activity at 2 days with normal osteoclast activity. This agrees with a previous report of significantly fewer osteoclasts and chondroclasts between 0.5-2 weeks post-irradiation (Margulies et al., 2003). However, others have observed significant increases in osteoclast number and surface as early as 3-days post-irradiation (Kondo et al., 2009; Willey et al., 2008). It is possible that there were more osteoclasts in the present study at 3-days, but there was no evidence observed of a significant increase in osteoclast activity or bone loss effects until 6 days.

A second possible explanation for the observed elevation in BV/TV at 2 days is a rapid mineralization response of the osteoid to radiation in young mice, which would also

coincide with the observed increase in osteoblast activity at 2 days. An early and transient increase in vBMD and mineral apposition rate has been reported within one week of radiation exposure (Willey et al., 2010), which may have significant additive effects before osteoclast over-activation in young mice. Furthermore, soft tissue ossifications have been observed in several diseases and post-traumatic clinical settings (Kalenderer et al., 2012), and hemophilia studies identified soft tissue calcifications and bone loss within 2 weeks of joint bleeds (Lau et al., 2014). We suspect that a similar mechanism of rapid mineralization may be contributing to the increase in bone at 2 days in young mice, possibly due to the shared characteristic of inflammation. Lack of clotting factors causes inflammation in joint bleeds as a result of trauma in hemophilia patients. In radiotherapy, radiation exposure is the trauma, and inflammation occurs as macrophages remove dead cells.

The large decline in BV/TV by 6 days post-irradiation was expected, as bone loss has been found to occur within 7-10 days of radiation exposure (Green et al., 2012; Kondo et al., 2009; Willey et al., 2010). This effect is largely attributed to osteoclast activity. Radiation is known to stimulate osteoclast differentiation (Yumoto et al., 2010), and increased numbers of osteoclasts and osteoclast expression have been reported multiple times after radiation exposure (Kondo et al., 2009; Margulies et al., 2003; Willey et al., 2008; Yumoto et al., 2010). The elevation of TRAP-5b serum levels and normal osteocalcin levels in our study agree with these observations. Inflammation due to radiation induced trauma also contributes to heightened osteoclast activity, as some inflammatory mediators also promote osteoclast differentiation and activity (Abu-Amer, 2009) and are known to correlate with bone loss in adults (Ding et al., 2008). Body mass is unlikely to have contributed detectable effects on bone structure due to the short time course of this study (Yumoto et al., 2010).

Sources of Variation

A large scattering in data is common in animal experiments on bone (Müller et al., 2014), and large variations in bone growth and metabolism are expected with growing subjects (Huang et al., 2011). While it is impossible to remove all variation among subjects and sources of variation, it is possible to reduce the amount of variation observed.

Animal mass and size is uncontrollable to the researcher for experiments that take place over several days. Although body mass would normally influence the amount of bone observed, animal growth or weight loss was less of a factor in this study due to the very short duration (Yumoto et al., 2010), despite inconsistent growth rates among growing animals. Nevertheless, at study onset mice were grouped to normalize weights among individuals to mitigate any variation that may occur.

Differences in individual developmental stage, particularly of the skeleton, are also a concern in growing animals. Peak skeletal growth occurs in mice between 6 and 12 weeks of age, but the growth plate never fully closes (Keenawinna et al., 2013). Skeletally immature bones are very porous and composed of woven bone that is replaced by lamellar bone with maturation (Humphries, 2011). Ossification occurs from diaphysis to metaphysis (Humphries, 2011), increasing bone density as the skeleton matures. Although mice are the same age, mice that are developing more rapidly would be expected to have greater bone density and less porosity than average. Furthermore, the rate of mineralization is likely different among individuals. Using mice that are the same age, grouping them based on body mass, and choosing short-duration time points are all attempts to reduce variability from animal growth and maturation.

μCT cortical and trabecular sections are created by manual delineation of the cortical boarder, introducing possible variation in borderline areas considered cortical or trabecular bone. This is especially difficult in young mice due to the porosity of the cortical bone in the metaphysis. To mitigate these effects, the same person traced all bones in the study and provided consistency with borderline decisions of cortical and trabecular bone.

μCT also requires the user to select a threshold for mineralized material to identify bone on a binary basis. This is an imperfect system especially with constant bone remodeling, as newly formed osteoid is not as dense as older bone and will not be identified as bone regardless of the quantity. Threshold selection must be made to include as much visible bone as possible while excluding artifacts to reduce this source of variation. Again, rate of mineralization among individuals plays a role in introducing variation, although the short duration of the study and choosing homogeneity of animal age and mass within groups reduces this effect.

Blood serum and ELISA assay materials can also introduce variation. There may be slight differences in the amounts of biomarker of interest distributed throughout the serum, skewing results depending on concentration in the amount tested. To account for this, serum is mixed before sampling, and multiple trials of the same sample are tested and averaged for each individual. Enzymes and antigens included in ELISA kits also have limited shelf-lives, which may affect biomarker detection. This variation is reduced by requesting materials manufactured at the same time from the supplier, and using kits soon after arrival.

Comparison Limitations

Several factors should be considered when comparing results of this study to those found in literature. First, radiation dose, type, and administration all affect study outcomes. X

rays were used in this study as opposed to other radiation types such as iron ions (Yumoto et al., 2010), cesium-137 (Kondo et al., 2009), and carbon ions (Sawajiri & Mizoe, 2003) seen elsewhere in literature. We used a single 8 Gy dose of radiation, while others have used amounts of 50 cGy (Yumoto et al., 2010), 2 Gy (Kondo et al., 2009; Willey et al., 2008; Willey et al., 2010; Yumoto et al., 2010), 5 Gy (Green et al., 2012; Wernle et al., 2010), and 20 Gy (Keenawinna et al., 2013; Wernle et al., 2010), and multiple fractions (Cao et al., 2011). Our study also used whole body irradiation, while others have irradiated only the hind limb, particularly in large doses (Keenawinna et al., 2013; Margulies et al., 2003; Sawajiri & Mizoe, 2003).

Second, study subjects chosen and time points analyzed provide different outcomes. It should be noted that C57BL/6 mice may have slightly different developmental trajectories than other strains or species (Li et al., 2002), such as Balb/c mice (Wernle et al., 2010) or Wistar (Ito et al., 2002; Sawajiri & Mizoe, 2003) or Sprague-Dawley rats (Margulies et al., 2003). The age of our animals was also quite young at 5-weeks, whereas other studies use skeletally mature mice, usually between 8-weeks and 20-weeks of age (Green et al., 2012; Keenawinna et al., 2013; Wernle et al., 2010; Willey et al., 2010). Different time points should also be taken into consideration, with our time points occurring early at 2, 4, and 6 days post-irradiation, while others commonly analyze bone over one week after (Green et al., 2012; Kondo et al., 2009; Willey et al., 2010) or within months (Keenawinna et al., 2013; Wernle et al., 2010) of exposure.

Lastly, analysis tools also have their limitations. Computed tomography analysis and finite elements are limited to certain resolutions and element size. Also, although models have been found useful to determine mechanical contributions of cortical and trabecular bone

(Ito et al., 2002), models assume a perfect engineering material with the properties specified by the user. This inherent limitation will always introduce at least minor differences between computer models and biological materials.

CHAPTER 6: CONCLUSIONS

Our hypothesis was correct that a marrow ablating dose of radiation would cause significant amounts of bone loss observable within days of radiation exposure with elevated osteoclast activity, and that this loss would have significant functional effects on the mechanical properties of bone. We characterized bone loss in young mice from a marrow-ablating dose of radiation by quantifying the amount of bone loss and changes in mechanical properties of whole, cortical, and trabecular bone, and provided evidence of the cellular role of osteoclasts at 6 days. We found a 70% reduction in BV/TV in irradiated mice compared to controls after exposure to an 8 Gy dose of X rays at 6 days, or about one week, as expected and observed by other groups (Green et al., 2012; Kondo et al., 2009; Willey et al., 2010). We saw higher TRAP-5b levels in irradiated mice than controls, evidence that osteoclast activity was heightened. We also observed significant 77% losses in trabecular bone volume and stiffness but 10% increased cortical volume and stiffness for overall maintenance of whole bone efficiency between irradiated and control groups. This suggests that an opportune time frame for intervention is within the first week after radiation exposure to mitigate or prevent radiation therapy induced bone loss in pediatric cancer patients.

However, we also conclude that the complete opposite of our hypothesis was true at 2 days post-irradiation in young mice. We unexpectedly observed that an 8 Gy dose of X rays resulted in significant increases in bone volume within 2 days of radiation exposure with elevated osteoblast activity, and that this increase had no functional effects on the mechanical properties of bone. We quantified a significant 16% increase in bone mass after a marrow

ablating dose of X rays, and saw evidence of osteoblast activity in the 17% increase of serum osteocalcin in irradiated mice. We also quantified zero significant changes in whole, cortical, or trabecular bone at 2 days post-irradiation. This suggests that the optimal time for intervention is around 2 days after radiation exposure to prevent radiation therapy induced bone loss or promote increased bone mass in pediatric cancer patients.

The overall goal of this research and subsequent studies that add bone marrow transplantation and chemotherapy is to develop a model that characterizes bone loss due to cancer treatment in ALL patients. Toward this goal, this study quantified a 70% loss of BV/TV and bone stiffness, and found evidence for heightened osteoclast activation for a marrow ablating dose of radiation 6 days post-irradiation. Although bone loss has been documented following radiation exposure, there are few studies that investigate the combination of young subjects and time points less than one week after exposure. This study characterizes the gap in knowledge of the effects of radiation exposure on young subjects to contribute to the improvement of care for pediatric ALL patients.

CHAPTER 7: IMPROVEMENTS AND FUTURE WORK

Introduction

This study characterized bone loss from a myeloablating dose of radiation in young mice. It will be used to understand treatment related bone loss in children undergoing radiation, chemotherapy, and bone marrow transplantation for ALL. Improvements to the current study include adding histology to quantify osteoblasts and osteoclasts, increasing group size to account for premature deaths, modifying the dose amount and administration to better reflect clinical experiences, and considering an alternative marker of bone formation. In the future, this study will be correlated to clinical findings of bone loss in pediatric cancer therapy patients, and the model will be expanded to include bone marrow transplantation and chemotherapy.

Improvements

The four main improvements to this study are to include histology, adjust the dose given to mice to correspond to the dose administered for ALL, use more mice per group to account for premature death, and use a different biomarker of bone formation.

Histology

Histology is needed to confirm osteoblast and osteoclast numbers and activity relative to controls. Serum chemistry was tested for concentrations of bone formation and resorption biomarkers (osteocalcin and TRAP-5b, respectively) using ELISAs. High concentrations suggest higher numbers and increased activity of osteoblasts or osteoclasts, but are not definitive because biomarker concentrations are measures of an effect of cell activity.

Histology will visibly look for the cells themselves in bone samples, and can quantify osteoblast and osteoclast numbers and surface area to determine whether increased biomarker levels are a result of increased cell numbers or activity. We would expect the number of osteoclasts to be heightened at 6 days post-irradiation to coincide with the increases in osteoclast number and surface area described previously in literature (Willey et al., 2008).

Corresponding Dose

The overall goal of this research is to use mice to model the effects of radiation, chemotherapy, and bone marrow transplantation treatments on bone in children with ALL. To more accurately portray bone loss from human clinical doses used in ALL treatment, the corresponding dose should be administered to mice and account for their differences in radioresistance. The median lethal dose for humans within 60 days is between 2.5 and 5 Gy, and cancer patients undergoing radiation therapy can experience up to a 12 Gy total dose administered by fractionation (Green & Rubin, 2014). The median lethal dose for C57BL/6 mice within 30 days is about 8 Gy (Green & Rubin, 2014). These limits and fractionation should be taken into account for subsequent studies to accurately portray the human condition, or may serve as a limiting factor for comparison of study results and clinical findings.

Increase Group Size

In our experiment, 20% of the mice in our irradiated group that were supposed to be analyzed in the 6-day time point did not make it to 6 days due to the decline of their overall health. Although this was not expected until later time points (Storer, 1966), knowing there is a risk of premature death within one week of radiation exposure allows compensations to be built into future studies. One possibility is to increase the number of mice in each group at

each time point by 5 mice, or one cage in this study. This would ensure enough samples to maintain statistical power and significance in the 6 day irradiated group even with the potential loss of a small number of individuals before 6 days. It would also provide a larger sample size that could help to reduce standard deviations in serum chemistry analyses due to individual responses. This may be useful with a combination of radiation exposure and BMT in a subsequent study due to the significant morbidity and mortality associated with BMT (Bashie & Champlin, 2014), even though BMT is intended to treat hematopoietic failure from irradiation (Domen et al., 2011) and thus improve overall survival after radiation exposure.

Alternative Bone Formation Biomarker

An alternative bone formation marker, such as BSAP or procollagen type 1 N-terminal propeptide (P1NP), may be preferred over osteocalcin in subsequent studies. Osteocalcin is a product of osteoblasts, deposited into the bone matrix by osteoblasts but released from the matrix by osteoclastic resorption (Rodrigues et al., 2010). It is present in the blood for bone turnover or formation, and there is a small amount present all the time that has been released from resorption adding to OC levels due to formation (Christenson, 1997). Osteocalcin may therefore reflect bone remodeling in general or different stages of osteoblast activity, not necessarily bone formation (Domen et al., 2011; Sebestyen et al., 2012). In addition, there are negative correlations between serum OC levels and bone density (Li et al., 2002), and serum OC and bone strength and stiffness (Rodrigues et al., 2010).

BSAP is not released from the matrix by osteoclast activity like osteocalcin, and it is also used clinically as an indicator of bone metabolism (Christenson, 1997). BALP also does not have a significant circadian variation, while osteocalcin can vary by 10-20% in children,

usually with higher values at night (Schönau & Rauch, 2003). BALP therefore would still be comparable to current clinical methods, and a possible replacement for osteocalcin testing. Both alkaline phosphatase (Yumoto et al., 2010) and osteocalcin (Willey et al., 2008) have been used to assess osteoblast activity and bone turnover in mice. Osteocalcin and BSAP are both commonly used to assess bone formation and bone turnover in children and adolescents (Fares et al., 2003; Huang et al., 2011; Ooi et al., 2012; Tuchman et al., 2008). P1NP has also been used for children (Huang et al., 2011) and adult samples (Rodrigues et al., 2010), although much less frequently.

Future Work

To model the effects of ALL treatment on the bones of young subjects, radiation, bone marrow transplantation, and chemotherapy all need to be taken into account and correlated to the clinical condition. This study characterized the effects for a marrow ablating dose of radiation on bone, the same type of dose used in ALL treatment. The next step is to correlate findings from this radiation study on young mice to those found in the hospital setting.

Findings from this study will be correlated to the clinical condition. We plan to assess bone biomarkers and DXA or CT scans from children undergoing radiation treatment for ALL in the University of North Carolina (UNC) Children's Hospital in Chapel Hill, North Carolina, and compare them to our current findings. Osteoclast activity is known to increase after radiation exposure (Green & Rubin, 2014), and elevated osteoclast numbers, TRAP-5b levels, and deoxypyridinoline/creatinine levels have increased after irradiation (Willey et al., 2008) and in children with chronic disease (Tuchman et al., 2008). BSAP was reduced in children with chronic disease (Tuchman et al., 2008) but is normally elevated along with

osteocalcin in adolescents (Fares et al., 2003), and our study found no change in osteocalcin levels at 4 and 6 days after irradiation in young mice. We would expect serum chemistry results to show similar trends to our study, and fall within the reference intervals established by Huang et al (Huang et al., 2011).

After the clinical assessment, bone marrow transplantation and chemotherapy treatment will be added to the model one at a time. Bone marrow transplantation is expected to improve long-term survival and must be performed soon after myeloablation to repopulate stem and immune cells. Clinical total body irradiation in preparation for bone marrow transplantation is most commonly combined with the chemotherapeutic drug cyclophosphamide (Mogul 2002). Cyclophosphamide and busulfan are both used as preparative regimens at UNC.

CHAPTER 8: IMPLICATIONS

Overall, this research adds to current knowledge of the effects of ALL and associated radiation, bone marrow transplantation, and chemotherapy treatments on bone, and completes another step toward improving the long-term quality of life in ALL survivors. This study is an illustration of the significant bone loss associated with radiation therapy in young subjects. It demonstrates that bone loss in young subjects occurs very quickly after radiation exposure, and suggests that bone loss intervention for the growing number of ALL survivors must occur within a few days of radiation exposure at the latest.

This study provides further evidence of bone loss associated with radiation therapy by demonstrating that there is significant bone loss in young subjects after radiation exposure. Total body irradiation is known as the primary contributor to reduced BMD in ALL patients (Weilbaecher, 2000) and poses a 75% greater risk of developing musculoskeletal abnormalities and impairment than children who do not receive radiation (Armenian et al., 2011). The greatest amount of bone loss occurs during therapy, as bone deterioration begins early and persists throughout treatment, and bone properties uncouple (Mussa et al., 2010). This is consistent with our observations that significant amounts of bone loss are observed even within the first week after irradiation.

This study demonstrates that bone loss in young subjects occurs very quickly after radiation exposure, and confirms that bone loss can be observed within one week (Willey et al., 2010) even in young subjects. This suggests a very limited window of opportunity after exposure for bone loss intervention for the growing number of ALL survivors, with a best-

case scenario of 6 days post-irradiation and an expected window of 4 days post-irradiation to maintain normal skeletal mineral density and microarchitecture. Therefore, patient bone mineral density should be monitored within the first days or weeks of treatment so that pharmacologic intervention can be initiated at a T-score of less than -1 to prevent fractures (Siris et al., 2004), not just 6 months after treatment when irreversible bone degradation has already occurred (Mussa et al., 2010).

By demonstrating bone loss from a clinical marrow ablating dose of radiation that occurs less than one week after exposure and providing evidence for the osteoclastic mechanisms through which it occurs, clinicians can increase their knowledge of treatment side effects and apply appropriate preventative measures to provide better care for their patients. Researchers can expand upon these findings to determine more precise causes of such a large acute loss, and develop treatments for specific targets in children exposed to radiation therapy. Translational research can and should continue to test current adult osteoporosis drugs for safety and efficacy in children, and should include research on safety and efficacy when used in combination with radiation, bone marrow transplantation, and chemotherapy.

APPENDIX A: TABLES OF AVERAGES, STANDARD DEVIATIONS, AND PERCENT DIFFERENCES FOR BODY MASS AND µCT, ELISA, AND FEA PARAMETERS

This appendix contains tables of averages, standard deviation, and percentage differences for µCT, ELISA, and FEA parameters. All data are presented as mean ± standard deviation. NR = non-irradiated, IRR = irradiated, %Diff = percentage difference between irradiated and non-irradiated averages on a given day. An asterisk (*) indicates statistical difference between irradiated and non-irradiated averages ($p < 0.05$). A pound sign (#) indicates the irradiated average is significantly different from irradiated averages at all other time points. A plus sign (+) indicates the non-irradiated average is significantly different from non-irradiated averages at all other time points. Two pound signs (##) indicate the irradiated average is significantly different from irradiated averages with the same designation. Two plus signs (++) indicate the non-irradiated average is significantly different from non-irradiated averages with the same designation.

Table A. 1: Body mass. Averages and standard deviations of body mass for irradiated and non-irradiated groups 2, 4 and 6 days post-irradiation.

	Non-irradiated (g)	Irradiated (g)	% Difference
Day 0			
Day 2	15.8 ± 0.06	14.5 ± 0.6	-8.2 *
Day 4	16.1 ± 0.9	14.8 ± 0.5	-8.1 *
Day 6	16.3 ± 1.0	13.8 ± 1.3 #	-15 *

Table A. 2: Cortical microarchitectural parameters (µCT). Averages and standard deviations of microarchitectural parameters from µCT analysis for irradiated and non-irradiated groups 2, 4 and 6 days post-irradiation.

		CtPo (%)	CtBv (mm^3)	CtTh (mm)	pMOI (mm^4)
Day 2	NR	31.6 ± 2.2 +	0.902 ± 0.077 ++	0.101 ± 0.008	0.719 ± 0.74
	IRR	32.5 ± 1.3	0.843 ± 0.042	0.097 ± 0.004 ##	0.644 ± 0.070
	% Diff	3.0	-6.4	-4.0	-10.4 *
Day 4	NR	34.1 ± 0.9	0.833 ± 0.071	0.096 ± 0.003	0.668 ± 0.091
	IRR	32.3 ± 3.4	0.864 ± 0.080	0.098 ± 0.012	0.648 ± 0.075
	% Diff	-5.1	3.8	2.5	-3.0
Day 6	NR	34.3 ± 1.5	0.830 ± 0.047 ++	0.099 ± 0.006	0.651 ± 0.043
	IRR	30.3 ± 1.4	0.913 ± 0.063	0.106 ± 0.008 ##	0.659 ± 0.070
	% Diff	-11.6 *	10.0 *	7.0	1.1

Table A. 3: Trabecular microarchitectural parameters (µCT). Averages and standard deviations of microarchitectural parameters from µCT analysis for irradiated and non-irradiated groups 2, 4 and 6 days post-irradiation.

		BV/TV	vBMD (mg HA/ccm)	TbTh (mm)	TbN (1/mm)	TbSp (mm)	ConnD (1/mm^3)
Day 2	NR	0.052 ± 0.010	35.0 ± 6.90	0.0306 ± 0.0014	3.88 ± 0.27	0.257 ± 0.018	43.8 ± 12.4
	IRR	0.061 ± 0.012 #	39.6 ± 8.1 #	0.0327 ± 0.0019	4.17 ± 0.31 #	0.240 ± 0.018 #	50.2 ± 23.0 #
	% Diff	16.15 *	12.9	6.8 *	7.6 *	- 6.8	14.8
Day 4	NR	0.045 ± 0.008	31.1 ± 5.86	0.0320 ± 0.0008	3.59 ± 0.34	0.279 ± 0.028	37.2 ± 18.7
	IRR	0.043 ± 0.009 #	30.1 ± 6.1 #	0.0350 ± 0.0014 #	3.39 ± 0.31 #	0.296 ± 0.029 #	20.0 ± 10.7
	% Diff	-5.9	-3.2	9.4 *	-5.5	6.0	-46 *
Day 6	NR	0.046 ± 0.008	32.0 ± 6.12	0.0321 ± 0.0010	3.71 ± 0.24	0.269 ± 0.020	39.3 ± 14.4
	IRR	0.014 ± 0.004 #	9.4 ± 2.9 #	0.0318 ± 0.0022	2.35 ± 0.24 #	0.439 ± 0.036 #	2.4 ± 1.0
	% Diff	-69.7 *	-71 *	-1.0	-36.6 *	62.9 *	-93.8 *

Table A. 4: Serum chemistry (ELISA). Averages and standard deviations of biomarkers of bone turnover from ELISA analyses for irradiated and non-irradiated groups 2, 4 and 6 days post-irradiation.

		Osteocalcin (ng/mL)	TRAP-5b (U/L)
Day 2	NR	573 ± 27 +	4.03 ± 1.05
	IRR	668 ± 37	6.37 ± 2.42
	% Diff	16.5 *	58.3
Day 4	NR	644 ± 26	4.24 ± 1.52
	IRR	666 ± 24	4.71 ± 1.42
	% Diff	3.3	10.9
Day 6	NR	651 ± 56	4.16 ± 1.69
	IRR	625 ± 33	12.31 ± 5.72 #
	% Diff	-4.1	195.8 *

Table A. 5: Whole bone structural parameters (FEA). Averages and standard deviations of structural parameters from FEA whole bone analysis for irradiated and non-irradiated groups 2, 4 and 6 days post-irradiation.

		Bone Volume (mm^3)	Stiffness (N/mm)	Efficiency ($N/mm/mm^3$)
Day 2	NR	0.901 ± 0.086 +	6261 ± 712	6944 ± 233
	IRR	0.854 ± 0.047	5892 ± 303	6908 ± 274
	% Diff	- 5.2	- 5.9	-0.5
Day 4	NR	0.819 ± 0.076	5803 ± 448	7097 ± 222
	IRR	0.845 ± 0.082	5792 ± 615	6858 ± 462
	% Diff	3.2	-0.2	-3.4
Day 6	NR	0.822 ± 0.047	5780 ± 393	7033 ± 213
	IRR	0.860 ± 0.075	5987 ± 582	6986 ± 295
	% Diff	4.6	3.6	-0.7

Table A. 6: Cortical bone structural parameters (FEA). Averages and standard deviations of structural parameters from FEA cortical bone analysis for irradiated and non-irradiated groups 2, 4 and 6 days post-irradiation.

		Bone Volume (mm^3)	Stiffness (N/mm)	Efficiency ($N/mm/mm^3$)
Day 2	NR	0.819 ± 0.073 +	5649 ± 582	6894 ± 275
	IRR	0.764 ± 0.047	5248 ± 271	6877 ± 312
	% Diff	- 6.7	- 7.1	-0.2
Day 4	NR	0.747 ± 0.065	5297 ± 408	7098 ± 226
	IRR	0.789 ± 0.076	5377 ± 616	6822 ± 505
	% Diff	5.5	1.5	-3.9
Day 6	NR	0.751 ± 0.043	5251 ± 336	6997 ± 266
	IRR	0.833 ± 0.059	5800 ± 434	7001 ± 374
	% Diff	11.0 *	10.4 *	0.1

Table A. 7: Trabecular bone structural parameters (FEA). Averages and standard deviations of structural parameters from FEA cancellous bone analysis for irradiated and non-irradiated groups 2, 4 and 6 days post-irradiation.

		Bone Volume (mm^3)	Stiffness (N/mm)	Efficiency ($N/mm/mm^3$)
Day 2	NR	0.082 ± 0.018	612 ± 168	7465 ± 807
	IRR	0.090 ± 0.022 #	644 ± 159 #	7237 ± 898
	% Diff	9.8	5.2	- 3.1
Day 4	NR	0.072 ± 0.018	505 ± 112	7129 ± 792
	IRR	0.057 ± 0.017 #	415 ± 110 #	7352 ± 812
	% Diff	-20.6	-17.9	3.1
Day 6	NR	0.071 ± 0.015	529 ± 106	7505 ± 791
	IRR	0.016 ± 0.006 #	123 ± 36 #	7917 ± 2124
	% Diff	-77.0 *	-76.7 *	5.5

REFERENCES

Aarden, E. M., Burger, E. H., & Nijweide, P. J. (1994). Function of Osteocytes in Bone. *Journal of Cellular Biochemistry, 55,* 287-299.

Abu-Amer, Y. (2009). Inflammation, cancer, and bone loss. *Current Opinions in Pharmacology, 9,* 427-433.

Allen, M. R. & Burr, D. B. (2014). Bone Modeling and Remodeling. In D.B.Burr & M. R. Allen (Eds.), *Basic and Applied Bone Biology* (pp. 75-90). San Diego, CA: Elsevier.

Armenian, S. H., Sun, C.-L., Kawashima, T., Arora, M., Leisenring, W., Sklar, C. A. et al. (2011). Long-term health-related outcomes in survivors of childhood cancer treated with HSCT versus conventional therapy: a report from the Bone Marrow Transplant Survivor Study (BMTSS) and Childhood Cancer Survivor Study (CCSS). *Blood, 118,* 1413-1420.

Barrett, A. (1999). Total Body Irradiation. *Rep.Pract.Oncol.Radiother., 4,* 47-64.

Bashie, Q. & Champlin, R. (2014). Hematopoietic Stem Cell Transplantation. In J.E.Niederhuber, J. O. Armitage, J. H. Doroshow, M. B. Kastan, & J. E. Tepper (Eds.), *Abeloff's Clinical Oncology* (5 ed., pp. 485-492). Elsevier.

Baxter, N. N., Habermann, E. B., Tepper, J. E., Durham, S. B., & Virnig, B. A. (2005). Risk of Pelvic Fractures in Older Women Following Pelvic Irradiation. *JAMA, 294,* 2587-2593.

Beamer, W. G., Donahue, L. R., Rosen, C. J., & Baylink, D. J. (1996). Genetic Variability in Adult Cone Density Among Inbred Strains of Mice. *Bone, 18,* 397-403.

Bellido, T., Plotkin, L. I., & Bruzzaniti, A. (2014). Bone Cells. In D.B.Burr & M. R. Allen (Eds.), *Basic and Applied Bone Biology* (pp. 27-45). San Diego, CA: Elsevier.

Beyzadeoglu, M., Ozyigit, G., & Ebruli, C. (2010). Clinical Radiation Oncology. In M.e.al.Beyzadeoglu (Ed.), *Basic Radiation Oncology* (pp. 145-173). Verlag Berlin Heidelberg: Springer.

BMJ (1968). Today's Drugs: Drugs In The Treatment of Leukaemia. *The British Medical Journal, 4,* 305-307.

BMJ (1969). Asparaginase. *The British Medical Journal, 2,* 465-466.

Bonewald, L. F. (2011). The Amazing Osteocyte. *Journal of Bone and Mineral Research, 26,* 229-238.

Boyle, W. J., Simonet, W. S., & Lacey, D. L. (2003). Osteoclast differentiation and activation. *Nature, 423,* 337-342.

Buck, D. W. & Dumanian, G. A. (2012). Bone Biology and Physiology: Part I. The Fundamentals. *Plastic and Reconstructive Surgery, 129,* 1314-1320.

Burr, D. B. & Akkus, O. (2014). Bone Morphology and Organization. In D.B.Burr & M. R. Allen (Eds.), *Basic and Applied Bone Biology* (pp. 3-25). San Diego, CA: Elsevier.

Campana, D. & Pui, C.-H. (2014). Childhood Leukemia. In J.E.Niederhuber, J. O. Armitage, J. H. Doroshow, M. B. Kastan, & J. E. Tepper (Eds.), *Abeloff's Clinical Oncology* (5 ed., pp. 1849-1872).

Cao, X., Wu, X., Frassica, D., Yu, B., Pang, L., Xian, L. et al. (2011). Irradiation induces bone injury by damaging bone marrow microenvironment for stem cells. *PNAS, 108,* 1609-1614.

Carlson, K., Simonsson, B., & Ljunghall, S. (1994). Acute Effects of High-Dose Chemotherapy Followed by Bone Marrow Transplantation on Serum Markers of Bone Metabolism. *Calcif Tissue Int, 55,* 411.

Chou, R. H., Wong, G. B., Kramer, J. H., Wara, D. W., Matthay, K. K., Crittenden, M. R. et al. (1996). Toxicities of total-body irradiation for pediatric bone marrow transplantation. *Int J Radiation Oncology Biol Phys, 34,* 843-851.

Christenson, R. H. (1997). Biochemical Markers of Bone Metabolism: An Overview. *Clinical Biochemistry, 30,* 573-593.

Crabbe, J. C., Cotnam, C. J., Schlumbohm, J. P., Rhodes, J. S., Metten, P., & Wahlsten, D. (2003). Strain differences in three measures of ethanol intoxication in mice: the screen, dowel and grip strength tests. *Genes Brain Behav., 2,* 201-213.

Damilakis, J., Adams, J. E., Guglielmi, G., & Link, T. M. (2010). Radiation exposure in X-ray-based imaging techniques used in osteoporosis. *European Radiology, 20,* 2707-2714.

de Beaumais, T. A., Fakhoury, M., Medard, Y., Azougagh, S., Zhang, D., Yakouben, K. et al. (2011). Determinants of mercaptopurine toxicity in paediatric acute lymphoblastic leukemia maintenance therapy. *British Journal of Clinical Pharmacology, 71,* 575-584.

de Beaumais, T. A. & Jacqz-Aigrain, E. (2012). Pharmacogenetic determinants of mercaptopurine disposition in children with acute lymphoblastic leukemia. *Eur J Clin Pharmacol, 68,* 1233-1242.

Despars, G. & St-Pierre, Y. (2011). Bidirectional interactions between bone metabolism and hematopoiesis. *Experimental Hematology, 39,* 809-816.

Ding, C., Parameswaran, V., Udayan, R., Burgess, J., & Jones, G. (2008). Circulating Levels of Inflammatory Markers Predict Change in Bone Mineral Density and Resorption in Older Adults: A Longitudinal Study. *J Clin Endocrinol Metab, 93,* 1952-1958.

Domen, J., Wagers, A., & Weissman, I. L. (2011). Bone Marrow (Hematopoietic) Stem Cells. *Regenerative Medicine,* 13-34.

Fares, J. E., Choucair, M., Nabulsi, M., Salamoun, M., Shahine, C. H., & Fuleihan, G. E. (2003). Effect of gender, puberty, and vitamin status on biochemical markers of bone remodeling. *Bone, 33,* 242-247.

Frost, H. M. (1990). Skeletal Structural Adaptations to Mechanical Usage (SATMU): 2. Redefining Wolff's Law: The Remodeling Problem. *The Anatomical Record, 226,* 414-422.

Girinsky, T., Briot, E., Bridier, A., & Beaudre, A. (1997). Principles of Total Body Irradiation. *Rep Pracr Oncol, 2,* 33-35.

Green, D. E., Adler, B. J., Chan, M. E., & Rubin, C. T. (2012). Devastation of Adult Stem Cell Pools by Irradiation Precedes Collapse of Trabecular Bone Quality and Quantity. *Journal of Bone and Mineral Research, 27,* 749-759.

Green, D. E. & Rubin, C. T. (2014). Consequences of irradiation on bone and marrow phenotypes, and its relation to disruption of hematopoietic precursors. *Bone, 63,* 87-94.

Guillerman, R. P. (2013). Marrow: red, yellow and bad. *Pediatric Radiology, 43,* S181-S192.

Haddy, T. B., Mosher, R. B., & Reaman, G. H. (2001). Osteoporosis in Survivors of Acute Lymphoblastic Leukemia. *Oncologist, 6,* 278-285.

Hadjidakis, D. J. & Androulakis, I. I. (2006). Bone Remodeling. *Annals of the New York Academy of Sciences, 1092,* 385-396.

Hamilton, S. A., Pecaut, M. J., Gridley, D. S., Travis, N. D., Bandstra, E. R., Willey, J. S. et al. (2006). A murine model for bone loss from therapeutic and space-relevant sources of radiation. *J Appl Physiol, 101,* 789-793.

Henderson, J. E., Gao, C., & Harvey, E. J. (2011). Skeletal Phenotyping in Rodents: Tissue Isolation and Manipulation. In G.Duque & K. Watanabe (Eds.), *Osteoporosis Research: Animal Models* (1 ed., pp. 13-28). London: Springer-Verlag.

Huang, Y., Eapen, E., Steele, S., & Grey, V. (2011). Establishment of reference intervals for bone markers in children and adolescents. *Clinical Biochemistry, 44,* 771-778.

Humphries, A. L. (2011). Basic Juvenile Skeletal Anatomy and Growth and Development. In A.H.Ross & S. M. Abel (Eds.), *The Juvenile Skeleton in Forensic Abuse Investigations* (pp. 19-31). Springer Science+Business Media, LLC.

Hyman, C. B. & Sturgeon, P. (1956). Prednisone therapy of acute lymphoblastic leukemia in children. *Cancer, 9,* 965-970.

Imbach, P. (2011a). Acute Lymphoblastic Leukemia. In P.Imbach, T. Kuhne, & R. J. Arceci (Eds.), *Pediatric Oncology: A Comprehensive Guide* (2 ed., pp. 5-20). Verlag Berlin Heidelberg: Springer.

Imbach, P. (2011b). General Aspects of Childhood Leukemia. In P.Imbach, T. Kühne, & R. J. Arceci (Eds.), *Pediatric Oncology* (pp. 1-4). Verlag Berlin Heidelberg: Springer.

Ito, M., Nishida, A., Koga, A., Ikeda, S., Shiraishi, A., Uetani, M. et al. (2002). Contribution of Trabecular and Cortical Components to the Mechanical Properties of Bone and Their Regulating Parameters. *Bone, 31,* 351-358.

Jagannathan-Bogdan, M. & Zon, L. I. (2013). Hematopoiesis. *Development, 140,* 2463-2467.

Jonsson, O. G. & Kamen, B. A. (1991). Methotrexate and Childhood Leukemia. *Cancer Investigation, 9,* 53-60.

Kalenderer, O., Bozoglan, M., & Agus, H. (2012). Heterotopic ossification in quadratus femoris muscle in a haemophilic patient. *Haemophilia, 18,* e13-e14.

Keenawinna, L., Oest, M. E., Mann, K. A., Spadaro, J., & Damron, T. A. (2013). Zoledronic Acid Prevents Loss of Trabecular Bone after Focal Irradiation in Mice. *Radiation Research, 180,* 89-99.

Khosla, S. (2013). Pathogenesis of Age-Related Bone Loss in Humans. *J Geronrol A Biol Sci Med Sci, 68,* 1226-1235.

Kim, J. Y., Kim, S. T., Nam, D.-H., Lee, J.-I., Park, K., & Kong, D.-S. (2011). Leukoencephalopathy Following Intrathecal Methotrexate Chemotherapy and Radiation Therapy for Central Nerve System Lymphoma or Leukemia. *J Korean Neurosurg Soc, 50,* 304-310.

Kondo, H., Searby, N. D., Mojarrab, R., Phillips, J., Alwood, J., Yumoto, K. et al. (2009). Total-Body Irradiation of Postpubertal Mice with Cs-137 Acutely Compromises the Microarchitecture of Cancellous Bone and Increases Osteoclasts. *Radiation Research, 171,* 283-289.

Lau, A. G., Sun, J., Hannah, W. B., Livingston, E. W., Heymann, D., Bateman, T. A. et al. (2014). Joint bleeding in factor VII deficient mice causes an acute loss of trabecular bone and calcification of joint soft tissues which is prevented with aggressive factor replacement. *Haemophilia, 20,* 716-722.

Li, X., Srivastava, A. K., Gu, W., Masinde, G., Mohan, S., & Baylink, D. J. (2002). Opposing Changes in Osteocalcin Levels in Bone vs Serum During the Acquisition of Peak Bone Density in C3H/HeJ and C57BL/6J Mice. *Calcif Tissue Int, 71,* 416-420.

Mandel, K., Atkinson, S., Barr, R. D., & Pencharz, P. (2004). Skeletal Morbidity in Childhood Acute Lymphoblastic Leukemia. *Journal of Clinical Oncology, 22,* 1215-1221.

Margulies, B., Morgan, H., Allen, M., Strauss, J., Spadaro, J., & Damron, T. A. (2003). Transiently Increased Bone Density After Irradiation and the Radioprotectant Drug Amifostine in a Rat Model. *Am J Clin Oncol (CCT), 26,* e106-e114.

Marie, P. J. (1998). Osteoblasts and Bone Formation. In *Advances in Organ Biology* (pp. 445-473). JAI Press Inc.

McClune, B., Polgreen, L., Burmeister, L., Blaes, A., Mulrooney, D., Burns, L. et al. (2011). Screening, prevention and management of osteoporosis and bone loss in adult and pediatric hematopoietic cell transplant recipients. *Bone Marrow Transplantation, 46,* 1-9.

Miyazaki, O., Nishimura, G., Okamoto, R., Masaki, H., Kumagai, M., Shioda, Y. et al. (2009). Induction of systemic bone changes by preconditioning total body irradiation for bone marrow transplantation. *Pediatr Radiol, 39,* 23-29.

Mogul, M. J. (2002). Guide to Pediatric Stem Cell Transplantation. 1-53. University of Florida School of Medicine.
Ref Type: Generic

Müller, R., Kampschulte, M., El Khassawna, T., Schlewitz, G., Hürter, B., Böcker, W. et al. (2014). Change of mechanical vertebrae properties due to progressive osteoporosis: combined biomechanical and finite-element analysis within a rat model. *Med Biol Eng Comput, 52,* 405-414.

Murre, C. (2009). Developmental trajectories in early hematopoieses. *Genes & Development, 23,* 2366-2370.

Mussa, A., Bertorello, N., Porta, F., Galletto, C., Nicolosi, M. G., Manicone, R. et al. (2010). Prospective bone ultrasound patterns during childhood acute lymphoblastic leukemia treatment. *Bone, 46,* 1016-1020.

O'Brien, M. M. & Lacayo, N. J. (2008). Acute Leukemia in Children. In R.E.Rakel & E. T. Bope (Eds.), *Conn's Current Therapy 2008* (pp. 446-453). Elsevier.

Oeffinger, K. C., Mertens, A. C., Sklar, C. A., Kawashima, T., Hudson, M. M., Meadows, A. T. et al. (2006). Chronic Health Conditions in Adult Survivors of Childhood Cancer. *The New England Journal of Medicine, 355,* 1572-1582.

Olsen, B. R., Reginato, A. M., & Wang, W. (2000). Bone Development. *Annu.Rev.Cell Dev.Biol., 16,* 191-220.

Ooi, H. L., Briody, J., McQuade, M., & Munns, C. F. (2012). Zoledronic Acid Improves Bone Mineral Density in Pediatric Spinal Cord Injury. *Journal of Bone and Mineral Research, 27,* 1563-1540.

Orkin, S. H. & Zon, L. I. (2008). SnapShot: Hematopoiesis. *Cell, 132,* 712-713.

Paessler, M. E. & Bourne, S. (2011). Bone Marrow. In L.M.Ernst & et al. (Eds.), *Color Atlas of Fetal and Neonatal Histology* (pp. 273-281). Springer Science+Business Media, LLC.

Plotkin, L. I. & Bivi, N. (2014). Local Regulation of Bone Cell Function. In D.B.Burr & M. R. Allen (Eds.), *Basic and Applied Bone Biology* (pp. 47-73). San Diego, CA: Elsevier.

Pui, C.-H. & Evans, W. E. (2006). Treatment of Acute Lymphoblastic Leukemia. *New England Journal of Medicine, 354,* 166-178.

Pui, C.-H., Robison, L. L., & Look, A. T. (2008). Acute Lymphoblastic Leukemia. *Lancet, 371,* 1030-1043.

Putman, M. S. & Gordon, C. M. (2014). Pediatric Bone Drugs: Calcium and Vitamin D. In G.L.Kline (Ed.), *Bone Drugs in Pediatrics: Efficacy and Challenges* (pp. 153-181). New York: Springer Science+Business Media.

Raj, T. A., Smith, A. M., & Moore, A. S. (2013). Vincristine sulfate liposomal injection for acute lymphoblastic leukemia. *International Journal of Nanomedicine, 8,* 4361-4369.

Rauchenzauner, M., Schmid, A., Heinz-Erian, P., Kapelari, K., Falkensammer, G., Griesmacher, A. et al. (2007). Sex- and Age-Specific Reference Curves for Serum Markers of Bone Turnover in Healthy Children from 2 Months to 18 Years. *The Journal of Clinical Endocrinology & Metabolism, 92,* 443-449.

Rodrigues, A., Perpétuo, I. P., Caetano-Lopes, J., Alexio, I., Pena, A., Faustino, A. et al. (2010). Negative correlation between osteocalcin serum levels and bone mechanical properties. *Bone, 47,* S88.

Rueegg, C. S., Gianinazzi, M. E., Rischewski, J., Popovic, M. B., von der Weid, N. X., Michel, G. et al. (2013). Health-related quality of life in survivors of childhood cancer: the role of chronic health problems. *J Cancer Surviv, 7,* 511-522.

Saha, V. & Lilleyman, J. S. (1998). Leukaemia. *Current Paediatrics, 8,* 73-77.

Sanders, J. E. (1990). Late effects in children receiving total body irradiation for bone marrow transplantation. *Radiotherapy and Oncology, Suppl. 1,* 82-87.

Sawajiri, M. & Mizoe, J. (2003). Changes in bone volume after irradiation with carbon ions. *Radiat Environ Biophys, 42,* 101-106.

Sawyers, C. L., Denny, C. T., & Witte, O. N. (1991). Leukemia and the Disruption of Normal Hematopoiesis. *Cell, 64,* 337-350.

Schimmer, A. D., Minden, M. D., & Keating, A. (2000). Osteoporosis After Blood and Marrow Transplantation. *BB & MT, 6,* 175-181.

Schönau, E. & Rauch, F. (2003). Biochemical Markers of Bone Metabolism. In F.H.Glorieux, J. M. Pettifor, & H. Jüppner (Eds.), *Pediatric Bone* (pp. 339-357). San Diego: Academic Press.

Schwen, L. O. & Wolfram, U. (2014). Validation of composite finite elements efficiently simulating elasticity of trabecular bone. *Computer Methods in Biomechanics and Biomedical Engineering, 17,* 652-660.

Sebestyen, J. F., Srivastava, T., & Alon, U. S. (2012). Bisphosphonates Use in Children. *Clinical Pediatrics, 51,* 1011-1024.

Shuler, F. D., Conjeski, J., Kendall, D., & Salava, J. (2012). Understanding the Burden of Osteoporosis and Use of the World Health Organization FRAX. *Orthopedics, 35,* 798-805.

Silva, M. J., Keaveny, T. M., & Hayes, W. C. (1997). Load sharing between the shell and centrum in the lumbar vertebral body. *Spine, 22,* 140-150.

Siris, E. S., Ya-Ting, C., Abbott, T. A., Barrett-Connor, E., Miller, P. D., Wehren, L. E. et al. (2004). Bone Mineral Density Thresholds for Pharmacologic Intervention to Prevent Fractures. *Arch intern Med, 164,* 1108-1112.

Staal, F. J. T., Pike-Overzet, K., & van Zelm, M. C. (2011). Hamatopoiesis and lymphocyte development: An Introduction. In F.P.Nijkamp & M. J. Parnham (Eds.), *Principles of Immunopharmacology* (3rd revised and extended ed., pp. 3-14). Springer Basel AG.

Storer, J. B. (1966). Acute Responses to Ionizing Radiation. In E.L.Green (Ed.), *Biology of the Laboratory Mouse* (2 ed., New York: Dover Publications, Inc.

Teitelbaum, S. L. (2000). Bone Resorption by Osteoclasts. *Science, 289,* 1504-1508.

The Jackson Laboratory (2006a). Densitometric survey of 11 inbred strains of mice. Mouse Phenome Database web site [On-line].

The Jackson Laboratory (2006b). Hematologic survey of 11 inbred strains of mice. Mouse Phenome Database web site http://phenome.jax.org [On-line].

Triffitt, J. T. & Oreffo, R. O. C. (1998). Osteoblast Lineage. In *Advances i nOrgan Biology* (pp. 475-498). JAI Press, Inc.

Tucci, F. & Aricò, M. (2008). Treatment of pediatric acute lymphoblastic leukemia. *haematologica, 93,* 1124-1128.

Tuchman, S., Thayu, M., Shults, J., Zemel, B. S., Burnham, J. M., & Leonard, M. B. (2008). Interpretation of Biomarkers of Bone Metabolism in Children: Impact of Growth Velocity and Body Size in Healthy Children and Chronic Disease. *J Pediatr, 153,* 484-490.

Turner, A. S. (2011). How to Select Your Animal Model for Osteoporosis Research. In G.Duque & K. Watanabe (Eds.), *Osteoporosis Research: Animal Models* (1 ed., pp. 1-12). London: Springer-Verlag.

van der Sluis, I. M., van den Heuvel-Eibrink, M. M., Hählen, K., Krenning, E. P., & de Muinck Keizer-Schrama, S. M. P. F. (2002). Altered bone mineral density and body composition, and increased fracture risk in childhood acute lymphobastic leukemia. *J Pediatr, 141,* 204-210.

von Scheven, E. (2007). Pediatric Bone Density and Fracture. *Current Osteoporosis Reports, 5,* 128-134.

Weilbaecher, K. N. (2000). Mechanisms of Osteoporosis After Hematopoietic Cell Transplantation. *BB & MT,* 165-174.

Wernle, J. D., Damron, T. A., Allen, M. J., & Mann, K. A. (2010). Local irradiation alters bone morphology and increases one fragility in a mouse model. *Journal of Biomechanics, 43,* 2738-2746.

Willey, J. S., Lloyd, S. A., Nelson, G. A., & Bateman, T. A. (2011). Ionizing Radiation and Bone Loss: Space Exploration and Clinical Therapy Applications. *Clin.Rev.Bone Miner.Metab., 9,* 54-62.

Willey, J. S., Livingston, E. W., Robbins, M. E., Bourland, D., Tirado-Lee, L., Smith-Sielicki, H. et al. (2010). Risedronate Prevents Early Radiation-Induced Osteoporosis in Mice at Multiple Skeletal Locations. *Bone, 46,* 101-126.

Willey, J. S., Lloyd, S. A. J., Robbins, M. E., Bourland, D., Smith-Sielicki, H., Bowman, L. C. et al. (2008). Early Increase in Osteoclast Number in Mice after Whole-Body Irradiation with 2 Gy X-rays. *Radiation Research, 170,* 388-392.

Yang, L. & Grey, V. (2006). Pediatric refernce intervals for bone markers. *Clinical Biochemistry, 39,* 561-568.

Yumoto, K., Globus, R. K., Mojarrab, R., Arakaki, J., Wang, A., Searby, N. D. et al. (2010). Short-Term Effects of Whole-Body Exposure to Fe-56 Ions in Combination with Musculoskeletal Disuse on Bone Cells. *Radiation Research, 173,* 494-504.

Zeman, E., Schreiber, E., & Tepper, J. (2014). Basics of Radiation Therapy. In J.E.Niederhuber, J. O. Armitage, J. H. Doroshow, M. B. Kastan, & J. E. Tepper (Eds.), *Abeloff's Clinical Oncology* (5 ed., pp. 393-422).